SHORELINE DATA ANALYSIS

A DISSERTATION SUBMITTED TO THE GRADUATE DIVISION OF THE UNIVERSITY OF HAWAIʻI AT MĀNOA IN PARTIAL FULFILLMENT OF THE REQUIREMENTS FOR THE DEGREE OF

DOCTOR OF PHILOSOPHY

IN

GEOLOGY AND GEOPHYSICS

AUGUST 2013

By

Tiffany R. Anderson

Dissertation Committee:

L. Neil Frazer, Chairperson
Charles Fletcher III
Janet Becker
Paul Wessel
Mark Merrifield

Keywords: Shoreline change, erosion, coastal storms, linear regression, coastal geology, shoreline data

ACKNOWLEDGMENTS

I would first like to thank my advisor, Neil Frazer, for providing guidance and pushing me to grow, both intellectually and personally. I am also very grateful to Chip Fletcher for encouraging my professional and individual development and providing funding for me over the years. Thank you Janet Becker for listening to my rambling of ideas and gracing me with your words of wisdom. I am thankful to Paul Wessel and Mark Merrifield for sharing their thoughts and ideas. I am indebted to Kaena Horowitz for help with editing and providing valuable feedback on portions of this dissertation. Current and former members of the University of Hawaii Coastal Geology Group contributed to the research in this dissertation, including Brad Romine, Matthew Barbee, Matthew Dyer, Haunani Kane, and Ayesha Genz. Courtney Schupp from the U.S. Army Corps of Engineers provided information on Assateague Island engineering projects and Emily Himmelstoss from the USGS helped with East Coast data. Funding was provided from the U.S. Geological Survey National Shoreline Assessment; U.S. Army Corps of Engineers Regional Sediment Management Program; Department of Interior Pacific Islands Climate Science Center; University of Hawaii Sea Grant College Program; Hawaii Department of Land and Natural Resources; Fred M. Bullard Endowed Graduate Fellowship; Kotaro Kodama Graduate Scholarship; ARCS Foundation Scholarship; and the Association for Women Geoscientists Foundation Chrysalis Scholarship.

ABSTRACT

In this dissertation, shoreline response to a storm is investigated, and two new empirical models for shoreline position change, over timescales of decades to centuries, are developed and compared with earlier empirical models. The new B-spline method and regularized-ST method avoid over-fitting of data, as predictions of future shoreline position can be wildly inaccurate if based on models that over-fit. They utilize a non-diagonal data covariance matrix, with correlations estimated from the data residuals, in order to carefully estimate the uncertainty of predictions, because uncertainty is as important to shoreline managers as the predictions themselves.

The first part of the dissertation investigates storm behavior at Assateague Island, MD. Earlier work showed that inclusion of a transient storm function improved statistical modeling of historical shoreline data. Here, it is found that the shoreline response to a storm has not only a transient component, as in our earlier work, but also a persistent component, and that both are required to fit the data.

The B-spline and regularized-ST methods focus on reducing model parameters in the alongshore direction. The traditional single transect (ST) method uses far more parameters than necessary because it assumes that long-term erosion/accretion varies independently at each alongshore location. The new models give shoreline change rates that vary more smoothly alongshore than ST rates do, but are generally consistent with rates from prior studies. Both new models successfully address problems with earlier models, notably Gibbs effect with polynomial basis functions and noise contamination with principal component basis functions.

TABLE OF CONTENTS

LIST OF TABLES

LIST OF FIGURES

Chapter 1
INTRODUCTION

1.1 Why analyze shoreline data?

Increasing concern for shore-related hazards to coastal properties continues to spur coastal studies (*e.g.*, Crowell *et al.*, 1997; Miller and Dean, 2007; Davidson *et al.*, 2013; Ford, 2013). Properties along the coast are often popular destinations for tourism and recreation. Consequentially, the American population continues to shift toward the coast, increasing coastal development, and making coastal properties some of the most valuable in the U.S. Often, coastal communities are planned with insufficient thought for natural hazards such as coastal erosion, and coastal structures built too close to eroding shorelines experience wave inundation and damage. In response, sea walls and other structures are built to protect coastal homes, hotels, and infrastructure; but these structures can lead to the total loss of the beaches that once fronted them (Fletcher *et al.*, 1997; Romine and Fletcher, 2012). As a result, numerous shoreline studies aim to quantify trends in shoreline migration (*e.g.*, Crowell *et al.*, 1991; Galgano, 2004; Morton and McKenna, 1999; Maiti and Bhattacharya, 2009; Romine and Fletcher, 2012; UGSG National Assessment of Shoreline Change). Shoreline studies are thus vital to the early stages of the decision-making process for planned coastal developments to mitigate the potential loss of buildings, infrastructure, and beaches.

Long-term (decadal) trends in data are of particular interest because coastal planning projects tend to be longstanding. The median lifespan of commercial buildings is 70-75 years (U.S. Department of Energy, 2011). But shorelines are dynamic in nature and coastal behavior is the complex result of multiple processes occurring and interacting on a variety of time and spatial scales. Some physical processes that drive shoreline

change include waves, currents, tides, storm surges, seasonal fluctuations, aeolian transport, and relative changes in sea level (Komar, 1998).

Many scientists agree that long-term prediction at the multi-decadal scale is best achieved by analyzing historical shorelines spanning at least 80 years (Crowell et al., 1993; Galgano and Leatherman, 1991; Galgano and Douglas, 2000). Yet this is problematic because the shoreline data available over time spans of this length are often noisy and sparse in time. There might be, for example, a single historical shoreline survey per decade of the area of interest. This under-sampling in time creates problems because often there is significant short-term variation in the shoreline due to natural processes such as tides, storms, seasons, and other incidents, which can mask the long-term signal (Honeycutt *et al.*, 2001; Zhang *et al*., 2002a). Storms, especially, wreak havoc on shoreline analyses (Douglas and Crowell, 2000). A 50-year storm event can move the shoreline inland over ten times the distance spanned by a normal seasonal cycle of accretion and erosion.

Consequentially, coastal decision-makers rely on simple models that often produce estimates with inadequate accuracy for prediction purposes. For example, the single transect (ST) methods – widely used, due to their simplicity – calculate an independent rate at regularly spaced intervals along the shoreline, ignoring the fact that sand between neighboring transects is shared. Furthermore, due to the small number of available shoreline surveys, individual rate calculations are often accompanied by large uncertainty values; sometimes several times the size of the estimated rate itself. If uncertainty values are not considered, planned development of properties could be at a high risk for wave inundation. This is currently the case in determining shoreline setbacks on the islands of Kauai and Maui, Hawaii.

Several new methods address alongshore correlations and large uncertainty values, but coastal managers have been reluctant to use these methods because they are often complex and unwieldy to implement. It is important, therefore, to continue to develop more realistic models, which will, in turn, become more accurate as more data becomes available, and user friendly as shoreline managers become better acquainted with them.

1.2 Overview of historical shoreline data analysis methodology

Historical shoreline data, in conjunction with statistical methods, can be analyzed to identify relevant information, provide insight, and support decision-making. These shoreline studies typically involve calculating long-term cross-shore shoreline change rates at evenly spaced alongshore locations. At each location, a time series of shoreline positions, relative to some baseline, is measured along a shore-normal line, called a transect. Further discussion of analysis methods continues below, after detailed discussion of the types of data employed.

For calculating erosion rates, many researchers recommend using the longest available record, usually containing NOAA topographic survey charts (T-sheets), provided there have been no physical changes in the system, such as construction of coastal armoring or inlets opening or closing (Crowell *et al*., 1997; Dolan *et al*., 1991; Leatherman and Crowell, 1997). Although some scientists question the accuracy of T-sheets (Smith and Zarillo, 1990; Dolan *et al*., 1980), others recognize that they provide greater temporal coverage, which greatly outweighs the relatively small increase in positional uncertainty (Crowell *et al*., 1992; National Research Council, 1990). Other commonly used shoreline data are digitally orthorectified aerial photographs (Fletcher *et al*., 2003), GPS surveys (Morton *et al*., 1993), laser altimetry (LiDAR, Sallenger *et al.,* 2003), and satellite imagery (Maiti and Bhattacharya, 2009; Ford, 2013). A reference feature, typically the high water line or the beach toe (Bauer and Allen, 1995), identifies the shoreline in aerial photos, T-sheets, GPS surveys, and satellite imagery. LiDAR derived shorelines are based on a sea level datum. Ruggiero and List (2009) provide methodology for using the feature-based and datum-based shoreline data concurrently in a single study.

Using this data, a variety of methods have been implemented to calculate independent change rates (accretion/erosion) at each transect, for example: end-point rate (EPR), least squares (LS), the jackknife (JK), average-of-rates (AOR), reweighted least squares (RLS) (Rousseeuw, 1990), minimum description length (MDL) (Fenster *et al*., 1993), and weighted least squares (WLS) (Genz *et al*., 2007). Several researchers have

found LS to be the most accurate method, given known storm shorelines (Crowell, *et al*., 1997; Dean and Malakar, 1999; Dolan, et al, 1991). A drawback to using LS for shoreline change analysis is its susceptibility to outliers, especially those caused by large storms (Fenster et al, 1993; Dolan et al, 1991; Foster and Savage, 1989).

Large storms often impact shorelines significantly, causing large deviations in shoreline positions (outliers), which contribute to large uncertainties in prediction, thereby rendering them unreasonable (Douglas and Crowell, 2000). Several solutions to this problem were proposed. Some researchers concluded that excluding storm surveys would greatly improve the accuracy of predictions (Honeycutt et al, 2001; Galgano et al, 1998; Galgano and Douglas, 2000). For example, RLS and reweighted weighted least squares (RWLS) use statistical methods to identify and exclude specific storm data (Genz et al, 2007). Conversely, Frazer, *et al* (2009b) explicitly included storms in the ST model, allowing all data to be used while gaining additional information about the storms. As an alternative to the previous two methods, Miller and Dean (2004) introduced a cross-shore change model, which assumes an equilibrium beach position to which the beach relaxes, as with perturbation due to storms. This method, utilizing relatively temporally dense (hourly) wave and water level data in addition to field surveys has the benefit of identifying shoreline changes over short time intervals, but does not accurately assess long-term shoreline change. Methods based on the disequilibrium concept (*e.g*., Yates *et al.,* 2009; Davidson *et al.,* 2013) demonstrated successful hindcasting of observed shoreline locations at selected sites over shorter time scales. However, these methods require additional shoreline, wave, and water level data not widely available, especially over long time scales.

As addressed above, storms are not the only problem facing statistical models. Typical ST methods assume that the data at each transect location is independent. However, adjacent transects often reflect similar behavior. Genz *et al.* (2007) found that similar rates can be binned into alongshore cells. Frazer *et al*. (2009a) expand on this binning method by using the Akaike Information Criterion (AIC) to statistically select bin sizes. This model is more parsimonious; it balances the accuracy of the prediction with the number of parameters used in the model. However, the rates generated by binning

are discontinuous at cell boundaries, causing large jumps in rates alongshore. Frazer *et al*. (2009a) and Genz *et al*. (2009) introduced alongshore basis functions to produce smooth rates alongshore, using a modified AIC to identify the number of basis functions needed to produce the most parsimonious model. However, none of these methods accounts for large storms in the data.

As these previous researchers illustrate, developing new methods to better understand and predict shoreline change is warranted.

1.3 Improving analysis methods

This dissertation addresses some of the deficiencies discussed above by developing and testing new shoreline change methods. In Chapter Two, the storm function introduced by Frazer *et al*. (2009b) is combined with the Eigenbeaches alongshore method (Frazer *et al.*, 2009a) to investigate transient and persistent shoreline behavior from a storm on a barrier island. Combining an alongshore basis function method with the storm function shows the potential benefit of reducing uncertainty in change rate estimates via the storm function and, at the same time, increasing model parsimony. Shoreline data from Assateague Island, MD, provides an excellent example of a strong storm signal and it is temporally dense, as compared to most long-term datasets. This also provides important insight into shoreline response to the storm over smaller times scales (months), which can be compared to assumptions about long-term shoreline behavior in temporally sparse datasets.

Two new shoreline change methods are introduced in Chapters Three and Four, following work done by Frazer *et al.,* (2009b) and Genz *et al.,* (2009). The prior studies address the issue of model parsimony by reducing the number of model parameters via alongshore basis functions. Chapter Three introduces a shoreline change method that uses spline basis functions (B-splines) to represent change rates and intercepts alongshore. The spline method addresses problems with previously used basis function methods, such as Gibbs effect in polynomial (Legendre, trigonometric) functions and noise contamination in principal components regression. This chapter also presents additional noise handling techniques that address spatially correlated data errors. Chapter

Four presents a regression methodology that reduces model complexity by "regularizing" ST rates and intercepts via second order Tikhonov regularization. The regularized-ST model may be more acceptable to shoreline managers than the spline model because it includes the ST method as a special case in an obvious way. The new methods described in Chapters Three and Four both employ an information criterion (IC) to select the appropriate level of model complexity. A comparison between the methods is given in Chapter 4.

Chapter 2

TRANSIENT AND PERSISTENT SHORELINE CHANGE FROM A STORM

Published as Anderson, T.R., Frazer, L.N., and C.H. Fletcher (2010), Transient and persistent shoreline change from a storm. *Geophysical Research Letters*, 37, L08401, doi:10.1029/2009GL042252.

Abstract – There is disagreement as to whether shoreline position eventually recovers from large storms. In an earlier paper we showed that statistical modeling of historical shoreline data was improved by including large storms in the model via a transient storm function. Here we show that, at shorter timescales of months to years, modeling of the shoreline at Assateague Island, MD is improved by a storm model with both transient and persistent components. We find that the shoreline recovers from the storm rapidly, almost within a year, but that the recovery is only partial, despite anthropogenic reconstruction of a pre-existing berm. The long-term trend of a shoreline (whether erosive, accretive, or stationary) can thus be regarded as the cumulative persistent component of successive storms, although most long-term data sets are too temporally sparse to make such a parameterization more useful than a steady long-term rate.

2.1 Introduction

Coastal managers need to know how the shoreline is moving over long periods of time in order to plan development. Douglas & Crowell (2000) showed that post-storm shoreline positions can be outliers with respect to the trend, and that removing post-storm data can improve the apparent precision of trend estimates. However, removal of shoreline data inevitably introduces a degree of subjectivity. Frazer et al. (2009b) (paper 1) showed that including large storms as part of the shoreline model can improve long-

term shoreline position prediction from sparsely sampled historical shoreline data, and that subjectivity in choice of which storms to model can be addressed by using an information criterion and by probability-weighted model averaging. In order to better understand how storms impact beaches, this study investigates shoreline response to a large storm on a time scale much shorter than that in paper 1. Here the time between most surveys is a few months.

The US mid-Atlantic coast is subjected to intense tropical storms, which usually move quickly, impacting a given shoreline area for only a day, as well as mid-latitude storms known as "northeasters" which move more slowly, impacting a given shoreline area during several tidal cycles. Thus northeasters trap high-tide water, causing waves to reach higher portions of the shore. These large storm waves move sand from the dunes and berm to the offshore (Short, 1979). Washover, aeolian transport and nearshore downwelling also remove sand and contribute to landward shoreline migration during a storm (Niedoroda, 1984; Kochel and Dolan, 1986; Leatherman, 1979).

In the intervals between storms, swell waves gradually move the offshore sand back onshore, and shoreline positions tend to recover from storms (Birkemeier, 1979; Kriebel, 1987; Morton, 1988; Morton et al., 1994). After a storm, the rate of shoreline change may return to its long-term trend (Galgano and Douglas, 2000; Zhang et al., 2002a) over 5–15 years, depending on the magnitude of the storm. Historical shoreline data sets may span 150 years or more, but the data are temporally very sparse, so the details of shoreline recovery from a storm are not apparent. Here we model data in two dimensions (alongshore position and time) from Assateague Island, MD, containing a large storm. Although the time window from March 1995 to September 2002 is relatively short, the data are relatively dense in time (24 surveys) and the behavior of the storm-influenced shoreline position is revealed in more detail. An onshore berm was leveled by the storm, and our model accounts for the effects of its replacement by coastal managers. Other forms of shoreline nourishment were used after the study interval.

2.2 Assateague Island

Assateague Island is a barrier island along the coasts of Maryland and Virginia (Figure 2.1). Its Atlantic side consists of coastal dunes that seldom reach elevations above 2 meters, and its landward side is a low-elevation back barrier flat, sand and tidal wetland. Dominant waves have an average height of 1 m (Schupp, 2007), and spring tides fluctuate between -1 and 3 m (Field, 1979). Ocean City Inlet formed during a hurricane in 1933. Jetties constructed on both sides of the inlet in 1935 interrupted alongshore sediment transport from the north, causing severe coastal erosion south of the inlet (Rosati and Ebersole, 1996). An ebb tidal delta subsequently formed and developed into a 300 m attachment bar connected to the shore about 650-950 m south of the inlet (Schupp, 2007; Rosati and Ebersole, 1996) thus restoring a portion of the alongshore sediment transport (Krauss, 2000).

In 1998, two large northeasters altered the study shoreline (Ramsey et al., 1998). On January 28, 1998, a low pressure system originating in Texas moved northeast, crossed the mouth of Chesapeake Bay and continued north with maximum wind gusts reaching almost 95 km/h and significant wave heights exceeding 7 m over an interval less than 24 hours. A few days later, on February 4, 1998, a stronger northeaster originating in the Gulf of Mexico crossed North Carolina and Virginia, and continued slowly north along the Atlantic Coast through February 6. This storm also produced significant wave heights exceeding 7 m, with maximum wind gusts near 95 km/h over a period greater than 24 hours. As the time interval between these two storms is much smaller than the interval between shoreline surveys, we model them as a single storm on February 4.

The large waves generated by the two northeasters washed over portions of Assateague Island just south of the Ocean City Inlet. As a breach in the island was then considered a possibility, an onshore berm was constructed by the Assateague Island National Seashore North End Restoration Project (ASIS) and was completed 8 months after the storm. About 153,000 m^3 of sediment were deposited onto the beach 5-7.5 km south of Ocean City Inlet (National Park Service (NPS), Assateague Island National Seashore North End Restoration Project Timeline, available at www.nps.gov/asis/naturescience/upload/ProjectTimeline.pdf, 2006). (Prior accretion

north of the jetties at Ocean City Inlet protected Ocean City from what might otherwise have been catastrophic erosion.)

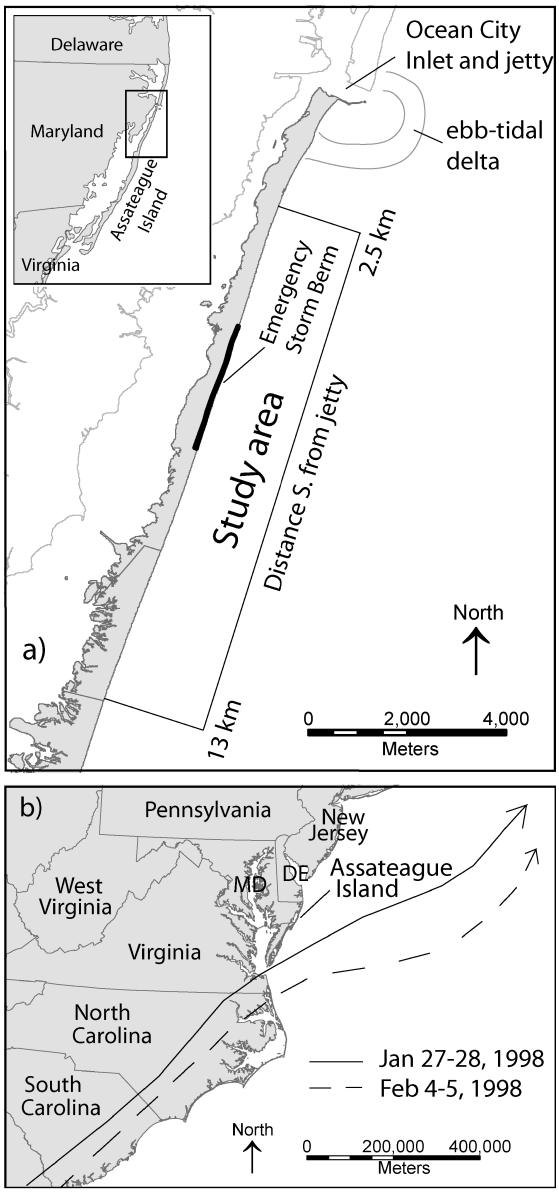

Figure 2.1 (a) Assateague Island, MD. (b) Tracks of the 1998 storms. See text for details.

2.3 Methods

Shoreline positions for the years 1995 to 2003 have been collected by ASIS North End Restoration Project (www.nps.gov/asis/naturescience/resource-management-documents.htm), which used a kinematic GPS mounted on an ATV to map the high tide,

high swash, wet/dry line four times a year. We used the Digital Shoreline Analysis System (DSAS) (Thieler et al., 2005) to cast cross-shore transect lines 10 m apart in the alongshore direction. The result is a matrix $Y_{ij} = y(x_i, t_j)$ of shoreline positions in which the row index is alongshore distance and the column index is time. Each row of *Y* (a transect) is a time series of shoreline positions at one alongshore location, and each column of *Y* (a survey) is a snapshot of the shoreline position at a particular time. Columns were then anti-alias filtered and re-sampled to 50 m transect spacing.

The traditional method of shoreline data analysis, called the single-transect method, models each transect independently, ignoring the lack of independence of the data at adjacent transects (Fletcher et al, 2003). We address the dependency issue as in Frazer et al. (2009a) and Genz et al. (2009) by the use of alongshore basis functions: We subtract the pre-storm survey temporally nearest to the storm, $y_{(0)}$, from all the columns of *Y* to obtain a matrix *Z*, find its singular value decomposition $Z = \sum_k \lambda_k u_{(k)} v_{(k)}^T$, then model each temporal coefficient $y_{(k)}(t_j) = \lambda_k v_{(k)}(t_j)$ as if it were a single transect. Our model for the data is thus

$$y(x,t) = y_{(0)} + \sum_k u_{(k)}(x) y_{(k)}(t) \tag{2.1}$$

in which the shoreline data mode $u_{(k)}(x)$ is the eigenvector of the matrix ZZ^T with eigenvalue λ_k^2. Only the first few modes are needed to model the data, but we modeled all temporal coefficients for completeness; the coefficients of modes higher than six were best modeled by noise.

Paper 1 gives our method for fitting time models to the temporal coefficients. Here our most complex time model is

$$\begin{aligned} y(t) = {} & b + rt + n(t) \\ & + s_T e_+^{-\gamma(t-t_s)} + s_P H(t - t_s) \\ & + v\, e_+^{-\gamma(t-t_v)} (1 - e^{-\gamma(t-t_v)}) \\ & + a_c \cos(2\pi t) + a_s \sin(2\pi t). \end{aligned} \tag{2.2}$$

The first line of equation (2.2) has the intercept, rate and noise terms; the second line has the transient and persistent parts of the storm function; the third line has the nourishment, and the fourth line has the seasonal component. The unit of time is years. In the storm function, t_s is the time of the storm, s_T is the amplitude of the storm transient, γ is the recovery rate, $H(t)$ is the unit step function, and s_P is the amplitude of the persistent component. The subscript "+" means that the storm transient $e_+^{-\gamma(t-t_s)}$ is zero prior to the storm. The shoreline displacement by the storm is the sum $s_T + s_P$. In the nourishment function, t_v is the time of the nourishment, which was 8 months following the storm (NPS, project timeline, 2006), and v is its amplitude. An information criterion (IC) — here the corrected Akaike Information Criterion (AICc)—is used to evaluate the likelihoods of models with various terms, and the model likelihoods are combined with prior model probabilities to generate model probabilities. Briefly, the posterior probability of the j^{th} model is proportional to $\pi_j e^{-\text{IC}_j/2}$, in which π_j is its prior probability, IC_j is its IC score, and $e^{-\text{IC}_j/2}$ is its likelihood. The final model is a probability-weighted average over all candidate models. The covariance matrix of residuals, a modeling diagnostic, is given in Appendix D.

Here all models with non-zero prior probability are given equal prior probability. Models with zero prior probability (excluded models) are:

1. Models with no storm component, unless the model is only noise.
2. Models for which transient and persistent components have opposite signs: for example, a positive persistent component and negative transient component. For such models, the shoreline displacement $s_T + s_P$ is reasonable, but s_T and s_P may individually have unreasonably large amplitudes.
3. Models with a transient component whose recovery rate γ approaches zero. For such models the transient component is redundant, and only a persistent component is needed.

Since all models not excluded are given the same prior probability, the model with the largest likelihood (lowest IC score) is the model with the largest posterior probability.

In view of the decomposition into data modes, and the modeling of temporal coefficients, the transient and permanent components of the modeled storm are the respective mode sums

$$s_T(x,t) = \sum_k s_T^{(k)} u_{(k)}(x) e_+^{-\gamma(t-t_s)} \tag{2.3a}$$

shown in Fig. 2.2c, and

$$s_P(x,t) = \sum_k s_P^{(k)} u_{(k)}(x) H(t-t_s) \tag{2.3b}$$

shown in Fig. 2.2d.

To estimate errors we make an adiabatic approximation, assuming that errors in one modal coefficient are unrelated to those of other coefficients. For example, the variance in the estimate of the transient component amplitude is

$$\sigma_{s_T}^2(x) \approx \sum_k (\sigma_{s_T}^{(k)})^2 (u_{(k)}(x))^2 \tag{2.4}$$

Calculation of quantities such as $\sigma_{s_T}^{(k)}$ includes model selection error and is given in the Appendix E. In regard of errors, Zhang et al. (2002b) found that the variability of the high water line at Duck, North Carolina, is significantly lower during summer than in other seasons. To test for an effect on our results we grouped residuals (predicted position from a model average with no seasonal function, minus the data) by seasons and tested for differences in mean and variance, finding no significant difference at the 95% level of confidence. We also re-ran our computations using the seasonal uncertainties from our residuals and found that our results did not change in any significant way. Seasonal variation of uncertainty would probably have affected our analysis more if the data set had fewer surveys.

2.4 Results

Figure 2.2 shows the analysis of shoreline data from Assateague Island, MD. Figure 2.2a is a 2D perspective plot of the original data, and Fig. 2.2b is the complete model including all modes. Fig. 2.2c shows the transient portion of the storm, and it can be seen that recovery is rapid, almost within 2 years for all portions of the beach. Fig. 2.2d shows the persistent component of the storm, which is lower in amplitude than the transient component, i.e., it does not account for as much of the initial shoreline displacement as the transient part of the model. Areas of the largest persistent shoreline change correlate roughly with areas of shoreline where the island was overwashed by the storm 5–8 km south of the inlet. Fig. 2.2e shows the modeled nourishment associated with the replaced onshore berm.

The first six modes have more than 99% of the data variance, and the temporal coefficients of the remaining modes are best modeled by noise. The first mode has 90.7% of the data variance, the second mode 5.0% and the third mode 1.9%. (See Appendix C for a table of modal contributions.) The temporal coefficient of the first mode is shown in Fig. 2.2g, and the temporal coefficients of modes 2 and 3 are given in the Appendix B. The first coefficient shows a strong storm signature with obvious transient and persistent components, and it is not surprising that the best model, i.e., the model with the largest posterior probability, is the model with rate, transient and persistent storm components. The probability-weighted average model, incorporating all possible models with likelihoods based on IC values, shows virtually no rate but a rapidly recovering transient storm component as well as a persistent component. There is also a small perturbation as a result of nourishment. The best model for the second mode coefficient (Appendix A) has rate, transient storm, and nourishment. The best model for the third mode coefficient has no rate, but a transient storm component and a larger nourishment term.

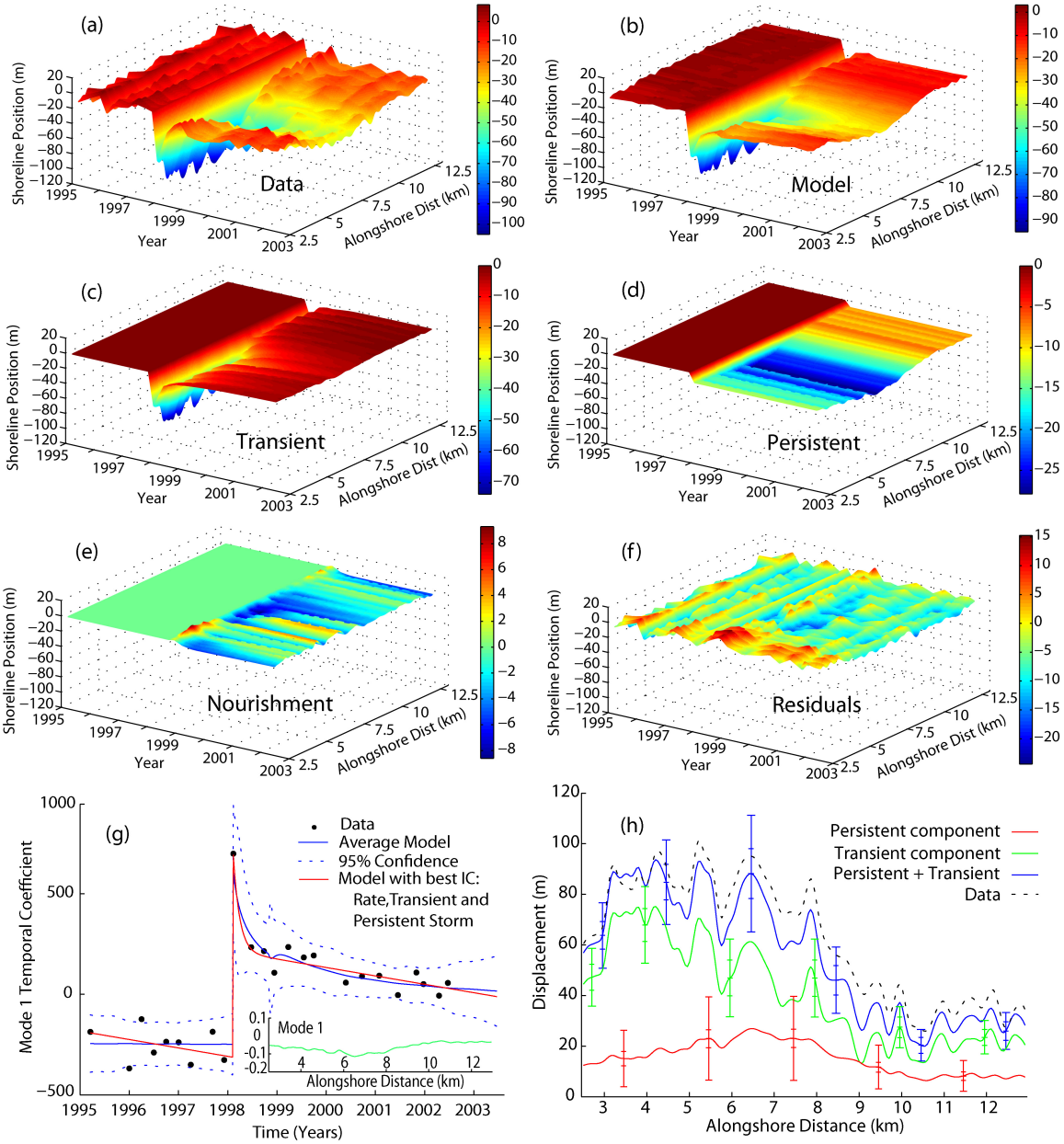

Figure 2.2 (a) Shoreline data from Assateague Island, MD. (b) Probability-weighted average model. (c) Transient component of storm related shoreline change. (d) Persistent component of storm-related shoreline change. (e) Nourishment component of model (see text). (f) Residuals = data – model prediction. (g) Temporal coefficient of the first shoreline data mode (filled circles), with best model (red) and probability-weighted average model (blue). (h) Transient and persistent parts of the storm; the transient part is evaluated at the time of the first post-storm survey for comparison with data. The dotted line (data) is the first post-storm survey minus the average of pre-storm surveys. On the error bars, the inner ticks are the standard error of the model-average computed using the method of paper 1, and the outer ticks include model selection error—see Appendix E for details.

Figure 2.2h shows shoreline displacement at the first survey after the storm (February 11, 1998). The black dashed line is the actual horizontal landward change in shoreline position seen in the data. The blue line is the model displacement due to the storm. The green and red lines show the transient and persistent shoreline change due to the storm respectively.

2.5 Discussion and Conclusions

The Assateague Island data suggest that storm-induced shoreline change can be modeled as the sum of a transient component that is recovered in a few years and a component that persists until sediment is mobilized by a subsequent storm. There is thus a suggestion that long-term shoreline change can be grossly modeled as the cumulative sum of persistent components from storms. Unfortunately, most historical shoreline data sets do not have the time resolution necessary to resolve the transient and persistent components, and it is probably better to model such data with a gradual trend (rate term) plus a sum of transients from the larger storms, as in paper 1. Still, a transient-persistent analysis may be useful in shoreline management. For example, in areas where multi-decade data are not available, a transient-persistent analysis of recent, temporally dense data containing a storm might be used to generate a very coarse estimate of long-term rate as the persistent component from the storm divided by the expected time interval between such storms.

2.6 Appendix A. Model Probabilities

The posterior probability of a model is proportional to the product of its likelihood and prior probability. As we give all models with non-zero prior the same prior probability, the model with the largest likelihood has the largest posterior probability; this is the model with the lowest IC score.

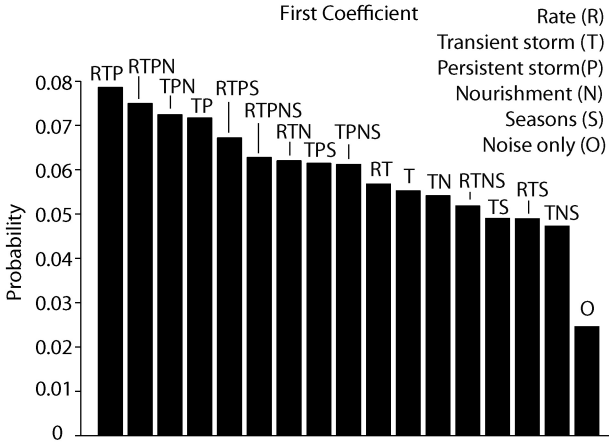

Figure 2.3 Posterior probabilities of models for the temporal coefficient of mode 1.

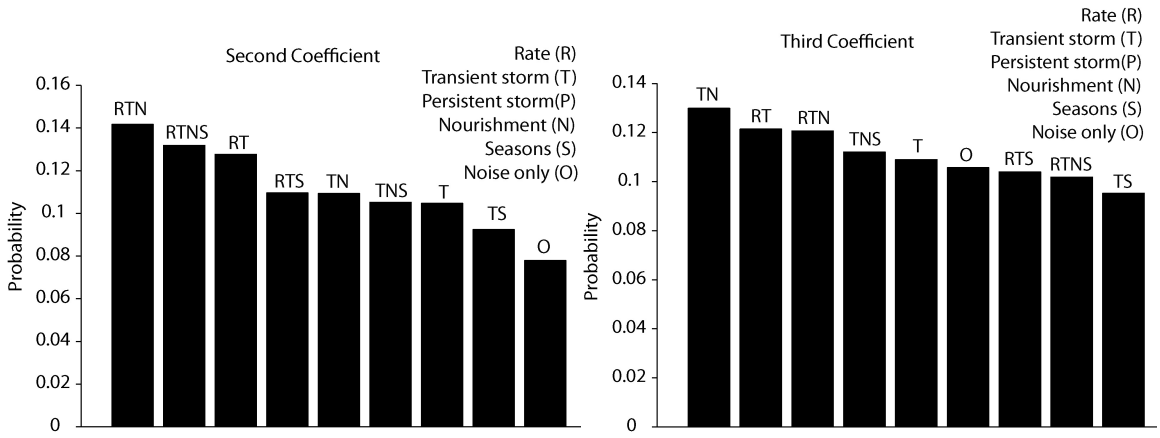

Figure 2.4 Posterior probabilities of models for the temporal coefficient of modes 2 and mode 3. Models assigned zero prior probability (see main text) are not displayed.

2.7 Appendix B. Temporal Coefficients of Modes 2 and 3.

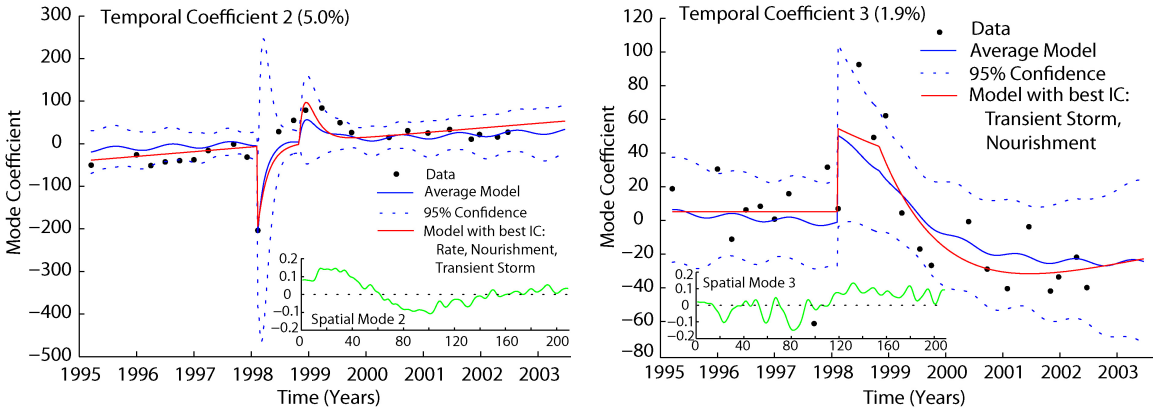

Figure 2.5 Left panel: mode 2. Right panel: mode 3. The red lines are the models with the lowest IC score (largest likelihood, largest posterior probability). The blue lines are the probability-weighted average models.

2.8 Appendix C. Modal Contributions

Table 2.1 Percent data variance contribution of each mode and cumulative percent.

Key: R-rate, T-transient storm, P-persistent storm, N-nourishment, S-seasons.

Mode	Data variance Contribution (%)	Cumulative Contribution (%)	Best-fit model
1	90.67	90.67	R,T,P
2	5.01	95.68	R,T,N
3	1.92	97.61	T,N
4	0.69	98.30	Noise
5	0.45	98.75	R,T,N
6	0.26	99.01	R,T,N
7	0.21	99.23	Noise
8	0.15	99.38	Noise
9	0.11	99.49	Noise
10	0.09	99.58	Noise
11	0.09	99.67	Noise
12	0.07	99.74	Noise
13	0.05	99.79	Noise
14	0.04	99.83	Noise
15	0.04	99.87	Noise
16	0.03	99.90	Noise
17	0.07	99.93	Noise
18	0.02	99.95	Noise
19	0.02	99.97	Noise
20	0.01	99.98	Noise
21	0.01	99.99	Noise
22	0.01	100	Noise
23	0	100	Noise
24	0	100	Noise

2.9 Appendix D. Prediction Error

Figure 2.6 shows the time averaged prediction error covariance matrix

$$\frac{1}{24}\sum_{k=1}^{24}\left[y_p(x_i,t_k)-y(x_i,t_k)\right]\left[y_p(x_j,t_k)-y(x_j,t_k)\right],$$

in which y is the data and y_p is the prediction from modeling. If our model for noise and signal corresponded exactly to reality, this matrix would be diagonal (a bright line along the diagonal of the figure with darkness off the diagonal), meaning that the prediction error at any alongshore location is uncorrelated with the error at any other alongshore location.

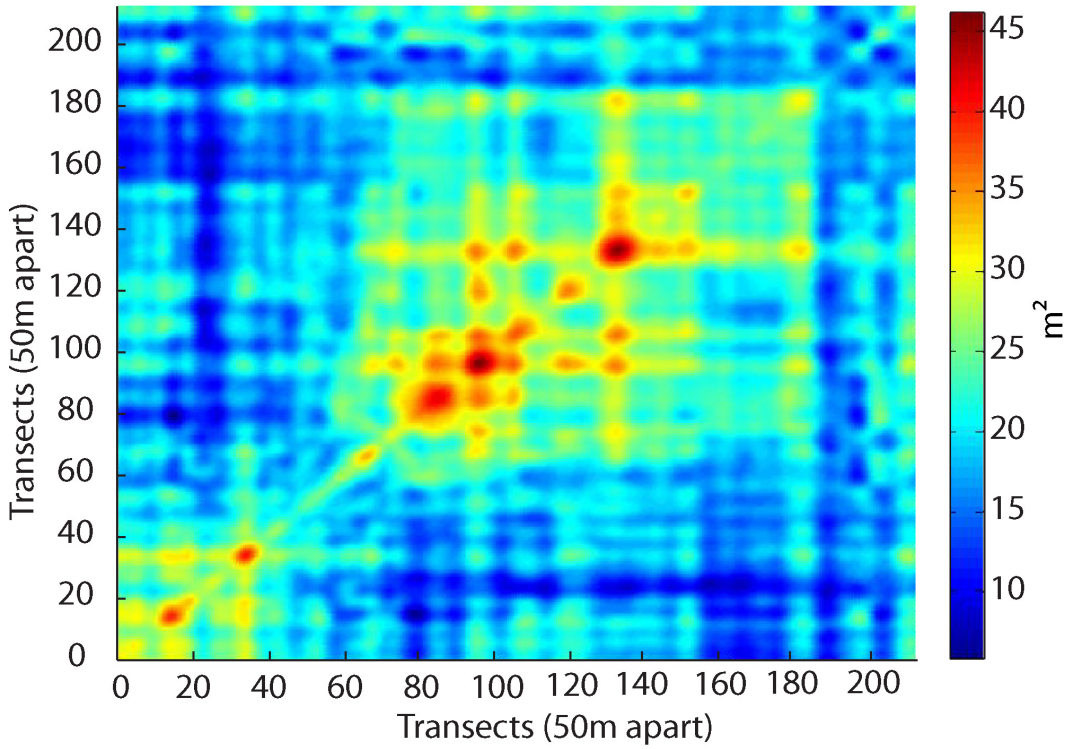

Figure 2.6 Time averaged prediction error covariance matrix.

2.10 Appendix E. Error Estimation

In the Auxiliary Material for Frazer et al. (2009b) (paper 1) there is a Section D, entitled "Variance of a model-averaged estimator," in which we derived an expression (equation D9) for the variance of a model-averaged estimate. Briefly, for any quantity of interest ϕ we calculated the variance, $\sigma^2_{\hat{\phi}}$, of the model-averaged estimate $\hat{\phi} = \sum_j p_j \phi_j$ in which ϕ_j is the estimate from the j^{th} model, and p_j is the posterior probability of the j^{th} model. (The posterior probability of a model is gotten by combining the prior probability of that model with the model likelihood computed from the data.) We calculated the variance by first calculating the variation $\delta\hat{\phi}$ with respect to a variation of the data δy, not neglecting the variation δp_j. The standard error indicated by the inner ticks on Figure 2.2(h) of this paper is the square root of that variance. That method of estimating errors was used in this paper and in paper 1 because it is analogous to the standard method of estimating error for any particular model and is thus comparable to most error estimates in the literature.

In this paper we also calculate model selection error (Buckland et al. 1997), which tends to be larger and is thus more conservative. We derive model selection error as follows by using probability density functions (pdf). Let $p(\phi \mid y)$ be the pdf of ϕ given data y. Then we may write

$$p(\phi \mid y) = \sum_i p(\phi \mid M_i, y) p_i \tag{2.E1}$$

in which $p(\phi \mid M_i, y)$ is the pdf of ϕ conditioned on M_i being the correct model. The expected value of ϕ for model M_i is thus

$$\phi_i = \int \phi p(\phi \mid M_i, y) d\phi \tag{2.E2}$$

and its variance, needed below, is

$$\begin{aligned}\sigma_{\phi_i}^2 &= \int (\phi-\phi_i)^2 p(\phi \mid M_i, y) d\phi \\ &= \int (\phi^2 - 2\phi\phi_i + \phi_i^2) p(\phi \mid M_i, y) d\phi \\ &= \left\langle \phi^2 \right\rangle_i - \phi_i^2 .\end{aligned} \tag{2.E3}$$

The model-averaged estimate of ϕ is

$$\begin{aligned}\hat{\phi} &= \int \phi\, p(\phi \mid y) d\phi \\ &= \int \phi \sum_i p(\phi \mid M_i, y) p_i d\phi \\ &= \sum_i p_i \int \phi\, p(\phi \mid M_i, y) d\phi \\ &= \sum_i p_i\, \phi_i\end{aligned} \tag{2.E4}$$

and the variance that includes model selection error is

$$\begin{aligned}\sigma_{\hat{\phi}}^2 &= \int (\phi-\hat{\phi})^2 p(\phi \mid y) d\phi \\ &= \int (\phi-\hat{\phi})^2 \sum_i p(\phi \mid M_i, y) p_i d\phi \\ &= \sum_i p_i \int (\phi-\hat{\phi})^2 p(\phi \mid M_i, y) d\phi \\ &= \sum_i p_i \int (\phi^2 - 2\phi\hat{\phi} + \hat{\phi}^2) p(\phi \mid M_i, y) d\phi \\ &= \sum_i p_i \left\{ \left\langle \phi^2 \right\rangle_i - 2\phi_i\hat{\phi} + \hat{\phi}^2 \right\} \\ &= \sum_i p_i \left\langle \phi^2 \right\rangle_i - 2\hat{\phi} \sum_i p_i \phi_i + \hat{\phi}^2 \sum_i p_i \\ &= \sum_i p_i \left\langle \phi^2 \right\rangle_i - 2\hat{\phi}^2 + \hat{\phi}^2 \\ &= \sum_i p_i \left\langle \phi^2 \right\rangle_i - \hat{\phi}^2 \\ &= \sum_i p_i \sigma_{\phi_i}^2 + \sum_i p_i \phi_i^2 - \hat{\phi}^2 .\end{aligned} \tag{2.E5}$$

The square root of this variance is indicated by the outer ticks on the error bars of Figure 2.2h of the paper.

Chapter 3

TOWARD PARSIMONY IN SHORELINE CHANGE PREDICTION: B-SPLINES AND NOISE HANDLING

In review for publication in the *Journal of Coastal Research* as Anderson, T.R. and L. N. Frazer, Toward parsimony in shoreline change prediction (III): B-splines and noise handling.

Abstract – The traditional single-transect method for predicting long-term shoreline change uses far more parameters than necessary because it assumes that erosion/accretion (change) rates at adjacent alongshore positions (transects) are independent. Such over-fitting can cause poor predictions of future shoreline location, so recent work has modeled change rates as linear sums of polynomials, or linear sums of principal components. Here we introduce an alternative method that uses linear sums of B-splines. As in earlier work, an information criterion is used to identify the optimal number of basis functions. The local nature of B-spline models makes them less susceptible to Gibbs effect than polynomial models, and their smoothness makes them more robust to noise than principal components regression. We also compare three noise-handling techniques by examining their effects on the posterior probability density functions of rates. We find that noise handling affects both predicted rate and its uncertainty, and that correlated noise is best addressed by iteratively constructing a full covariance matrix from data residuals. We illustrate our procedure using shoreline data from Assateague Island and Ocean City, Maryland and a synthetic dataset.

3.1 Introduction

Quantifying trends in shoreline position is necessary for managing natural coastal environments and human communities. Models for shoreline change range from simple empirical relations, such as the model of this paper, to physics-based models. Empirical models gain parsimony (require fewer parameters) by ignoring waves, currents and bathymetry. Physics-based forward modeling systems, such as Delft3D, developed by Delft Hydraulics (Roelvink and van Banning, 1994), include those phenomena, but must contend with limited availability of required data (*e.g.*, wind, wave, high resolution bathymetry) and large propagated errors. Semi-empirical models (e.g. Miller and Dean, 2004; Yates, Guza, and O'Reilly, 2009; Davidson, Splinter, and Turner, 2013) must also contend with limited data availability and propagated errors, but to a lesser extent. Recently, Maged *et al*. (2011) incorporated wave spectra from airborne synthetic aperture radar (SAR) data into a long-term shoreline change model. Technical innovations such as GPS (e.g. Dail, Merrifield, and Bevis, 2000), LiDAR (e.g. Stockdon *et al*., 2002), and video imagery (e.g. Plant *et al*., 2007; Becker *et al*., 2007) are greatly improving the quality and quantity of shoreline data, but available time series are not long enough to reveal trends over decades to centuries. In order to extract such trends, we are still largely dependent on historical shoreline surveys.

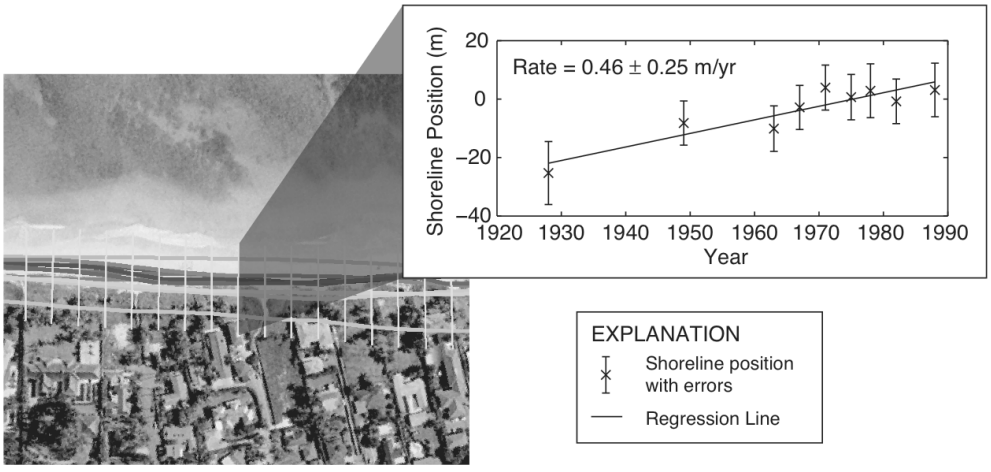

Figure 3.1 Weighted least squares linear regression of shoreline data along a single transect.

One of the simplest and most widely used methods of estimating long-term shoreline change is the single-transect (ST) method (Figure 3.1). It is an empirical method in which equally spaced cross-shore transects (*e.g*., 20 to 50 m apart) are analyzed independently. The mathematical model for each transect is usually $y = rt + b$ in which y is shoreline position in the cross-shore (i.e., landward-seaward) direction, r is the rate of erosion or accretion, and b is an intercept that depends on the baseline relative to which y is measured. The data consist of historical shorelines at each transect (Honeycutt, Crowell, and Douglas, 2001; Fletcher *et al.,* 2003; Genz *et al*., 2007; Thieler *et al.,* 2009; etc.) The ST method is attractive because it is simple to understand and easy to implement, especially over large spatial regions. Also, it provides shoreline change statistics at a high spatial frequency along the shoreline. However, it ignores correlation between the rates at different transects, and thus creates a model shoreline that can have large excursions that increase unrealistically as the model prediction is extended further into the future. Moreover, for shorelines in which rates change little from transect to transect, the ST method is highly unparsimonious; it has far more parameters than are independent, as indicated by the wide autocorrelation of ST rate parameters along 40 km of shoreline centered on Ocean City Inlet, Maryland, shown in Figure 3.2. Here, we focus on long-term (decades) and large-scale (kilometers) shoreline trends, attempting to

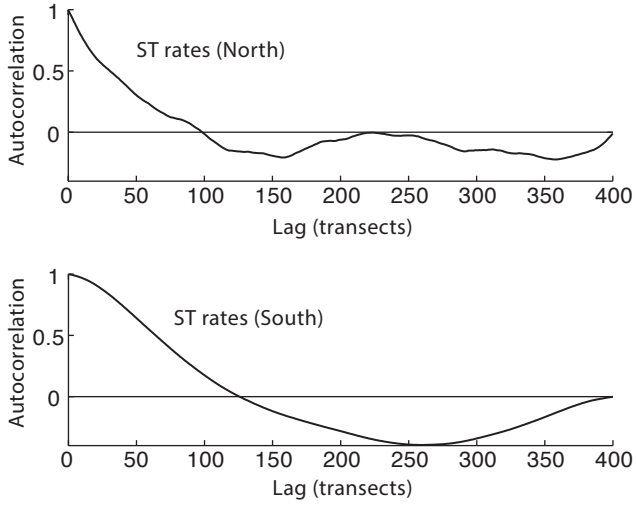

Figure 3.2 Autocorrelation of rates calculated by the ST method for the north (top) and south (bottom) study areas.

improve on the ST method. Frazer, Genz, and Fletcher (2009), and Genz, Frazer, and Fletcher (2009) also addressed the over-fitting issue of ST, and the procedure of this paper extends their work by the use of different basis functions and by an improved treatment of noise.

Frazer, Genz, and Fletcher (2009) examined three types of basis functions: polynomials, eigenbeaches (principal components), and piece-wise constant "bins." Examples of Legendre polynomials and eigenbeaches are shown in Figure 3.3d,e. Polynomials are subject to Gibbs effect (Bracewell, 2000) when modeling shorelines with

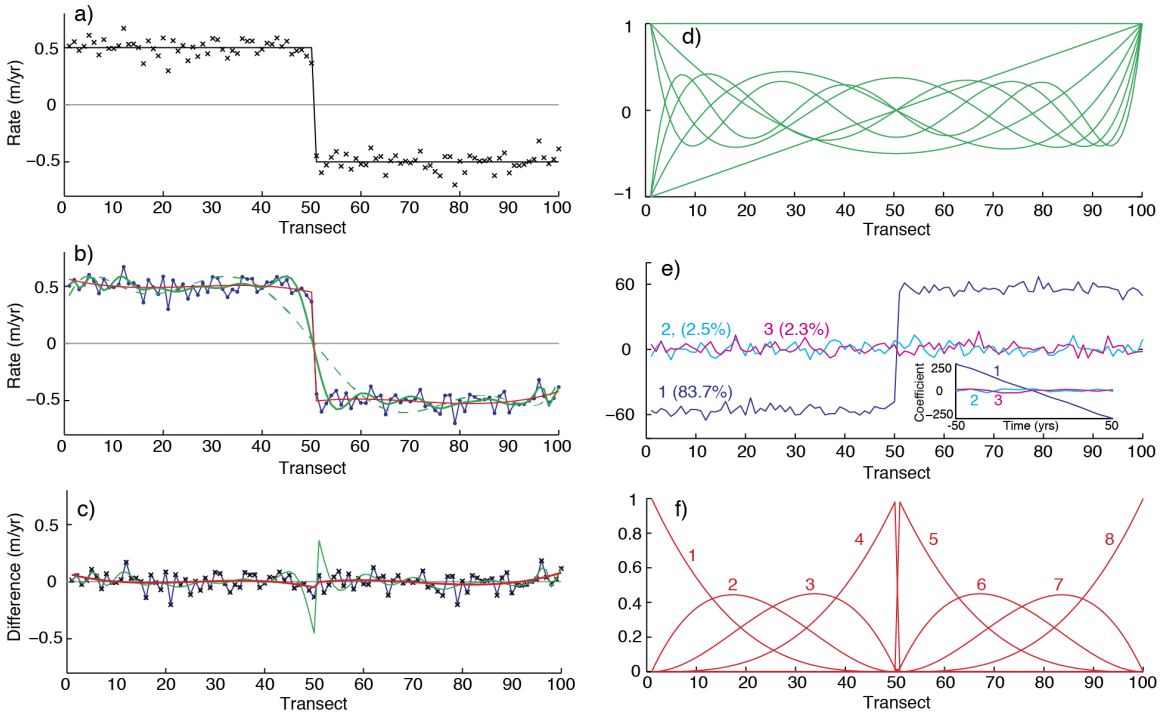

Figure 3.3 Results from modeling a synthetic data set consisting of eleven shorelines ten years apart. Additive noise in the data is from $N(0, (7.5\text{m})^2)$. (a) Solid line shows the true rates, constant on each side of a jump between transects 50 and 51; black crosses are the rates estimated by ST. (b) Rates estimated using 30 Legendre polynomials (green, solid), eight Legendre polynomials (green, dashed), eight B-splines (red), and one eigenbeach (blue). (c) Errors in rate [estimated - true] for ST (black crosses), 30 Legendre polynomials (green), 8 splines (red) and one eigenbeach (blue). (d) The Legendre polynomials. (e) The three most dominant eigenbeaches with percent variance. (f) The eight B-splines. Note Gibbs effect and noise in (b) and (c). The location of the rate jump was assumed known prior to modeling.

sudden alongshore variations in rate (Figure 3.3b,c). Eigenbeaches automatically does away with Gibbs effect by using principal components of the shorelines themselves as the basis functions, but those basis functions are contaminated by process and measurement noise in the data (Figure 3.3b,c).

In this paper we model cross-shore rate with a cubic spline defined by its value at alongshore locations called "knots" (de Boor, 1978). Splines avoid Gibbs effect, if extra knots are added at alongshore locations where rate changes rapidly, and they are not contaminated by noise (Figure 3.3b,c). We use B-splines (de Boor, 1978) as basis functions for the spline because of their simplicity. Following the methodology in Frazer, Genz, and Fletcher (2009), the parameters of our model are the coefficients of the basis functions; least squares regression is used to estimate those coefficients and an information criterion (IC) is used to select the optimal number of basis functions. We improve on the noise methodology of Frazer, Genz, and Fletcher (2009) by iteratively estimating the spatial covariance of the data noise.

We illustrate the new procedures using barrier island shoreline data from Assateague Island and Ocean City, Maryland. We examine 40 km of shoreline centered on Ocean City (OC) inlet, as seen in Figure 3.4a. Inlet jetties disrupt alongshore sediment transport from the north, resulting in episodes of sand bypassing (Kraus, 2000; Schupp, Bass, and Grosskopf, 2007). The coast is mostly developed north of OC Inlet, and is undeveloped south of the Inlet where Assateague Island National Park is located.

3.2 Methodology

3.2.1 Historical Shoreline Data

Our data consist of 12 historical shoreline surveys (1849–2000) obtained online as GIS shape files from the United States Geological Survey (USGS) National Assessment of Shoreline Change for the New England and Mid-Atlantic Coasts (Himmelstoss *et al*., 2010). Table 3.1 lists the range of years for USGS shorelines derived from different data sources, and their average uncertainty values calculated from

Table 3.1 Shorelines used in the study. (HWL – high water line; MHW – mean high water; # Shore – number of shorelines; Unc. – average uncertainty from quantifiable sources)

Date	Source	# Shore	Indicator	Unc. (m)
1849-1942	T-sheet	6	HWL	10.8
1962-1976	T-sheet	2	HWL	5.1
1980-1989	Air photo	3	HWL	3.2
2000	LiDAR	1	MHW	5.3

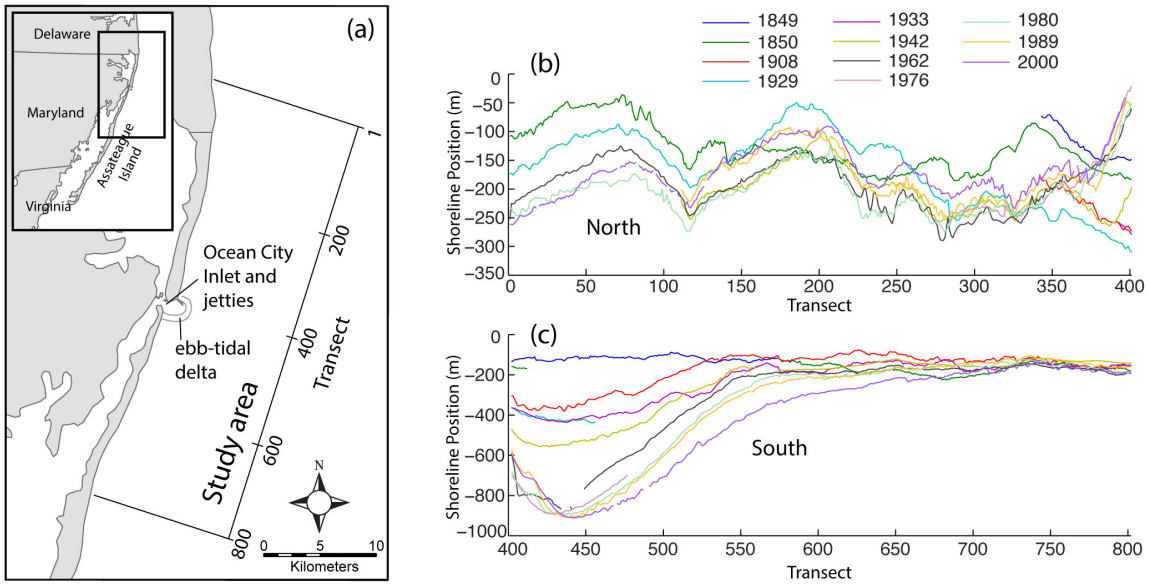

Figure 3.4 (a) Study area and (b-c) shoreline data relative to offshore baseline for sections north and south of Ocean City Inlet. Transects are spaced 50 meters apart.

quantifiable sources of error (Hapke *et al*., 2010). Shorelines are extracted from T-sheets and air photos by digitally identifying the high water line (HWL) from georeferenced maps and photos. Mean high water (MHW) indicates shoreline position in LiDAR (light detection and ranging) derived shorelines. Details of data extraction and error quantification procedures are available in Hapke *et al*. (2010). To correct for the horizontal difference between the MHW and HWL, we shift the LiDAR shoreline landward by the proxy-datum bias values in Himmelstoss *et al*. (2010). The baseline, a

proxy for a mean shoreline shape, is also obtained from the USGS online. We cast cross-shore transects perpendicular to the baseline, and record the distance between each shoreline and the baseline at each transect using the Digital Shoreline Analysis System (DSAS) Version 4.2 (Thieler *et al*., 2009). There is a gap in the shoreline where OC inlet cuts through the barrier island, so we model the 20 km sections north and south of the inlet separately (Figure 3.4b,c).

3.2.2 Summary of Procedure

Spline models are distinguished by the number and location of their knots. For the Assateague data analyzed here, it is sufficient to count basis functions because we use knots that are regularly spaced, except for coincident knots at endpoints. For each model, we create a spline matrix; each column of the matrix is a B-spline evaluated at each transect. We use the matrix in a generalized least squares regression model that includes iterative estimation of the data covariance matrix. From the residuals and the number of model parameters, including the parameters required for covariance, we calculate an information criterion (IC) statistic. We take the model with the lowest IC to be the best model, and we use it to predict shoreline positions at specified times within the study area. We also generate the posterior probability density function for rate at each transect.

3.2.3 B-splines as Basis Functions

A cubic spline is a linear sum of cubic B-splines (de Boor, 1978). Each B-spline is defined everywhere, but it vanishes outside an interval that spans five knots in a prescribed knot sequence. Its first and second derivatives vanish at the endpoints of that interval, so each B-spline has a continuous second derivative, and thus the linear sum also has a continuous second derivative. Figure 3.5a shows 11 B-splines (solid lines) generated from a knot sequence consisting of 15 knots: 9 evenly spaced knots (dashed lines), 50 transects apart, between transects 0 and 400, with 4 knots at each endpoint. (The three extra knots at each endpoint cause the spline to vanish outside the interval.) The heavy line in Fig. 3.5a is the B-spline with support from transect 50 to transect 250.

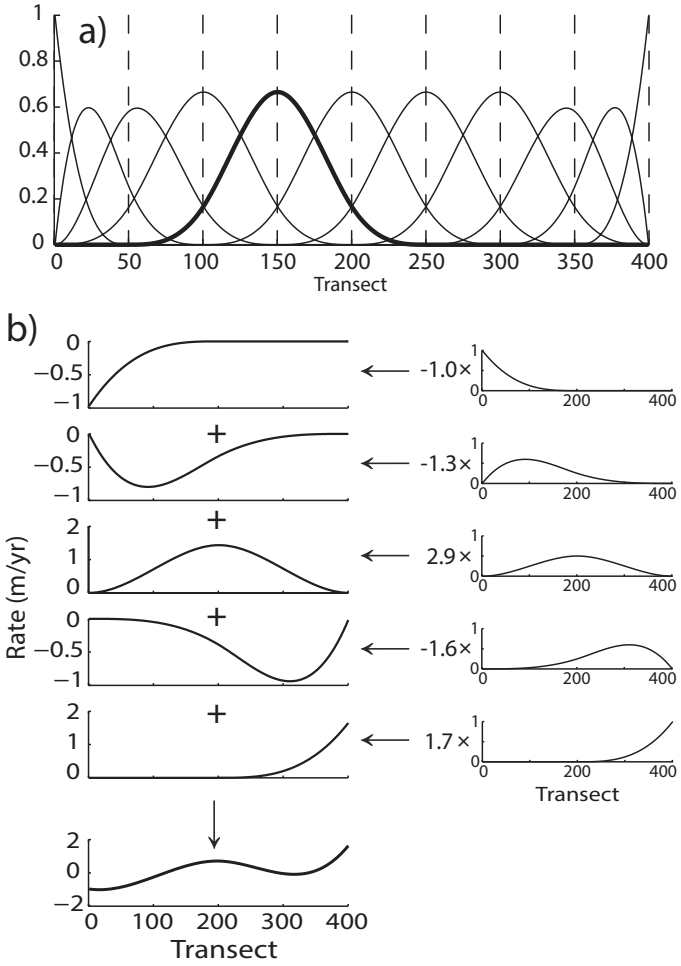

Figure 3.5 (a) Cubic B-splines. (b) Five B-splines multiplied by coefficients (right column) form a linear combination of B-splines to create a spline function (left column at bottom).

The shape of the B-spline shows how it acts as a local weighted average. The B-splines near the ends have smaller apertures than the interior B-splines because of the duplicate knots at the ends. Although the B-splines in the figure were generated using evenly spaced interior knots, the spacing can be allowed to vary if there is compelling *a priori* information that warrants it. For example, if there were a geologic or structural feature, such as a stream mouth or pier in the middle of an otherwise uniform sandy shoreline, one could add additional knots in the vicinity of the feature, allowing more basis functions to capture the higher spatial frequencies, as in Figure 3.3f.

The number of knots at a knot location determines the smoothness at that point. More knots allow less continuity. For example, if there are two knots at the same location, the resulting spline will have a continuous first derivative at that point, but not necessarily a continuous second derivative. Four knots at the same location allow a zeroth-order discontinuity there.

Suppose for a moment that we are modeling only rate. We use B-splines to create a spline matrix V which linearly transforms a short column vector of spline coefficients $\tilde{m}$ to a much longer $I \times 1$ column vector of rates r, with one rate for each transect. (The tilde notation is called for because, in order to be consistent with single-transect, we refer to r as the rate model, and below we will include rates and intercepts in a model vector m.) Each column of the spline matrix is a B-spline generated using the recursion relation of de Boor (1978, p. 131), and the modeled rate at transect $1 \le i \le I$ is

$$r_i = V_{i,}\tilde{m}\,, \tag{3.1}$$

in which $V_{i,}$ denotes the i^{th} row of V.

3.2.4 Shoreline Change Model

Here we apply B-splines to the simple, time-linear model $y = rt + b$. Let $y(x_i, t_j)$ represent the cross-shore shoreline position at alongshore location x_i and time t_j, for $i = 1:I$ transects and $j = 1:J$ shoreline surveys. Our shoreline equation is $y(x_i, t_j) = b_i + (t_j - \bar{t})r_i + n_{ij}$, where r_i and b_i are the rate and intercept, respectively, at the i^{th} transect; n_{ij} is the noise for shoreline position $y(x_i, t_j)$; and $\bar{t}$ is the mean of shoreline survey years. Shifting the time origin to $\bar{t}$ helps condition the system matrix for regression, without affecting rate parameters.

Frazer, Genz, and Fletcher (2009) and Genz, Frazer, and Fletcher (2009) used an additional acceleration term in some of their models. Frazer, Anderson, and Fletcher (2009) and Anderson, Frazer, and Fletcher (2010) included a storm function in the time component of their shoreline model. We do not include acceleration or storms here

because preliminary testing showed no significant acceleration or storm signals in this dataset. However, both storms and acceleration terms may also be expressed as linear combinations of spline basis functions.

Here we use splines to model the alongshore variation in intercept as well as rate, so we construct the matrix V as a block-diagonal matrix with two blocks of splines, one for rates, and one for intercepts. The two blocks have different numbers of columns if the number of splines needed for intercept differs from the number needed for rate. The vector $\tilde{m}$ contains the spline coefficients for both rate and intercept. Combining the time-linear model with spline modeling of rate and intercept gives

$$\begin{aligned} y(x_i,t_j) &= b_i + (t_j - \overline{t})r_i + n_{ij} \\ &= V_{i,}\tilde{m} + (t_j - \overline{t})V_{I+i,}\tilde{m} + n_{ij} \end{aligned}. \tag{3.2}$$

3.2.5 Basic GLS

Our generalized least squares (GLS) model is similar to that given in Frazer, Genz, and Fletcher (2009), but is presented here in a slightly different way so that the matrix of spline basis functions is explicit. In the following section, and in the appendix, we present our method for handling spatially correlated noise. The GLS model for the single-transect method is written as

$$d = Gm + \eta, \tag{3.3}$$

in which $N = I \times J$ is the number of data points, d is an $N \times 1$ vector of shoreline positions relative to the baseline; G is an $N \times 2I$ system matrix; m is a $2I \times 1$ vector of parameters (I rates and I intercepts); η is an $N \times 1$ vector of noise with zero mean and covariance matrix C_{dd}. To reduce the number of parameters in the model, we set

$$m = V\tilde{m}, \tag{3.4}$$

in which V is the $2I \times M$ spline matrix described above, and $\tilde{m}$ is an $M \times 1$ vector of spline coefficients with $M << 2I$. Substituting (3.4) into (3.3), and introducing the notation $\tilde{G} = GV$, gives the familiar GLS form $d = \tilde{G}\tilde{m} + \eta$, still with noise covariance C_{dd}.

In basic GLS there is only one noise parameter. One begins with an *a priori* estimate of the covariance $\tilde{C}_{dd}$, then scales it using a scaling factor that maximizes the fit of the model to the data. The basic GLS estimator of $\tilde{m}$ is the usual relation

$$\hat{\tilde{m}} = (\tilde{G}^T \tilde{C}_{dd}^{-1} \tilde{G})^{-1} \tilde{G}^T \tilde{C}_{dd}^{-1} d \quad , \tag{3.5}$$

with parameter covariance matrix (*e.g.*, Menke 2012)

$$\hat{C}_{\tilde{m}\tilde{m}} = (\tilde{G}^T \hat{C}_{dd}^{-1} \tilde{G})^{-1}, \tag{3.6}$$

in which the estimated data covariance $\hat{C}_{dd} = \hat{\alpha} \tilde{C}_{dd}$ contains the best-estimate constant of proportionality

$$\hat{\alpha} = (N - M)^{-1} (d - \tilde{G}\hat{\tilde{m}})^T \tilde{C}_{dd}^{-1} (d - \tilde{G}\hat{\tilde{m}}). \tag{3.7}$$

The estimated parameter vector $\hat{m}$ containing rates and intercepts at each transect, is now

$$\hat{m} = V\hat{\tilde{m}} \tag{3.8}$$

with associated covariance matrix,

$$\hat{C}_{mm} = V\hat{C}_{\tilde{m}\tilde{m}} V^T. \tag{3.9}$$

Shoreline positions are predicted using the best-fit shoreline model. The predicted shoreline position $\hat{y}(x_i, t)$ at desired time *t* and transect location x_i is

$$\hat{y}(x_i,t) = q_i^T V\hat{\tilde{m}} = q_i^T \hat{m} \ , \tag{3.10}$$

in which $q_i = q_i(t)$ is a $2I \times 1$ column vector, which we refer to as a prediction kernel. The variance of the prediction is

$$\hat{\sigma}^2(x_i,t) = q_i^T V\hat{C}_{\tilde{m}\tilde{m}}V^T q_i \ = q_i^T \hat{C}_{mm} q_i, \tag{3.11}$$

where $\hat{C}_{\tilde{m}\tilde{m}}$ (Eq. 3.6) is the parameter covariance matrix, and $\hat{C}_{mm}$ (Eq. 3.9) is the covariance matrix for modeled rates and intercepts (Eq. 3.8). Confidence intervals are calculated by multiplying the square root of the above variance by the Student's t-statistic $t_{\nu,1-\varepsilon/2}$ where ν is the number of independent observations minus the number of parameters used to model the data, and $100(1-\varepsilon)$ is the percent confidence level.

3.2.6 Data Covariance Estimation

Ideally, the GLS model outlined in the previous section would contain a data covariance matrix C_{dd} that is known. In reality, the covariance matrix is rarely known *a priori*, even to within a scaling factor, and must be estimated. In the problem of this paper, the structure of the covariance matrix may be simplified by noting that shoreline surveys are typically dense in space but ~10 years apart in time. Therefore it is a good approximation to assume that data errors are correlated in the alongshore direction but weakly correlated in time.

Frazer, Genz, and Fletcher (2009) and Genz, Frazer, and Fletcher (2009) addressed alongshore correlation by fitting the data residuals from the ST method to a decaying exponential, then using that exponential to generate the rows of the covariance matrix. Another method for handling correlated noise is to inflate a diagonal covariance matrix by using $N^* - M$ instead of $N - M$ in equation (7), where N^* is the effective number of independent observations (Bayley and Hammersely, 1946). That is essentially

what others (e.g. Hapke *et al*., 2010; Kane *et al*., 2012) have done to estimate the variance in the average of correlated rates; we refer to that method as W_{N*}.

Here, in what we refer to as the C_{full} method, we estimate the full covariance matrix for each spline model by an iterative process in which each successive covariance matrix is calculated from the residuals of the previous iteration (*e.g*., Dosso, Neilsen, and Wilmut, 2006). Below, in the context of the spline model, we compare differences in the posterior probability density function (pdf) for all three methods of noise estimation: uncorrelated (W_{diag}), inflated variance based on an effective number of data (W_{N*}), and full covariance (C_{full}).

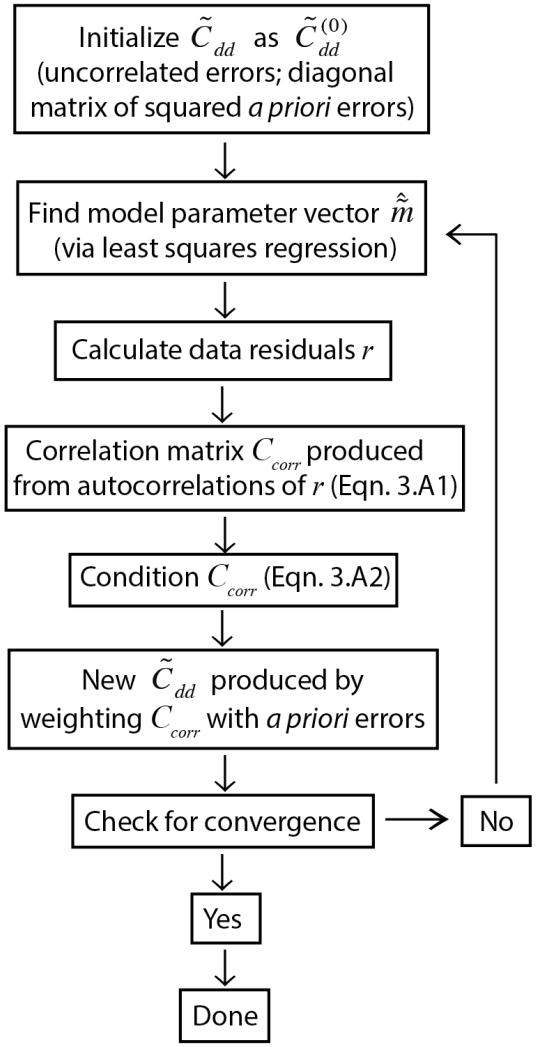

Figure 3.6 Flowchart for estimating the unscaled covariance matrix $\tilde{C}_{dd}$ (before scaling by $\hat{\alpha}$).

Each of the noise handling methods incorporates in some way the shoreline position uncertainties provided by the USGS (Himmelstoss *et al*., 2010). Let $\tilde{C}_{dd}^{(0)} = diag(w_{ij}{}^2)$ be the diagonal matrix containing USGS uncertainty estimates w_{ij} at locations *i* and times *j*. In the uncorrelated noise method (W_{diag}) we use $\tilde{C}_{dd}^{(0)}$ as the *a priori* estimate of $\tilde{C}_{dd}$. In the noise estimation method (W_{N*}) we also use $\tilde{C}_{dd}^{(0)}$ as the *a priori* estimate $\tilde{C}_{dd}$, but we increase the constant of proportionality $\hat{\alpha}$ by substituting the effective number of independent data *N** for the actual number of data *N* in equation (3.7). In the full-covariance (C_{full}) method we iteratively construct $\tilde{C}_{dd}$ from the data according to the flowchart in Figure 3.6, and then multiply by the best-estimate constant of proportionality $\hat{\alpha}$. We limit the number of noise parameters associated with the scaled autocorrelation by assuming that it is independent of time and alongshore distance. Details of the flowchart procedure are given in Appendix A.

In our study area, iteration for $\tilde{C}_{dd}$ converged for each spline model, but at different rates. Most models essentially converged within two to three iterations, although we used a more conservative stopping criterion for iteration (see Appendix A). Table 3.2 contains the left hand side of the convergence criterion for each iteration of the two best models. The misfit value *LL* (defined as -2 times the logarithm of the likelihood) is also displayed; *LL* decreases in value as model likelihood increases, and it is used in IC calculations. The covariance scaling factor $\hat{\alpha}$ is also shown, since it is used in calculating *LL*, although it is not needed in the iteration for covariance.

To test the goodness of our covariance matrix estimate, we compare the autocorrelation function for raw data residuals $\rho = d - \tilde{G}\tilde{m}$ with the autocorrelation function for standardized residuals defined as $\tilde{\rho} = \hat{C}_{dd}^{-1/2}\rho$. In GLS regression, the standardized residuals are minimized, and the autocorrelation function of the standardized residuals indicates the accuracy of the data covariance matrix estimate. Figure 3.7 shows the autocorrelations of raw residuals (left) and standardized residuals (right) for two survey years. The delta-like autocorrelation of the standardized residuals indicates considerable improvement over the diagonal covariance assumption.

Table 3.2 The decline in *LL* during iteration shows how an improved estimate of the covariance matrix gives a model with higher likelihood. ΔLL is the change in *LL* between successive iterations. $\hat{\alpha}$ is the covariance scaling factor needed to calculate *LL*, but is not used in the iteration process. $\|\cdots\|_1$ is the matrix L_1 norm of the difference in estimated covariance matrices between iterations. The iteration process on the left is for the best model in the north region, comprised of 6 rate and 72 intercept basis functions. The best model in the south region (right) has 10 rate and 62 intercept basis functions. Convergence is essentially complete within two iterations.

	North Section			South Section		
Iteration	$(\Delta LL)/LL_{it-1}$	$\hat{\alpha}$	$\left\|\tilde{C}_{dd}^{(it)}-\tilde{C}_{dd}^{(it-1)}\right\|_1\left\|\tilde{C}_{dd}^{(it-1)}\right\|_1^{-1}$	$(\Delta LL)/LL_{it-}$	$\hat{\alpha}$	$\left\|\tilde{C}_{dd}^{(it)}-\tilde{C}_{dd}^{(it-1)}\right\|_1\left\|\tilde{C}_{dd}^{(it-1)}\right\|_1^{-1}$
0	--	24.2	--	--	46.2	--
1	-8.35×10^{-1}	16.8	7.23×10^{1}	-9.17×10^{-1}	25.9	8.10×10^{1}
2	-2.51×10^{-3}	24.0	2.71×10^{-1}	-3.56×10^{-4}	27.7	1.11×10^{-1}
3	-6.40×10^{-5}	25.2	2.10×10^{-2}	-1.67×10^{-4}	28.1	8.04×10^{-3}
4	-4.78×10^{-6}	25.3	1.73×10^{-3}	2.79×10^{-6}	28.1	8.57×10^{-4}
5	-4.14×10^{-7}	25.3	1.53×10^{-4}	-7.79×10^{-7}	28.1	6.28×10^{-5}
6	-3.61×10^{-8}	25.3	1.37×10^{-5}	2.33×10^{-8}	28.1	5.58×10^{-6}
7	-3.21×10^{-9}	25.3	1.23×10^{-6}	--	--	--

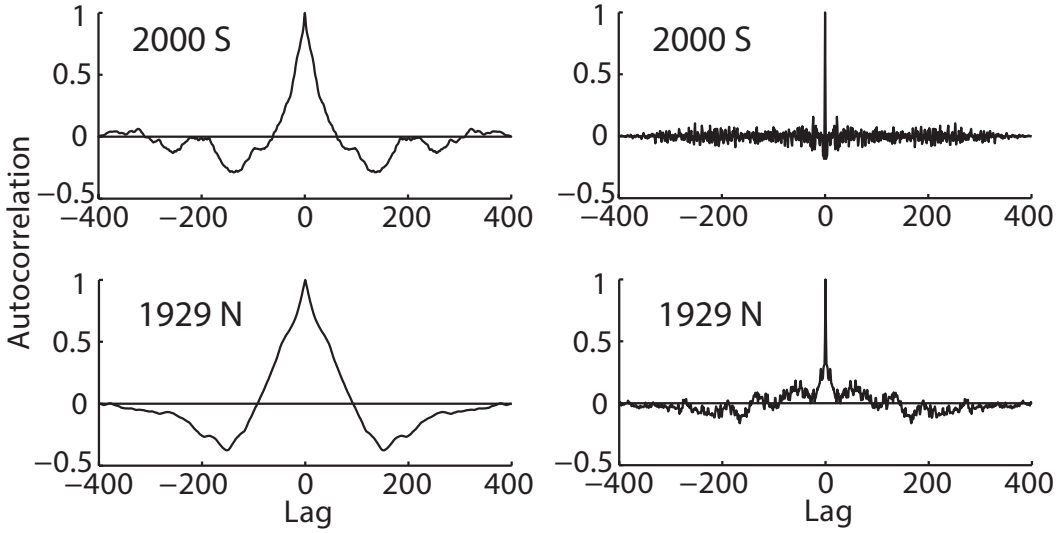

Figure 3.7 Selected autocorrelation functions for raw residuals (left column) and standardized residuals (right column) show the improvement due to a full covariance matrix.

3.2.7 Information Criterion

Within a given family of models, the best model is the one with the minimum information criterion (IC) statistic (score, value). An IC statistic is the sum of two penalty terms: one term, the misfit, increases with the data residuals, and the other term increases with the number of parameters. Increasing the number of parameters reduces the first term and increases the second term. The IC score thus helps prevent one from fitting the noise instead of the data. For further reading on IC use in regression, see McQuarrie and Tsai (1998) or Frazer, Genz, and Fletcher (2009). This paper uses the corrected Akaike information criterion (AICc) (Hurvich and Tsai, 1989; Sugiura, 1978). Our formula for AICc includes additional terms that were unnecessary in Frazer, Genz, and Fletcher (2009) because they were constant across all models. Since our method of estimating the covariance matrix produces matrices with different off-diagonal behavior, we use the more general expression

$$\mathrm{AICc} = \log\left(\left|\hat{C}_{dd}\right|\right) + (N - M) + 2KN/(N - K - 1), \tag{3.12}$$

where $\log(...) + (N - M)$ represents the misfit and $2KN/(N - K - 1)$ penalizes the model based on parameter count. Here K is the number of parameters used in the modeling process; it is the sum of M and the number of parameters used to model variance. Table 3.3 summarizes parameter counts for different methods. For uncorrelated noise (W_{diag} method), only one parameter (the covariance scaling factor $\hat{\alpha}$) is associated with variance. The inflated diagonal covariance technique (W_{N*}) uses two parameters for variance, one for the covariance scaling factor, and one associated with calculating the effective number of independent data, N^*. For model selection in the W_{N*} method, we substitute N^* for N in Eq. 3.12.

Since the C_{full} procedure uses an estimated autocorrelation function, one may first think to count the number of autocorrelation lags as the number of parameters associated with correlation. However, correlations for large lags contribute little to the covariance estimation, and they are poorly estimated, so we damp them in estimating the autocorrelation (Box, Jenkins, and Reinsel 1994). The effective number of parameters

Table 3.3 Model parameter counts and relative AICc scores of methods with differing covariance estimators. (ST_{ind} – Single Transect with variance calculated independently at each transect; W_{diag} – Spline method with weighted diagonal covariance matrix; W_{N*} – Spline method with inflated weighted diagonal covariance calculated using the effective number of data; C_{full} – Spline method with full covariance matrix; n_r – number of parameters used to model rates; n_b – number of parameters used to model intercepts; n_{var} – number of parameters used to estimate variance; K – IC parameter count ($n_r + n_b + n_{var}$); N – number of data; N^* – effective number of data; ΔAICc – the AICc score minus the lowest AICc score.)

	North Section						South Section					
Method	n_r	n_b	n_{var}	K	N^* (N=2819)	ΔAICc	n_r	n_b	n_{var}	K	N^* (N=3321)	ΔAICc
ST_{ind}	401	401	401	1203	--	13248	401	401	401	1203	--	17269
W_{diag}	8	34	1	43	--	9084	16	11	1	28	--	14787
W_{N*}	8	20	2	30	276	13439	7	6	2	15	196	21463
C_{full}	6	72	101	179	--	0	10	62	101	173	--	0

associated with spatial correlation is thus the integral of the damping function given in Appendix A.

When comparing IC scores for models with different noise handling methods, it is helpful to understand how the misfit term is related to the likelihood of a model. Since we assume Gaussian noise, the likelihood function for parameter vector m, given data d, is

$$L(m \mid d) = (2\pi)^{-N/2} \left| C_{dd} \right|^{-1/2} \exp\left[-\frac{1}{2} (d - Gm)^T C_{dd}^{-1} (d - Gm) \right].$$

As noted above, the misfit LL, is defined as -2 times the logarithm of the likelihood function. Therefore, smaller LL values correspond to models with higher likelihood. The $(\Delta LL)/LL$ values in Table 3.2 show LL decreasing (model likelihood increasing) during iteration toward the full covariance matrix, with convergence after 2-3 iterations.

3.3 Results and Discussion

3.3.1 Model Selection: AICc

Figure 3.8 shows the ΔAICc scores, the difference in AICc from the lowest-scoring model, for each combination of rate and intercept parameters (up to 40 rate and 100 intercept parameters). The lowest AICc score in the north section corresponds to the model with 6 basis functions for rate and 72 basis functions for intercepts (see Table 3.3). Many more basis functions are required for modeling alongshore variations in intercept because the mean shoreline location depends on the shape of the baseline, and the baselines used in the USGS study are straight lines over large geographic regions, lines that do not mimic the mean shoreline shape on smaller scales. Alongshore variations in

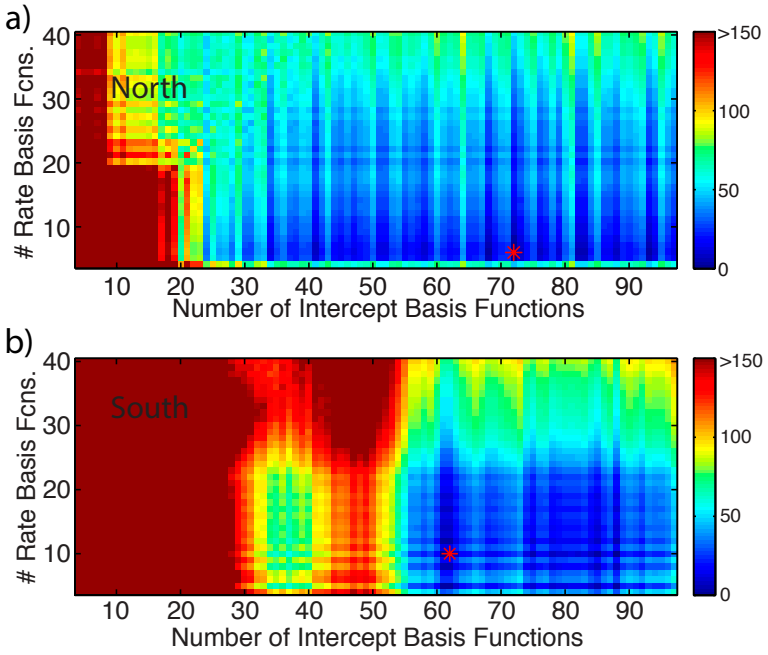

Figure 3.8 ΔAICc scores for each combination of rate and intercept basis functions North (a) and South (b) of OC Inlet. Red stars indicate the minimum AICc values.

rate, however, are insensitive to cross-shore shifts in mean shoreline position. In fact, if only rates are desired, one could simply remove the mean of each transect, as was done in Frazer, Genz, and Fletcher (2009) and Genz, Frazer, and Fletcher (2009). Calculated shoreline positions, however, depend on intercepts, so reducing the number of intercept

parameters is desirable for parsimony in shoreline prediction models. The same phenomenon is reflected in the AICc scores for the southern study region where 10 rate basis functions and 62 intercept basis functions were found optimal.

3.3.2 Modeled Rates and Intercepts

Modeled rates and intercepts produced from the optimal number of basis functions are shown in Figure 3.9, along with rates and intercepts calculated from the ST method. The two methods generally agree, indicating long-term erosion from the northernmost location (transect 0), turning to accretion, which is greatest just north of the OC Inlet. In the south section, erosion is most severe near the Inlet, in agreement with previous studies which found that the OC Inlet jetties have disrupted the natural long-term sediment transport to the south, causing sand to accumulate just north of the Inlet while retreating landward south of the Inlet (Dean and Perlin, 1977; Leatherman, 1984; Kraus, 2000; Buttolph *et al*., 2006).

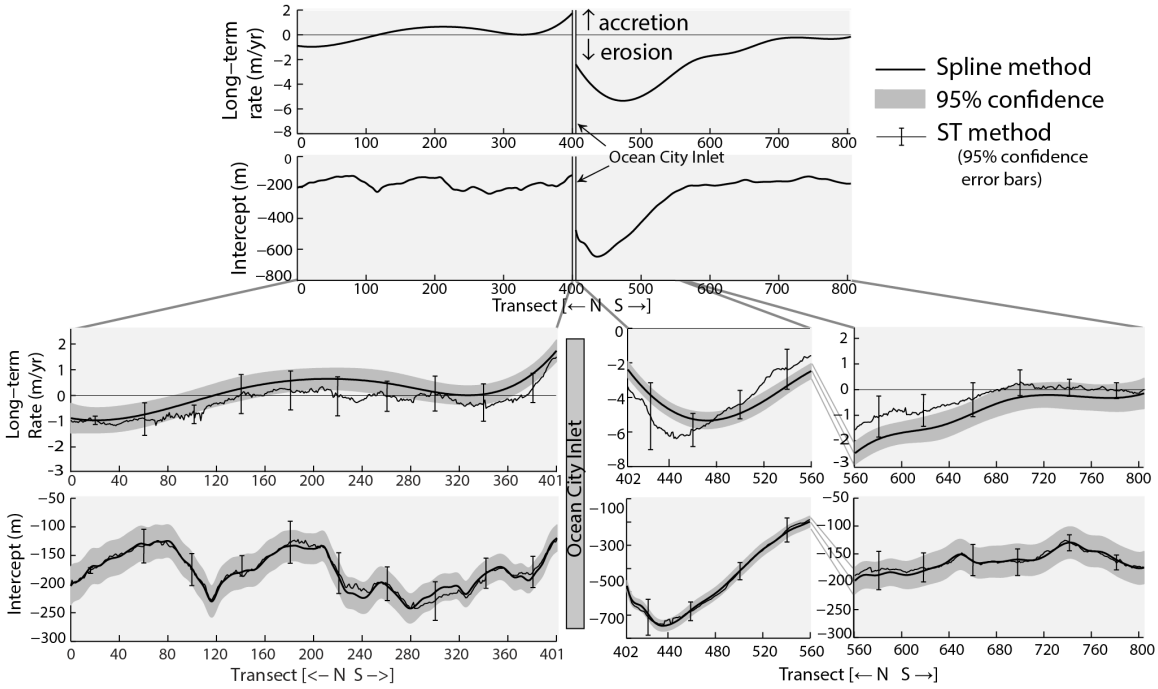

Figure 3.9 Modeled rates and intercepts along the coast of Ocean City and Assateague Island, MD using the spline model and ST model. For clarity, the lower middle panels are plotted with a different vertical scale.

For the north and south regions, we also computed an average change rate with 95% confidence interval by assuming a constant rate over each region, and inverting for that rate directly. For that calculation we shifted the y-baseline to zero, so the intercept is zero, and the spline matrix was reduced to an $I \times 1$ column vector of ones. A large difference is apparent between the constant rates calculated for the beaches north (0.31 ± 0.28 m/yr) and south (-2.40 ± 0.69 m/yr) of OC Inlet, due to disruption of longshore transport by OC Inlet jetties.

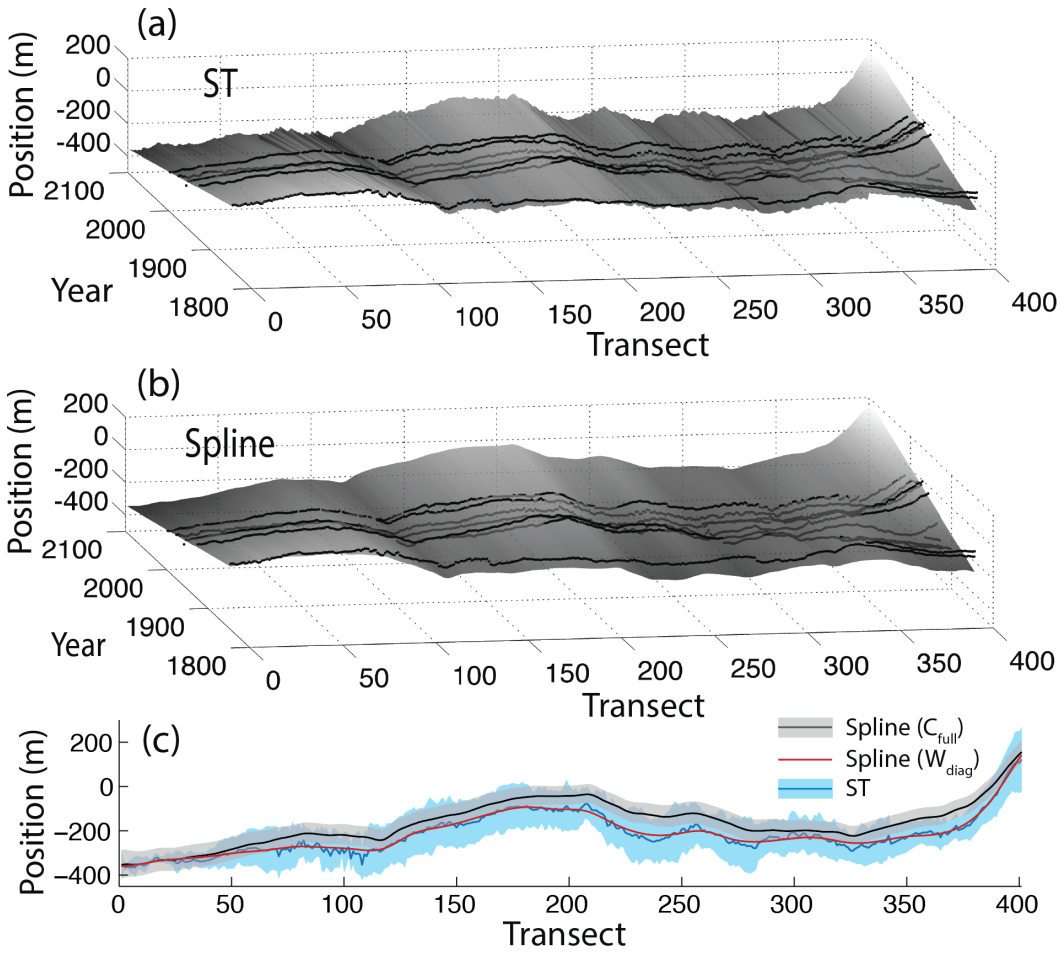

Figure 3.10 North section predicted shoreline positions (grayscale) for (a) ST and (b) C_{full} spline methods. Data are shown in black. Predictions are for the time span 1849 – 2100, a 100-year extension from the latest data. (c) Predicted shoreline positions in year 2100 for the ST and two spline methods reveals the unrealistic amplification of high spatial frequencies by ST. The spline model with noise treated as uncorrelated (W_{diag}) gives predictions similar to smoothed ST predictions.

The spline and ST rates have similar long-wavelength shapes, but deviate at shorter length scales, as expected. Areas with the largest deviations correspond generally to areas where ST estimates have the largest uncertainty estimates, especially in the southern portion closest to OC Inlet. The spline intercepts resemble the ST intercepts because many spline basis functions were needed to model the intercepts. If one continues to increase the number of basis functions used to model intercept and rate, the spline results would approach ST estimates because the single transect method is the end member of basis function saturation – equivalent to having delta-like spline basis functions at each transect. If we also then applied the correlated noise handling technique to ST, the estimates would be identical.

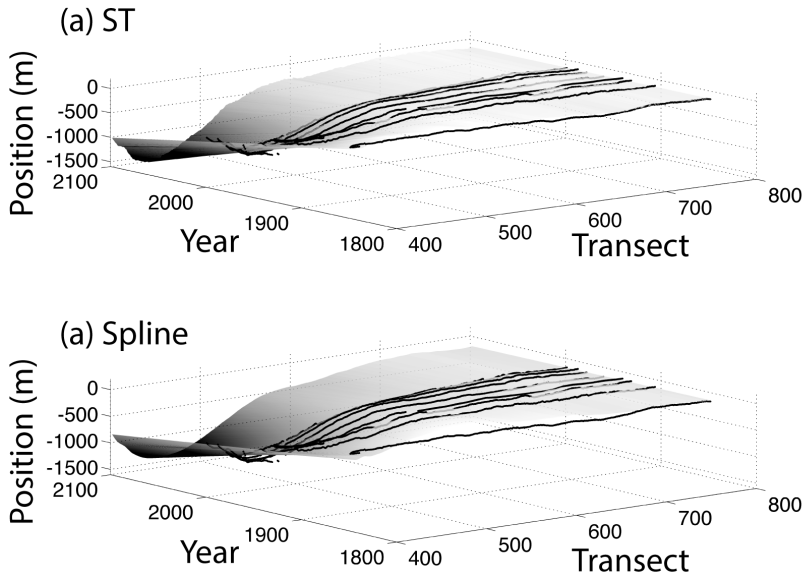

Figure 3.11 South section predicted shoreline positions for the (a) ST and (b) C_{full} spline methods during the time span 1849 – 2100.

3.3.3 Predicting Future Shorelines

Figure 3.10 shows predicted spline and ST shorelines, for the northern section of the study site, from 1849 to 2100, a 100-year extension to the time span of the original data. With time, the high spatial frequencies in the ST method are amplified, producing unrealistic variations between neighboring transects, inconsistent with the smoothing

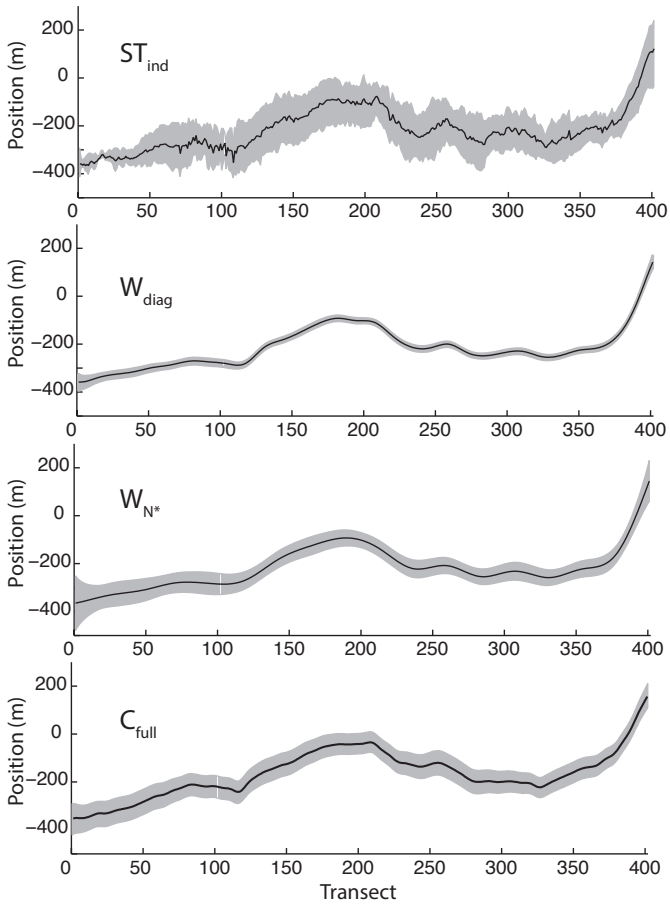

Figure 3.12 Northern section predictions for the year 2100, with 95% confidence intervals.

processes observed over time in natural coastal environments. The spline methods, however, give smooth shoreline predictions (Fig. 3.10c). Figure. 3.11 shows the corresponding results for the southern section. Figure 3.12 shows confidence intervals for the northern section predictions for the year 2100, using ST and all four spline methods, and it is interesting that the C_{full} spline method allows more alongshore detail than the W_{diag} and W_{N*} spline methods because it fits the data better (next section). Moreover, the W_{diag} result shows that if correlations in the noise are not properly handled, the erroneously low estimates of parameter variance results in erroneously narrow confidence intervals. For example, the average standard error of W_{diag} predicted positions in 2100 is roughly six meters, which is significantly less than the ≈11 meters of

actual shoreline position uncertainty (including variability in the shoreline indicator (high water line) due to seasonal and tidal influence) estimated by Douglas and Crowell (2000) at nearby Cotton Patch Hill, DE.

3.3.4 Comparing Noise Handling Techniques

As mentioned above, we processed the data using our spline method in conjunction with several different noise handling techniques. It is worth noting that the issue of spatially correlated noise spans all modeling techniques, no matter how unparsimonious they may be. One could apply all of the noise handling techniques we present (W_{diag}, W_{N*}, C_{full}), to the ST method because ST is just a spline method with delta-like splines at each transect. Since ST is so widely employed, we present only the standard ST noise methodology of estimating uncertainty independently at each transect, comparing that with our spline models. When comparing the ST method to our spline models, we denote the method as ST_{ind} as a reminder of the noise handling in the ST method.

Table 3.3 contains, for each noise method, the optimal number of basis functions used to model rate (n_r), intercept (n_b), and variance (n_{var}). The total number of parameters used in the IC calculations, K, is also shown. The ST_{ind} method naturally has the largest number of model parameters – a rate, intercept, and variance at each transect. The W_{diag} method requires far fewer parameters, with the W_{N*} method requiring even fewer parameters due to a much reduced effective number of data N^*. In the north section, N^* is 276 compared to the actual number of data $N = 2819$. In the south section, N^* is 196, out of $N = 3321$ actual data. The W_{diag} method also has reduced AICc values compared to ST in both the northern and southern portions, mainly due to the large reduction in parameters since IC scores balance model misfit (LL) with parameter count. The W_{N*} method, on the other hand, actually has the highest AICc score of all due to its high LL. The high AICc score is mainly due to the unlikely large variance in combination with assumed uncorrelated errors, and may not reflect actual accuracy (see Synthetic Data section below). The C_{full} method (splines with full covariance matrix) has a similar number of rate and intercept basis functions as the other two spline methods, but

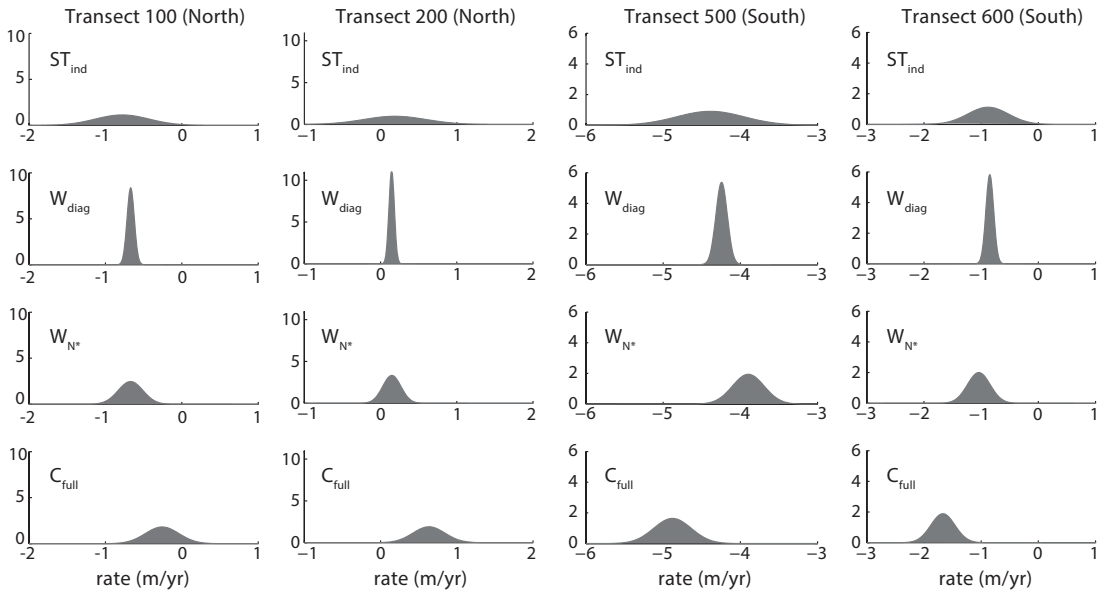

Figure 3.13 Posterior probability density functions for rate at four locations using: the single transect method with noise calculated independently at each transect (ST_{ind}); the spline method with uncorrelated noise (W_{diag}); the spline method with inflated diagonal (W_{N*}); and the spline method with full covariance (C_{full}). The change in mean rate between ST_{ind} and W_{N*} occurs because the IC allows the W_{N*} method fewer basis splines.

needs extra parameters to estimate the covariance matrix; even with the extra parameters, its lower *LL* gives it the lowest AICc score.

Notably, the different noise handling methods change not only the variance of the parameter estimates, but also their means. The posterior pdfs of rate at four locations are shown in Figure 3.13. The pdfs of the ST_{ind} method are typically the broadest because of the relatively small amount of data at each transect. The pdfs for the W_{diag} method are more localized due to the increased number of data used to estimate each rate in the spline method. In the W_{diag} method each B-spline coefficient is essentially a weighted average, and since the data are assumed independent and identically distributed, the variance of the average is smaller than that of any individual datum. This illustrates how when correlation is ignored, estimates of parameter uncertainty are erroneously low. On the other hand, the W_{N*} noise model gives rates with broader pdfs than the W_{diag} noise model because of the inflated variances; using N^* in lieu of N reduces the number of parameters allowed by the IC because the fit is degraded, and that changes the mean of

the rate pdf while increasing the variance. The pdfs for the C_{full} spline method are also broader than those in the W_{diag} method because covariance terms are included. Nevertheless, as Figure 3.12 shows, the C_{full} method reveals more alongshore detail because it is allowed more model parameters by the IC—because it fits the data better.

3.3.5 Comparing Basis Functions

The choice of basis function used in an analysis depends on both the analysis objective and the geology of the study area. No single type of basis function is superior in all situations, as summarized in Table 3.4. The ST method, although not truly a basis function method, is included in the table because it is equivalent to using delta-like basis functions at each transect.

All of the basis function methods produce more parsimonious models than ST, but they require careful handling of spatially correlated data errors. If the geology of the region warrants an alongshore discontinuity in rate (or intercept), B-splines and eigenbeaches (principal components) address the Gibbs effect (Figure 3.3) inherent in

Table 3.4 The effects of using different basis functions on model estimates.
*Eigenbeaches basis functions are not independent of the data; additional care is required for selecting a parsimonious number of basis functions (*e.g.*, cross-validation)
**Requires careful knot placement to circumvent Gibbs effect
[1]Correlated errors – covariance matrix must account for spatially correlated errors
[2]Nonparametric – requires nonparametric estimation method (*e.g.*, bootstrap)

Method	Parsimonious	Defined Everywhere?	Gibbs Effect	Error Estimation Assumptions
ST	N	N	N	Independent
Spline (B-splines)	Y	Y	N**	Correlated errors[1]
Polynomial (Legendre, Trigonometric)	Y	Y	Y	Correlated errors[1]
Eigenbeaches (Principal components)	Y*	N	N	Correlated errors[1]; Nonparametric[2]

polynomial (Legendre, trigonometric) basis functions, but not without added complication. The spline requires careful knot placement alongshore to circumvent the Gibbs effect. Eigenbeaches are contaminated by noise because they are derived from the data, requiring additional care in model selection and error estimation. Only the polynomial and spline basis functions are defined at every alongshore location, not just at each transect, a property that could be important if transects are widely spaced. If estimates are needed between transect locations, interpolation is required in the ST and eigenbeaches methods.

3.3.6 Limitations of the Time-Linear Model

All models tested here have the same shoreline change assumption in time – that shorelines erode or accrete at rates that are constant over decade to century time scales. This limitation affects predictions on either side of the OC Inlet jetties because shoreline behavior has changed, perhaps even reversed, over the time span of our data. The predicted shoreline locations for all models just north of the inlet actually exceed the seaward extent of the northern jetty. Since the jetty is the cause of sand accumulation to the north of the inlet, it is obviously incorrect to predict that the shoreline will continue to accrete past the seaward extent of the jetty. Given persistent coastal conditions, shorelines tend to move only when perturbed by a disruption, then gradually re-equilibrate to a stable state. Accordingly, the time component of our shoreline change model might be improved by incorporating relaxation in the time domain, following work done by Miller and Dean (2004) or Yates, Guza, and O'Reilly (2009). Incorporating our alongshore spline methods and noise handling into the Kalman Filter shoreline evolution framework described in Long and Plant (2012) might also provide additional improvement.

3.3.7 Confirmation with Synthetic Data

We analyze a synthetic dataset to support our modeling results. Ten cubic B-splines represent alongshore rates; intercepts are defined as zero everywhere. From the defined rates and intercepts, eleven synthetic shorelines at ten-year intervals are sampled

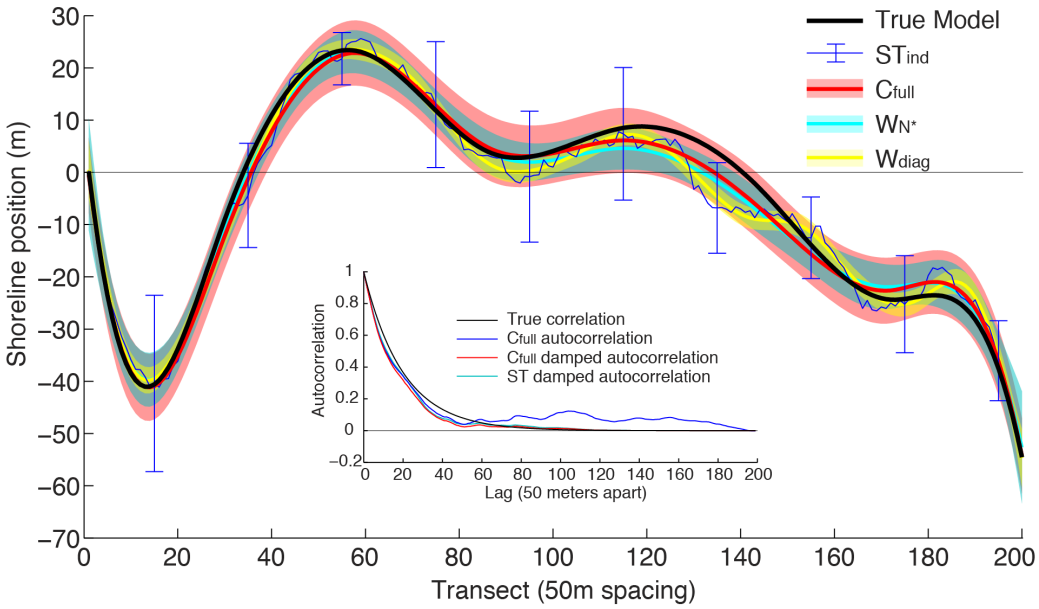

Figure 3.14 True (black line) and modeled (colored) most-recent synthetic shoreline. Inset shows true alongshore correlation and modeled correlation. Damped ST autocorrelation is not used in modeling, but has a similar shape to the C_{full} model autocorrelation.

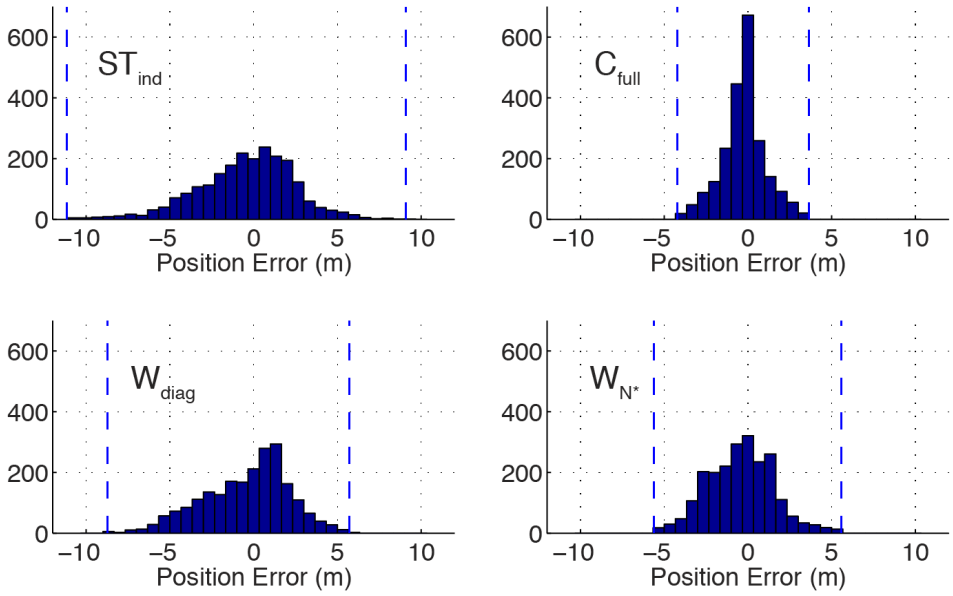

Figure 3.15 Histograms of shoreline position errors (estimated – true) for ST_{ind}, W_{diag}, C_{full}, and W_{N*} methods. Minimum and maximum error values for each method are indicated by vertical blue dashed lines.

at 50-meter increments alongshore. Correlated, zero-mean noise (Figure 3.14, inset) is weighted by *a priori* uncertainty estimates of 10 meters for the four oldest shorelines and 7.5 meters for the remaining seven shorelines, and added to the synthetic data. We model the data using the ST_{ind}, W_{diag}, W_{N*}, and C_{full} methods.

The C_{full} model is unique in identifying the true number of rate (ten) and intercept (one) B-splines used to create the synthetic data (Table 3.5). Its low relative AICc score indicated that the C_{full} model is also the most probable. The W_{N*} method also selects ten rate B-splines, but uses four B-splines to model intercepts alongshore, indicating that W_{N*} estimates represent slightly more noise than C_{full} estimates. As in the real data example, the W_{N*} method has the highest AICc due to the unlikeliness of its inflated variance. The W_{diag} and ST_{ind} methods use the most B-splines (Table 3.5) to model alongshore parameters indicating that they model more noise than the C_{full} and W_{N*} methods do.

Histograms of shoreline position errors (estimated – true) (Figure 3.15) show the C_{full} model to be the most accurate, followed closely by the W_{N*} model, then the W_{diag} and ST_{ind} models. The modeled noise correlation in the C_{full} method resembles the true correlation (Figure 3.14, inset). Autocorrelation of ST residuals are also similar to the true correlation. Model predictions of the most recent shoreline are shown in Figure 3.14; the synthetic data test also confirms that the uncertainty in the W_{diag} model is underestimated as seen in Figure 3.14 where the estimate does not overlap the true signal.

Table 3.5 Model parameter counts and relative AICc scores of methods with differing covariance estimators for synthetic data. (True – true model; ST_{ind} – Single Transect with variance calculated independently at each transect; W_{diag} – Spline method with weighted diagonal covariance matrix; W_{N*} – Spline method with inflated weighted diagonal covariance calculated using the effective number of data; C_{full} – Spline method with full covariance matrix; n_r – number of parameters used to model rates; n_b – number of parameters used to model intercepts; ΔAICc – the AICc score minus the lowest AICc score)

Method	n_r	n_b	ΔAICc
True	10	1	--
ST_{ind}	401	401	5674
W_{diag}	12	20	5036
W_{N*}	10	5	7133
C_{full}	10	1	0

3.4 Conclusion

Alongshore correlated data in shoreline change prediction is addressed by using a linear combination of B-splines to represent spatial variations of model parameters. B-splines avoid problems with Gibbs effect at abrupt discontinuities in rates (if knots are properly chosen) in previously used Legendre polynomial, sinusoid, and principal component basis functions, and they avoid problems with noise contamination in the latter. In addition to model parsimony, proper treatment of correlated noise is significant because differences in noise handling techniques affect mean parameter estimates, as well as estimated uncertainties. Treating correlated noise as if it were uncorrelated results in erroneously low variance estimates. Inflating variance estimates via an effective number of data to account for the lack of off-diagonal covariance terms limits the number of model parameters allowed, causing an increase in the misfit. Correlated noise was best addressed by including a full covariance matrix, constructed iteratively from data residuals. Although our method addresses both parsimony and noise handling, the shoreline near Ocean City Inlet reveals the usual limitations of the underlying time-linear assumption.

3.5 Appendix A: Estimating the Data Covariance Matrix

Following the flowchart in Figure 3.6, we begin by initializing $\tilde{C}_{dd}$ as the diagonal matrix $\tilde{C}_{dd}^{(0)} = diag(w_{ij}{}^2)$, where w_{ij} are the USGS *a priori* error estimates at locations *i* and times *j*. A diagonal covariance matrix represents uncorrelated data errors. Using $\tilde{C}_{dd}^{(0)}$, we invert for model parameter vector $\hat{\tilde{m}}$ (Eq. 3.5), and subsequently calculate residuals $\rho = d - \tilde{G}\hat{\tilde{m}}$. The correlation matrix C_{corr} is then constructed using the following equation

$$c_{ii'jj'} = \left(\sum_j \sum_i \rho_{i,j}^2\right)^{-1} \sum_{j=1}^{J} \sum_{k=1}^{I-|i'-i|} \rho_{k,j}\rho_{k+|i'-i|,j} \cdot \delta_{jj'} \qquad (3.A1)$$

in which i and i' are location indices ranging from 1 to I, j and j' are time indices ranging from 1 to J, and $\delta_{jj'}$ is the Kronecker delta which enforces our assumption that data are not correlated in time. If the data vector in the GLS problem is arranged such that data are grouped by time, and ordered spatially, the correlation matrix is block diagonal with each block equal and in Toeplitz form. Figure 3.16, left column, shows the spatial autocorrelation of shoreline residuals (first row of one block) for the north and south study sections.

To condition the matrix and ensure that it is positive definite, each autocorrelation in the correlation matrix is damped with the taper function

$$T\left(\left|i'-i\right|\right)=\cos^{l}\frac{\pi\left|i'-i\right|}{2(I-1)} \text{ (Fig. 3.16c),} \tag{3.A2}$$

in which the exponent l controls the rate of decay as data are spatially farther apart. We tested the values l = 3,6,10, and 20 for selected combinations of basis functions, and found that they all produced nearly identical parameter vectors. We used $l=6$ in our study, which causes the correlation to go nearly to zero by about lag 3/4 I. Fig. 3.16(a,b) shows the damped autocorrelation of residuals versus lag.

One of the $I\times I$ blocks within the block-diagonal C_{corr} matrix (J blocks total – one for each shoreline survey time) for the north section is shown in Fig. 3.16(e). The correlation matrix is subsequently weighted by the product of corresponding *a priori* uncertainty estimates $w_{ij}w_{i'j'}$ to produce a new $\tilde{C}_{dd}$

$$\tilde{C}_{dd}^{(1)}=\tilde{C}_{dd}^{(0)1/2}C_{corr}\tilde{C}_{dd}^{(0)1/2}. \tag{3.A3}$$

The USGS estimated errors for the year 2000 LiDAR-derived shoreline in the North are shown in Fig. 3.16d, with the accompanying weighted correlation matrix (Fig. 3.16f). We then use the new full covariance matrix to invert for an updated parameter vector $\hat{\tilde{m}}$, and use that parameter vector to estimate yet another covariance matrix and

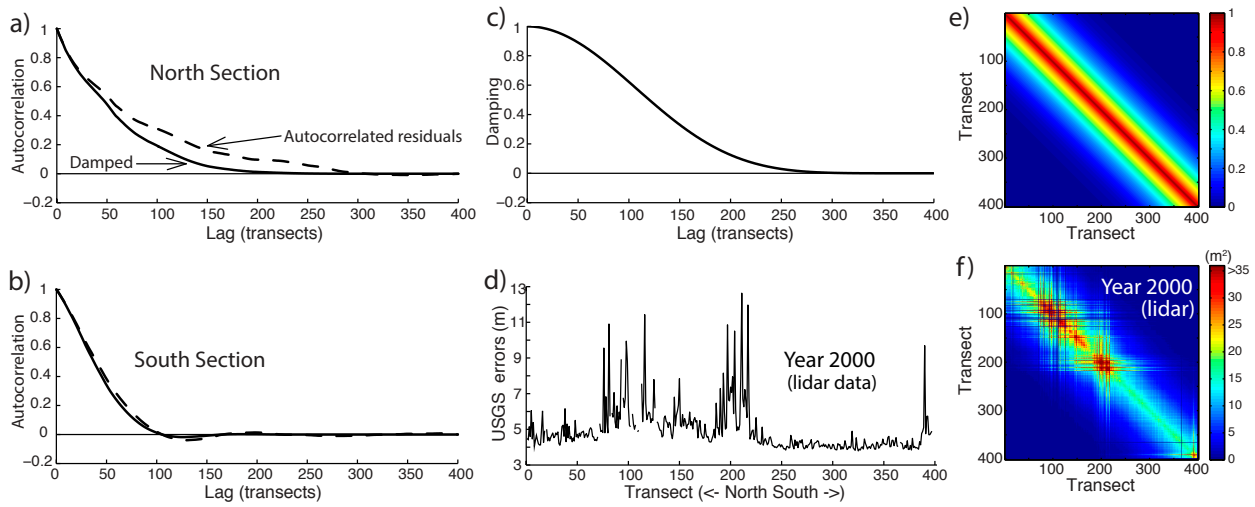

Figure 3.16 (a-b) Autocorrelation (dashed) and damped autocorrelation (solid) of residuals for north (a) and south (b) portions of the study area, (c) the cosine damping function (l = 6), and (e) the resulting autocorrelation matrix for each year in the north section. (d) The *a priori* error estimates for the 2000 LiDAR shoreline fluctuate alongshore (north section). (f) The result of weighting the correlation matrix in (e) by the error estimates in (d). For years in which *a priori* shoreline error estimates do not vary alongshore (shorelines not derived from LiDAR data), the entire block is simply scaled by the constant.

model pair, and so on, until the covariance matrix is sufficiently similar to the one from the previous iteration. Our convergence criterion is $\left\|\tilde{C}_{dd}^{(u)} - \tilde{C}_{dd}^{(u-1)}\right\|_1 < 10^{-5}\left\|\tilde{C}_{dd}^{(0)}\right\|_1$, where u is the number of iterations, and $\|\cdots\|_1$ denotes the matrix L_1-norm. Notice that it is not necessary to calculate the constant of proportionality $\hat{\alpha}$ until the iterations have converged, because it drops out of equation 3.5, the GLS estimator of parameter vector $\tilde{m}$.

Chapter 4

LONG-TERM SHORELINE CHANGE AT KAILUA, HAWAII, USING REGULARIZED-ST

In preparation for publication submission as Anderson, T.R., L. N. Frazer, and C.H. Fletcher, Long-term shoreline change at Kailua, Hawaii, using regularized-ST.

Abstract – We use second-order Tikhonov regularization to model long-term shoreline change at Kailua, Hawaii. As a check on our regularized-ST method, we also analyze the data with the traditional single-transect method (ST) and with B-splines. All three methods indicate long-term accretion, especially near the opening of an offshore sand-filled channel toward the middle of Kailua Beach, consistent with earlier work by others. The regularized-ST and B-spline models both give shoreline change rates that vary more smoothly alongshore than the rates from ST. In regularized-ST, the alongshore smoothness is controlled by two regularization parameters, one for rate and one for intercept, which can vary continuously and are chosen using a Bayesian information criterion. Setting those parameters to zero gives traditional ST. In the B-spline method, smoothness is controlled by the spline counts for rate and intercept, and changing the number of splines causes the location of the splines to shift, thus linking model smoothness to other aspects of the model. This is a disadvantage compared to regularized-ST, although splines have the compensating advantage of being defined at every alongshore point, a convenience if transects are widely spaced. Regularized-ST is more straightforward to implement than splines, especially when modeling data with alongshore discontinuities. Regularized-ST may also be preferable because of its continuous connection with the familiar ST method.

4.1 Introduction

Shoreline change studies are becoming increasingly vital to coastal managers as chronic erosion, storms, limited sediment supplies, coastal development, and rising sea levels continue to damage coastlines. Many states rely on quantitative measures of shoreline behavior, such as shoreline change rates, to implement building setback policies. Given that the median lifespan of commercial buildings is 70-75 years (U.S. Department of Energy, 2011), it is desirable to predict shoreline locations 70 to 100 years into the future.

Data limitations present challenges to long-term shoreline prediction because of the complexity of coastal dynamics, especially drivers of shoreline change such as wave energy, storm surge, tides, seasonal variations, aeolian transport, and changes in relative sea level which occur over a wide range of time and spatial scales (Miller and Dean, 2004). Highly sophisticated three-dimensional physics-based models (*e.g.*, Delft3D-MOR (Lesser *et al*., 2004)) adequately represent shoreline behavior over short time spans, but are limited in their long-term predictive capabilities. Empirical models, on the other hand, can identify long-term trends in historical shoreline position data, which are typically very sparse in time and contain large scatter due to short-term beach processes (*e.g.*, Galgano and Douglas, 2000; Honeycutt, Crowell, and Douglas, 2001). For example, it is common that only 5 to 10 historical shoreline positions, unevenly spaced over approximately 80 years, are available for a shoreline. As more data becomes available, modeling efforts progress toward assimilating the various time resolutions (*e.g.*, Long and Plant, 2012; Davidson, Splinter, and Turner, 2013).

Long-term shoreline change modeling techniques have developed incrementally. Least squares regression has replaced the once-favored end-point method (*e.g.*, Crowell, Douglas, and Leatherman, 1997; Galgano and Douglas, 2000; Honeycutt, Crowell, and Douglas, 2001). Least squares regression uses all available shoreline positions, whereas the end-point rate method used only two shoreline positions to calculate a cross-shore change rate at each alongshore location. Genz *et al*. (2007) investigated different forms of regression analyses such as least absolute deviation, weighted least squares, and least median of squares. Frazer, Anderson, and Fletcher (2009) added a storm function to the

typical rate-only regression equations, improving long-term shoreline change estimates. Improvements in quantifying error and bias in data derived from different sources (*e.g.*, LiDAR, aerial photographs) have also improved shoreline change statistics (Douglas and Crowell, 2000; Fletcher *et al*., 2003; Ruggiero and List, 2009).

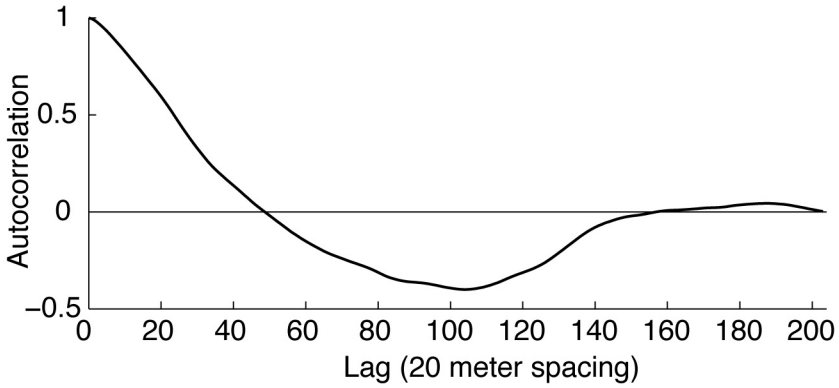

Figure 4.1 Autocorrelation of shoreline change rates at 20 meter increments along Kailua Beach.

The single transect method (ST) is still the typical procedure for calculating a shoreline change rate at each shore-normal transect alongshore. It assumes that the data and noise at each transect are independent, which results in more parameters being used to fit the data than are necessary. As an example, Figure 4.1 shows the autocorrelation of long-term rate parameters that were calculated independently at 20-meter increments (transects) along Kailua Beach, Hawaii. The slow decay of the autocorrelation in the alongshore direction shows that rates are highly correlated. Frazer, Genz, and Fletcher (2009) and Genz, Frazer, and Fletcher (2009) reduced this overfitting by representing change rates as the sum of alongshore basis functions. The basis functions they used were Legendre polynomials, trigonometric functions, and principal components. They followed Fenster, Dolan, and Elder (1993) by using an information criterion to select the most parsimonious model. Anderson, Frazer, and Fletcher (2010) combined alongshore basis functions with the storm function (Frazer, Anderson, and Fletcher, 2009) in their modeling technique to investigate transient and persistent storm components. Recently, Anderson and Frazer (in review) investigated B-spline basis functions as a way to avoid the Gibbs effect; they also compared different methods of handling correlated data errors,

showing that approximating correlated errors by uncorrelated errors affects rate as well as uncertainty.

Regularization is a technique often used in regression analysis to improve the condition of matrix inverses, but it can also be used to avoid overfitting (Aster, Borchers and Thurber 2012). In zeroth-order Tikhonov regularization, solutions are penalized for distance from a reference model, as well as for misfit; in first-order Tikhonov regularization, solutions are penalized for their variability, including linear variation; in second-order Tikhonov regularization, solutions are penalized for roughness but not for locally linear behavior. In this paper we use second-order Tikhonov regularization to make the traditional ST method more parsimonious. Regularization can be applied to any model, but it is most useful when the basis functions of the model are localized. In the spline method, the width of the basis functions is controlled to avoid overfitting, so regularization isn't necessary, but in the traditional ST method, the basis functions are delta-like, and regularization is highly beneficial. From the point of view of Bayesian statistics, regularization consists of multiplying the likelihood function by a prior, but is implemented numerically by adding more equations to the linear system.

We begin with the ST method. At each transect location, the shoreline position $y(x,t)$ is estimated by $\hat{y}(x,t) = \hat{r}(x)(t-\overline{t}) + \hat{b}(x)$, where $\hat{r}(x)$ and $\hat{b}(x)$ are the least squares rate and intercept, respectively, for alongshore location x. These parameters are found by minimizing the residual sum of squares (RSS), or misfit, in the equation $y = rt + b$ at each alongshore location x. As an example, the circles in Figure 4.2 show rate parameters $\hat{r}(x)$, calculated using ST at transects spaced 20 meters apart for Kailua Beach, Hawaii. A much less complex relationship results when the difference between ST rates at adjacent transects is constrained to be constant, giving the smoothest representation possible: a straight line (Figure 4.2, dashed line). That alongshore-linear rate model does not fit the data nearly as well as the ST model but it is very parsimonious. The preferred model lies somewhere between the two extremes of fitting the data well at each transect and limiting the alongshore variability. The regularized model parameters are found by minimizing

$$\phi(m) = \mathrm{RSS}(m) + \gamma^2 \{\text{roughness penalty}(m)\}, \quad \gamma \geq 0,$$

where *m* is a vector of parameters, RSS is the (Mahalanobis) residual sum of squares, γ is the regularization parameter, and the roughness penalty is the sum of the squared alongshore second derivative of parameters. When γ is zero, there is no penalty, and the model reverts to ST. As γ increases, the penalty for alongshore variation increases, and parameters are forced to vary smoothly. In Figure 4.2, the solid line represents rates in which alongshore variation is constrained by a large penalty; as γ approaches infinity, the parameters approach a straight line.

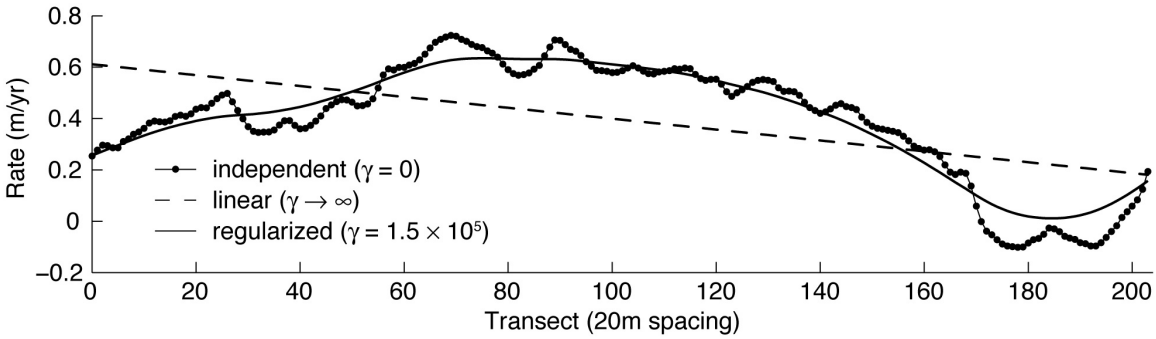

Figure 4.2 Rates from ST (dots), rates from regularized-ST with very large γ (dashed line), and rates from regularized-ST with moderate γ (solid line).

As an alternative to choosing basis functions, regularization has some practical advantages. For example, polynomial basis functions usually require separate analysis of shoreline sections that are separated by small gaps of missing data, but regularization allows for one-time processing of shorelines with alongshore data gaps. We find regularized ST easier to implement than basis functions methods, and many routines used in regularization are available in software packages such as Matlab (www.mathworks.com) and R (www.r-project.org).

In regularization, some criterion is required for selecting the appropriate regularization parameter(s). This is comparable to selecting the optimal number of basis function using basis function methods (Frazer, Genz, and Fletcher, 2009). After experimenting with the traditional L-curve method (Aster, Borchers and Thurber 2012), and various information criteria, we elected to use the simple Bayesian Information

Criterion derived in Appendix B. As with any information criterion, the best model is the one whose BIC score is the lowest.

Below we present our regularization methodology and use it to analyze historical shoreline data at Kailua Beach, Oahu, Hawaii. To buttress our findings at Kailua we compare results for three different shoreline change methods: standard ST, regularized-ST, and B-spline basis functions. We also discuss model selection in regularization, practical issues in applying different methods, and the estimation of parameter uncertainty.

4.2 Kailua Beach, Hawaii

4.2.1 Physical Setting

Kailua Beach is located on the windward side of the Hawaiian island of Oahu (Figure 4.3). The 4-kilometer carbonate sand beach is bounded by limestone to the north at Kapoho Point and basalt at Alala Point to the south. A wide fringing reef platform provides moderate protection to the beach from year-round northeast trade wind waves, and winter (October-March) north swells. The reef platform is bisected by a winding 200m wide sand-floored channel that widens toward the shore into a broad sand field at the center of the beach. The residential area of Kailua sits upon a low-lying expansion of Holocene-age carbonate dune ridges and terrestrial lagoon deposits (Harney and Fletcher, 2003). Low vegetated dunes front many oceanfront homes. The Kaelepulu Stream empties into the ocean near the south end of Kailua Beach. Episodic removal and occasional redistribution of sand near the stream mouth began in the 1980s. A boat ramp, constructed between 1949 and 1963 at the south end of Kailua Beach, generally inhibits sediment moving toward the north, as evidenced by sediment accumulation on the south side, and deprivation on the north of the boat ramp in the majority of post-1949 historical aerial photos available online from the University of Hawaii Coastal Geology Group (http://www.soest.hawaii.edu/coasts/erosion/mosaics.php?sArea=kailua).

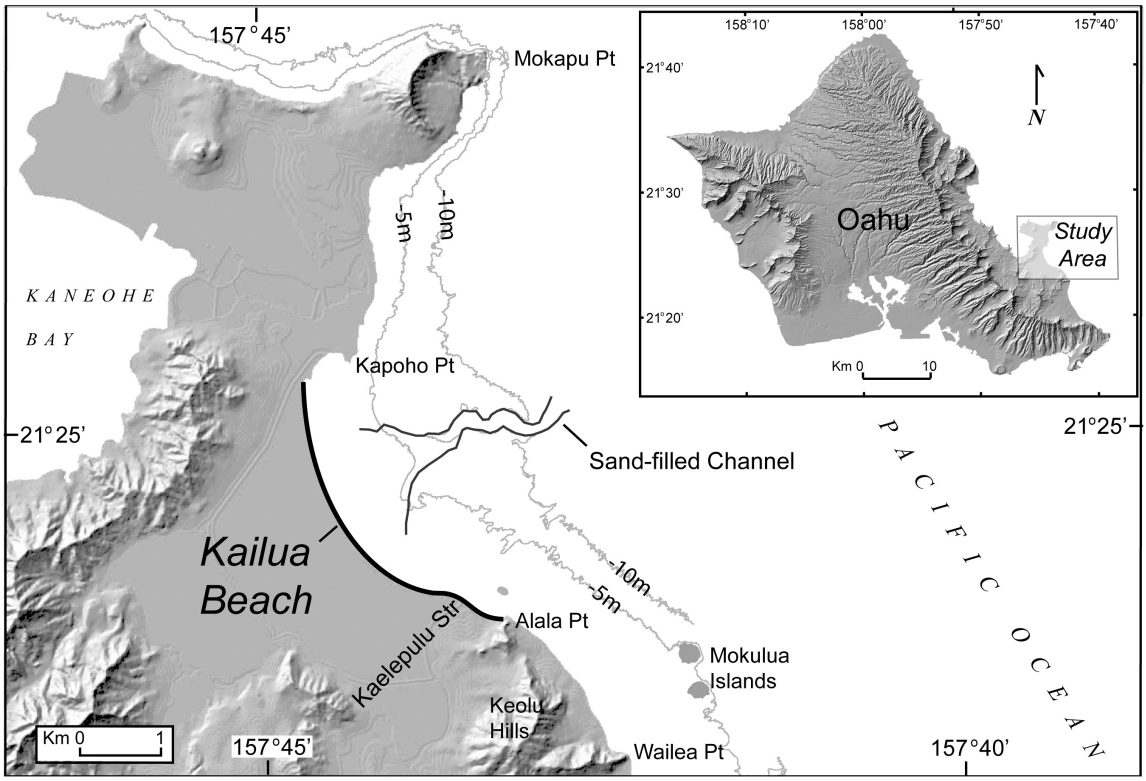

Figure 4.3 Kailua Beach, Oahu, Hawaii. (Adapted from Romine *et al.*, 2009)

4.2.2 Kailua Beach Data

Data used in the study are cross-shore distances relative to a user-defined baseline (Figure 4.4 inset). Historic shorelines extracted from aerial photographs and T-sheets dating between 1928-2005 were obtained from the University of Hawaii Coastal Geology Group as GIS shapefiles (see Romine *et al*., 2009 for shoreline extraction procedure). Dates, origins, and total position errors for each survey, calculated by Romine *et al*., (2009), are shown in Table 4.1. Approximately shore-normal transects, spaced 20 meters apart, are cast off of a smooth baseline that follows the general shape of the shoreline. Here, the baseline is a spline fitted to the average shoreline position (Figure 4.4). At each transect location x_i along the baseline, the relative distance from the shoreline to the baseline y_{ij} is calculated for shoreline times t_j. Thus, $y_{ij} = y(x_i, t_j)$, where transect index i ranges from 0 to I-1, and time index j ranges from 1 to J. The Kailua Beach data set is the collection of cross-shore positions relative to the baseline over all transects (Figure 4.5).

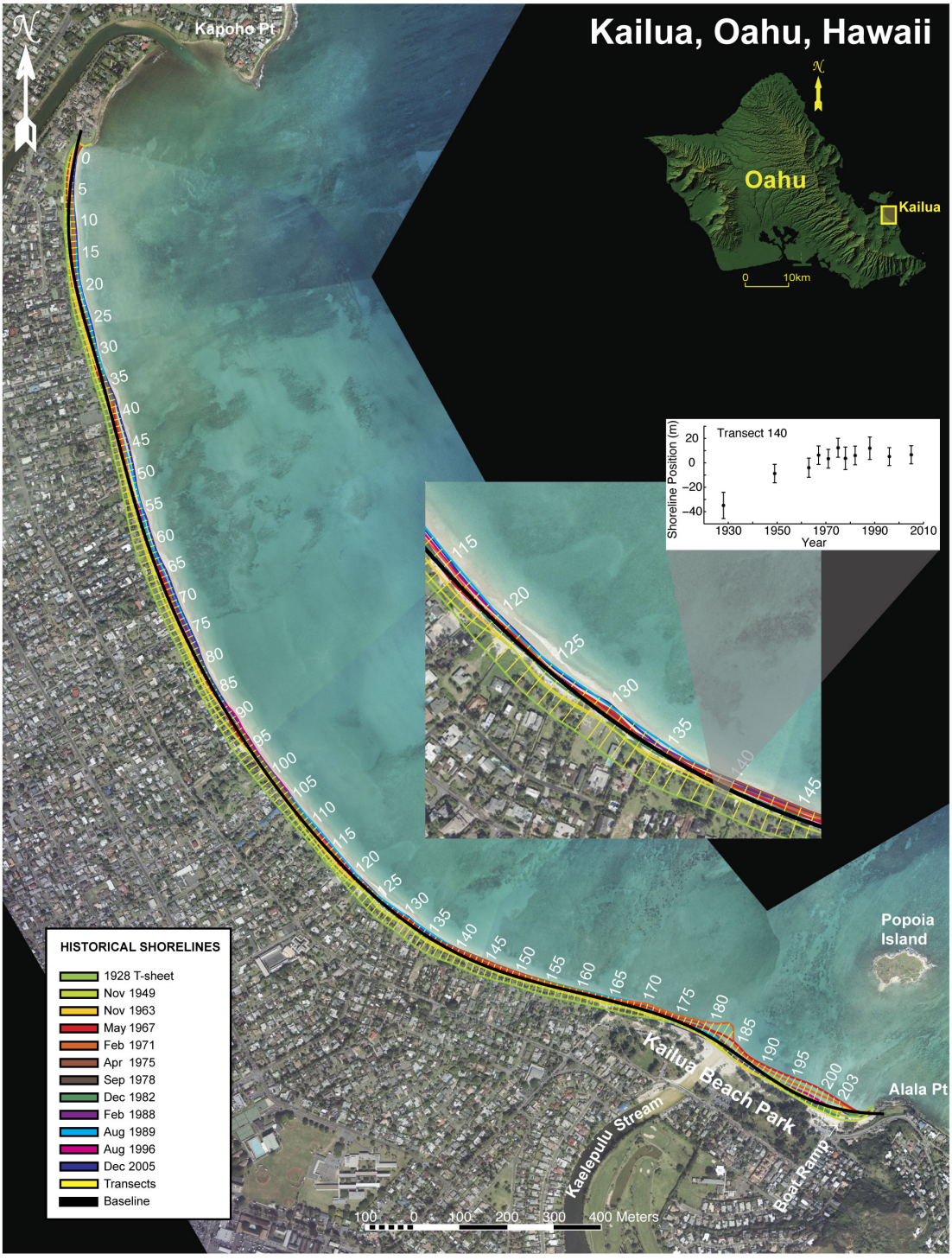

Figure 4.4 Shoreline vectors are overlaid on a 2005 aerial photomosaic (from the University of Hawaii Coastal Geology Group) of Kailua Beach. Shore-normal transects (thin yellow lines) are cast off a baseline (black line) that follows the general shape of the coast. Inset shows a small-scale shoreline deviation from the baseline, following the near-shore topography. Upper inset shows a plot of cross-shore position versus time, along one transect

Table 4.1 Dates of shoreline surveys, sources of data, and estimated position errors.

Date	Source	Error (m)
1928	T-Sheet	10.78
1949	Aerial Photo	7.56
1963	Aerial Photo	7.79
1967	Aerial Photo	7.53
1971	Aerial Photo	7.70
1975	Aerial Photo	7.77
1978	Aerial Photo	9.22
1982	Aerial Photo	7.63
1988	Aerial Photo	9.18
1996	Aerial Photo	7.35
2005	Aerial Photo	7.41

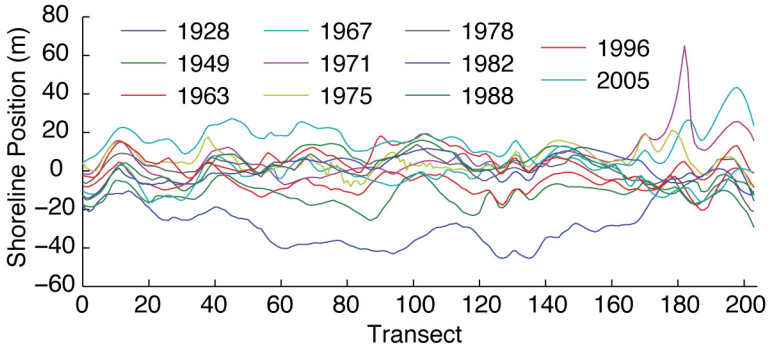

Figure 4.5 Shoreline data, relative to baseline, from Kailua, Hawaii. Transects are spaced 20 meters apart.

4.3 Procedure

We use least squares regression to estimate parameter values for a system of shoreline equations penalized by an additional set of equations. The influence that the penalty equations have on the estimates is governed by regularization parameters. We employ the BIC statistic to find the appropriate value of the regularization parameter.

We use the following simple forward model for shoreline change over time:

$$y_{ij} = b_i + r_i(t_j - \overline{t}) + n_{ij}, \tag{4.1}$$

in which b_i and r_i are the intercept and rate, respectively, at alongshore location x_i, and n_{ij} is noise. It is straightforward to include additional terms in this model, such as acceleration (e.g., Frazer, Genz, and Fletcher, 2009; Romine *et al*., 2009) or a storm function (Anderson, Frazer, and Fletcher, 2010). We opted not to include acceleration here because it can result in unstable long-term (decades) predictions. Also, a previous study by Romine et al. (2009) found that purely linear models outperformed models with acceleration terms in fitting data at Kailua Beach with polynomial basis functions. We do not include a storm function because we found no storm signal in the Kailua Beach data set. However, such terms are easily added to the shoreline change equation above and incorporated into the remaining procedure.

As a comparison to regularized-ST, we also analyzed the data using cubic B-splines as alongshore basis functions (Anderson and Frazer, in review). In basis function methodology, the parameter vector consists of basis function coefficients; Frazer, Genz, and Fletcher (2009) present a thorough explanation of basis functions in shoreline change modeling. The forward model for B-splines is

$$y_{ij} = \sum_{k_0=0}^{K_0} \tau_{k_0}^{(0)} B_{k_0}(x_i) + (t_j - \overline{t}) \sum_{k_1=0}^{K_1} \tau_{k_1}^{(1)} B_{k_1}(x_i) \tag{4.2}$$

where the $B_k(x)$ are cubic B-splines and the τ_k are their coefficients.

4.3.1 Second Order Regularization

Regularization is most easily implemented by adding constraint equations in the following way. Consider the system of equations (4.1) in matrix form as $d = Gm + \eta$, where d is an $N \times 1$ column vector of N observed shoreline positions, m is an $M \times 1$ column vector of M model parameters, G is an $N \times M$ system matrix, and η is an $N \times 1$

column vector of errors with zero mean and covariance matrix C_{dd}. We control model roughness by augmenting the system with equations that set the second alongshore derivative of the parameters to zero. We approximate the second derivative by the centered second difference matrix L,

$$L = \frac{1}{(\Delta x)^2}\begin{bmatrix} 1 & -2 & 1 & & & \\ & 1 & -2 & 1 & & \\ & & & \cdots & & \\ & & & 1 & -2 & 1 \end{bmatrix}, \tag{4.3}$$

where Δx is the spacing between transects. Thus Lm approximates the second derivative of the parameter vector m. In coding, the equation $Lm = 0$ becomes $\mathbf{0} = \gamma Lm + \varepsilon$, where $\mathbf{0}$ is an $(M-2)\times 1$ column vector of 0s, ε is an $(M-2)\times 1$ column vector of independent and identically distributed (iid) errors with zero mean and unit variance (*i.e.* the covariance matrix is the identity matrix), and γ is the regularization parameter.

Together the forward shoreline model equations and the roughness constraints are:

$$\begin{aligned} d &= Gm + \eta \\ \mathbf{0} &= \gamma Lm + \varepsilon \end{aligned} \tag{4.4}$$

with $\eta \sim N(0, C_{dd})$ and $\varepsilon \sim N(0, \mathrm{I})$. It follows that the least squares solution to the augmented system of equations (4.4) is found (*e.g.* Hastie, Tibshirani, Friedman, 2009) by minimizing

$$(d - Gm)^T C_{dd}^{-1} (d - Gm) + \gamma^2 m^T L^T L m . \tag{4.5}$$

It can be seen that when $\gamma = 0$, the regularization terms disappear, leaving only the sum of squared residuals typically seen in least squares regression. As γ approaches infinity,

the second derivative penalty term is given so much weight that the parameters are forced to be linear in the alongshore direction.

Taking the differential of (4.5) and setting it to zero, we find that the model vector *m* that minimizes (4.5) for a given γ is

$$\hat{m} = (G^T C_{dd}^{-1} G + \gamma^2 L^T L)^{-1} G^T C_{dd}^{-1} d \tag{4.6}$$

with estimated model covariance matrix (*e.g.*, Menke, 2012)

$$\hat{C}_m = \left(G^T C_{dd}^{-1} G + \gamma^2 L^T L\right)^{-1}. \tag{4.7}$$

The vector of fitted values is then

$$\hat{d} = Hd \tag{4.8}$$

where

$$H = G(G^T C_{dd}^{-1} G + \gamma^2 L^T L)^{-1} G^T C_{dd}^{-1} \tag{4.9}$$

is the data resolution matrix, also known as the "hat" matrix.

Future shoreline location is predicted by extrapolating from the model whose parameters we have just estimated. For future time t_f, and location x_i, let $q_{x_i} = q_{x_i}(t_f)$ be an $M \times 1$ column vector, which we refer to as the prediction kernel. The predicted position of the shoreline at location x_i and future time t_f is then

$$\hat{y}(x_i, t_f) = q_{x_i}^T \hat{m} \tag{4.10}$$

with estimated variance

$$\hat{\sigma}_{x_i}^2 = q_{x_i}^T \hat{C}_m q_{x_i} . \tag{4.11}$$

A $100(1-\varepsilon)\%$ confidence interval for $\hat{y}$ is given by

$$\hat{y}(x_i, t_f) = q_{x_i}^T \hat{m} \pm z_{1-\varepsilon/2} \hat{\sigma}_{x_i} \tag{4.12}$$

in which $z_{1-\varepsilon/2}$ is the value of the standard normal distribution with associated cumulative distribution $1-\varepsilon/2$. When the data variance is estimated, Student's *t*-distribution is used to estimate confidence intervals for parameters. Here we assume a known variance estimated as in Romine *et al*. (2009), so the posterior distribution is normal.

Although errors are assumed *a priori* for each data value, we do estimate the correlations between these errors as in Chapter 3. Our procedure for estimating error correlations is given in Appendix A. Correlations appear in an $N \times N$ matrix called the covariance structure matrix C_{corr}. The structure matrix is then scaled by the *a priori* error estimates to obtain the data covariance matrix as

$$C_{dd} = W^{1/2} C_{corr} W^{1/2}, \tag{4.13}$$

where $W^{1/2}$ is the diagonal matrix containing the *a priori* error estimates,

$$W^{1/2} = \text{diag}(\tilde{\sigma}_1, \tilde{\sigma}_2, ..., \tilde{\sigma}_N). \tag{4.14}$$

Due to the large time intervals between surveys (~10 years), data are not considered correlated in time. However, data correlation in the alongshore direction is present because of the small spacing (20 meters) between transects. Violation of assumption of data independence "can cause dramatic differences in the inferences which may be legitimately drawn from a set of observations, Box (1954), Zellner and Tiao, (1964)" (from Box and Tiao, 1973). Anderson and Frazer (in review) confirm that

different assumptions about data independence caused differences in parameter estimates and their uncertainties in the shoreline problem.

4.3.2 Selecting the Regularization Parameter

We take a Bayesian approach to model selection, and determine the appropriate regularization parameter by means of the BIC given in Appendix B. Alternative model selection techniques are deferred to the Discussion section. The BIC is a statistic that is a measure of posterior model probability (see Appendix B). As with other information criteria, the lower the BIC, the better the model. We cannot minimize the BIC analytically, so we find the minimum by searching over a range of regularization parameters, calculating the BIC statistic for each parameter value. In order to use the spline method for comparison we also give an analogous BIC for that method; the BIC for spline selection is a simplification of the one for regularization. The residual sum of squares,

$$\mathrm{RSS} = (d - G\hat{m})^T C_{dd}^{-1} (d - G\hat{m})$$

appears in both BIC equations. For selecting the optimal number of basis functions in the spline method we use

$$\mathrm{BIC}_1 = \mathrm{RSS} + \ln\left|C_m^{-1}\right|. \tag{4.15}$$

Here, $\left|\cdots\right|$ denotes the matrix determinant and C_m is the model covariance matrix (Eqn. 4.7). For selecting the optimal regularization parameters we use

$$\mathrm{BIC}_2 = \mathrm{BIC}_1 + \gamma_r^2 \hat{r}^T L^T L \hat{r} + \gamma_b^2 \hat{b}^T L^T L \hat{b} - 2(M/2 - 2)\ln(\gamma_r \gamma_b), \tag{4.16}$$

in which L is the second derivative operator (Eqn. 4.3) with $M/2-2$ rows, γ_r is the regularization parameter for rate, γ_b is the regularization parameter for intercept, and M is the length of the parameter vector $m=[r^T, b^T]^T$. For the purposes of model selection, the covariance matrix C_{dd} is assumed constant; it is possible to compare models with different C_{dd} and L, but additional terms are required (see Appendix B). Figure 4.6a shows the ΔBIC scores, the BIC score relative to the lowest (best) score, for all pairs of regularization parameters tested. The model with the lowest BIC score has a rate regularization parameter of 3.2×10^5 and an intercept regularization parameter of 9.0×10^2.

As the numerical values of the regularization parameters have no intuitive value it is desirable, though not strictly necessary, to estimate the effective number of model parameters associated with each regularization parameter. In regression methodology, this number is called the regression degrees of freedom. For basis function methods, this number is simply the number of basis functions, *i.e.*, the number of components in the parameter vector m. For regularization, the length of the parameter vector is fixed at the number of transects, but as the regularization parameter increases in value, the effective number of parameters declines. The regression degrees of freedom df_γ is defined as the trace of the data resolution matrix (hat matrix) given in Eqn. 4.9 (*e.g.*, Hastie, Tibshirani, and Friedman, 2009), or

$$df_\gamma = trace(H). \tag{4.16}$$

To see why the trace of the hat matrix is an intuitively reasonable measure of effective number of parameters, first note that the trace of the hat matrix is also the trace of the model resolution matrix, $G^{\#}G$, where $G^{\#}$ is the generalized inverse matrix on the right hand side of equation (4.6). Now consider a simple regression system for which $G^{\#}G$ is the identity matrix; in that system, the regression degrees of freedom is clearly the number of parameters. Finally, consider a system in which $G^{\#}G$ is a [1/4 1/2 1/4] smoothing matrix, which has the value 1/2 for each diagonal entry. The effective number

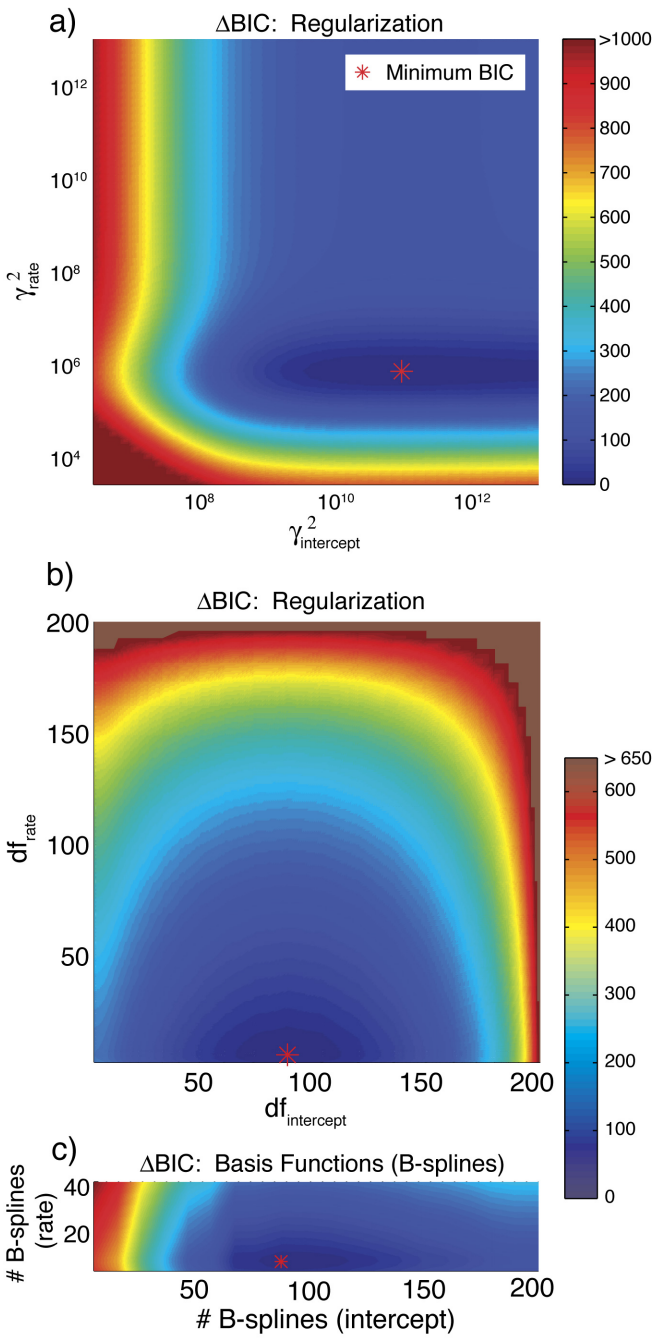

Figure 4.6 (a) ΔBIC values for regularization models shown plotted against (a) the squared regularization parameters and (b) regression degrees of freedom. In (c) the ΔBIC values for the B-spline models are plotted against the number of splines used for intercept and rate.

of parameters for this system is the actual number of parameters divided by 2, consistent with what one would expect from averaging two parameters into one. Figure 4.6b shows

the ΔBIC values from regularization models as in Figure 4.6a, but plotted against corresponding regression degrees of freedom for rate and intercept parameters. The regularization model with the lowest BIC score for Kailua Beach had roughly six (5.5) degrees of freedom for rate parameters and 89 degrees of freedom for intercept parameters. This agrees well with the most parsimonious spline model (Figure 4.6c), which had six rate basis functions and 82 intercept basis functions.

4.4 Kailua Beach Results

We find that Kailua Beach is generally accreting, with an overall long-term rate of 0.36 m yr^{-1} (± 0.06 m yr^{-1} standard deviation). There is general agreement, as shown in Figure 4.7a, among the shoreline change rates calculated by the three methods of analysis that we tested. Maximum accretion rates for each of the three methods are between 0.61

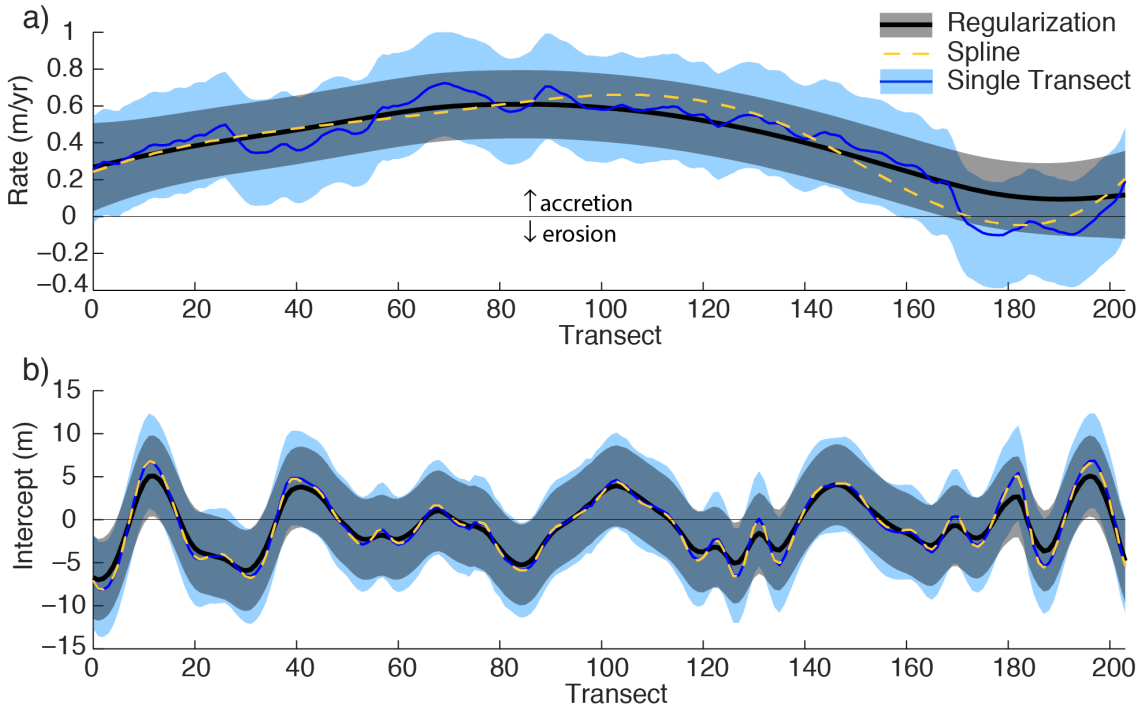

Figure 4.7 Shoreline change rates (a) and intercepts (b) calculated via three methods: 1) regularization, 2) B-spline basis function, and 3) single transect are shown surrounded by their 95% confidence bands. The confidence intervals for the spline method are similar in size to those for regularized-ST.

Table 4.2 For each method, the number of parameters Np or regression degrees of freedom *df* are given for rate and intercept. For the regularization method, the square of the regularization parameter γ is given in brackets. Minimum and maximum rates calculated by the different methods are given along with corresponding transect locations in brackets. The total change in area estimated by each model over years 1928-2005 are denoted by ΔArea. The overall bias in predicted change shows that both the regularization and spline models imposed biases toward net accretion, but the biases are not significant given the uncertainty in ΔArea.

	ST	Regularized-ST	Spline
Np_{rate} / df_{rate} [γ^2_{rate}]	204	5.5 [1.1×10^9]	6
Np_{int} / df_{int} [γ^2_{int}]	204	89 [8.0×10^5]	82
Max rate (m/yr) [transect]	0.61 [69]	0.72 [84]	0.66 [105]
Min rate (m/yr) [transect]	-0.10 [178]	0.09 [190]	-0.05 [183]
ΔArea ± std (m^2)	124,459 (± 44,649)	126,899 (± 35,852)	124,785 (± 37,440)
Bias (m^2)	--	2440	325
Bias/Area	--	0.0026	0.020

and 0.72 m yr^{-1} (Table 4.2), and are located near the center of the beach. Romine *et al*. (2009) analyzed Kailua Beach data using polynomial basis functions with similar results. This is consistent with the occurrence of seaward moving vegetated dunes that have formed on the ocean side of many coastal properties.

The regularized-ST rates are the smoothest alongshore. Because of this, the regularized-ST method is the only one whose long-term rates do not indicate erosion at Kailua Beach Park, located at the south end of the study area, from the Kaelepulu Stream to the Kailua boat ramp (transects 170-203). However, the 95% confidence intervals for these rates indicate the possibility of long-term erosion in this area. Erosion rates at the beach park were found to be minimal by the spline and ST methods, as illustrated by seventy-year model predictions (Figure 4.8). Short-term erosion since 2000 has occurred at Kailua Beach Park where trees have been undermined, leaving a scarp in the shorefront dune. Historic shorelines appear to be highly variable in this portion of the beach. Evidence of grading and redistribution of sediment in the area can be seen in past aerial

Figure 4.8 Seventy-year shoreline prediction for ST (cyan), spline (yellow), and regularized-ST (black). Ninety-five percent confidence bands are shown for the regularized-ST. The most recent (2005) shoreline (low water mark) is shown in dark blue for reference.

photographs. Recent attempts have been made to mitigate erosion at the park by placing sand, collected from Kaelepulu Stream mouth, onto the beach face fronting the park.

The maximum accretion rates for the three methods that we tested are all located within a stretch of shoreline (transects 69, 84, and 105) adjacent to a broad sand field at the head of a winding, and roughly shore-normal sand channel. Our analyses indicate that sediment is accumulating mostly near the head of the sand channel, but they do not tell us the alongshore direction of net sediment movement.

Noda (1989) found that Kailua Beach does not receive significant sand influx from neighboring shorelines because it is bounded by basalt and limestone. Harney and Fletcher (2003) found that less than 2% of the sediment that seasonally moves on and off of Kailua Beach is from modern sand production. Since accretion cannot be accounted for by new sediment production from the reef, Norcross, Fletcher, and Merrifield (2002) suggest that the source of accretion is found in offshore sand deposits. With the zone of maximum accretion found to be close to the sand channel, it is possible that offshore sand travels landward via the sand channel, and is deposited onto Kailua beach. Richmond *et al*. (2002) and Cacchione *et al*. (2002) documented onshore sediment transport within the sand channel during weak to moderate trade wind conditions; and offshore transport with stronger trade winds. They were unable to identify net annual or seasonal transport. Norcross, Fletcher, and Merrifield (2002) also found high shoreline variability in the alongshore direction which they propose is the result of seasonal wind and wave climates causing sand to move in alternating directions along the beach.

4.4.1 Method Comparison for Kailua Beach

Of the three modeling techniques that we tested, rates calculated by the single transect method vary the most, as expected, while the regularized rates and spline rates both have a significantly smoother, long wavelength signal alongshore (Figure 4.7). The most parsimonious spline model was found to have six basis functions for representing rates alongshore, consistent with the roughly six regression degrees of freedom for rates from the most parsimonious regularization model. This is reflected in the similar "smoothness" of the modeled rates alongshore (Figure 4.7a). However, the two methods

differ in the shape that the rates follow alongshore, especially toward the south end of the beach. In the spline model, each spline basis function (B-spline) has a prescribed shape that is scaled by a coefficient value. Figure 4.9 shows the six B-splines (not scaled) used

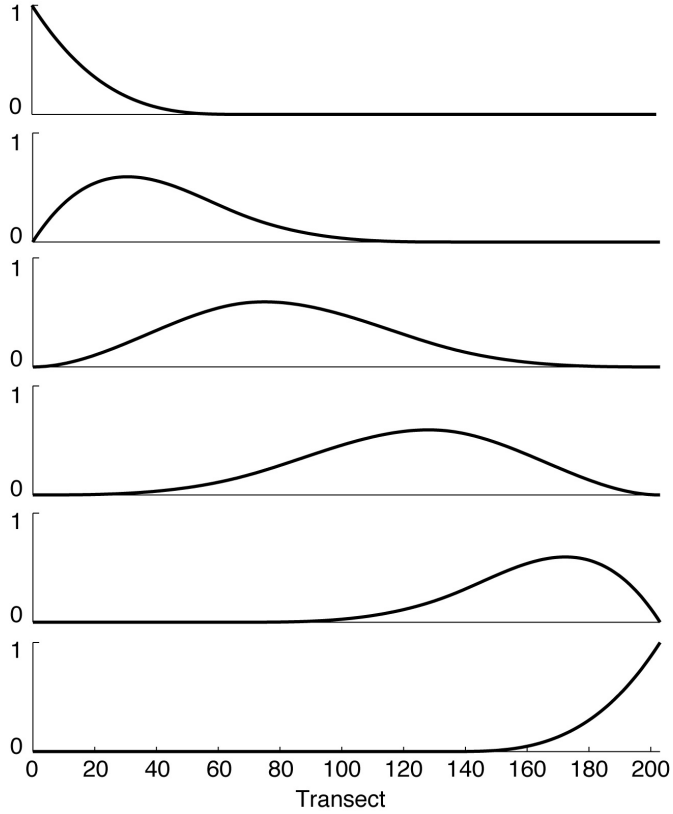

Figure 4.9 The six cubic B-splines (alongshore basis functions) used to represent rate parameters alongshore in the spline model.

in representing rates. The shape of each B-spline influences the final shape of the spline, and it can be seen that the B-splines near the ends are narrower than those toward the center. This has a noticeable effect on the final model when only a few B-splines are used, as in the Kailua Beach rates. The regularized rates, on the other hand, are not confined to any particular alongshore shape, but they are constrained to be smooth by constraining their second derivatives.

The intercept parameters (Figure 4.7b), which represent mean shoreline positions relative to the baseline, are better resolved in the alongshore direction, than are rates. Some of these fluctuations around the baseline can be linked to details in reef topography near the shoreline. For example, between transects 120 and 135, intercept values follow

a sinuous pattern which mimics the shape of the landward extent of the offshore reef (Figure 4.4 inset). Other deviations from the baseline may be due to persistent physical conditions in combination with reef topography that are not apparent in aerial photos, or simply due to noise inherent in the data. Given the large number of parameters allowed by the BIC in determining intercepts alongshore, reducing intercept parameters in the alongshore direction may provide only a small benefit as opposed to calculating an intercept at each transect. Anderson and Frazer (in review) found the same disproportionally high number of intercept parameters compared to rate parameters using B-splines when they analyzed shoreline data from Assateague Island and Ocean City, Maryland. This suggests that calculating the mean shoreline position at each transect and using this as a new baseline, as done by Frazer, Genz, and Fletcher (2009), simplifies the modeling process without greatly compromising model parsimony.

If both the regularization and spline models are permitted to have the maximum number of parameters, both will approach the ST model. Thus, we can use the difference between parsimonious shoreline model estimates and ST estimates as an indicator of the bias that has been traded for model simplicity. For each method, we hind-cast shoreline positions and calculate the total change in area over the 77-year time span of our data set (1928-2005). The formula for total area change is

$$\Delta A = \sum_{i=0}^{I-1} (\Delta x)(y_{i1} - y_{iJ}),$$

where Δx is the distance between transects (20 meters). The total area added to Kailua Beach between 1928 and 2005 is estimated at $1.24\ (\pm\ 0.46) \times 10^5$ m^2, $1.25\ (\pm\ 0.37) \times 10^5$ m^2, and $1.27\ (\pm\ 0.36) \times 10^5$ m^2 by the ST, spline, and regularization models, respectively. The bias in overall area for the spline method is 325 m^2; about 10 times smaller than the 2440 m^2 bias for the regularization method.

Upon inspection of the estimated rate parameters, the bias in the regularization model appears to be primarily due to rates showing more accretion at the southern end of the beach. Additionally, both of the bias values are significantly less than the standard

errors for each calculated total area, which were roughly 36,000 m^2. We do not believe that the positive bias indicates an overall accretionary bias in regularization methodology over all datasets, but rather it reflects the bias over a specific portion of shoreline that is known to be highly variable. Application of the regularization method to many datasets is needed to better assess bias.

Biases in intercept and rate both contribute to the resulting bias in the predicted shoreline location; but the influence of rate bias on a future shoreline location is significantly greater than that of the intercept. This is because change in shoreline position over time does not depend on the intercept parameter.

4.5 Discussion

4.5.1 Model Selection

Model selection is a very active area of research in which consensus is rare. Recent reviews are given by Claeskens and Hjort (2008), and Ando (2010). For selecting regularization parameters we tested the L-curve method (Aster, Borchers, and Thurber, 2012; Hansen and O'Leary, 1993), and well-known information criteria such as AIC (Burnham and Anderson, 2002). We also investigated the generalized cross-validation method (Golub, Heath, and Wahba, 1979; Wahba, 1990). None of them were entirely satisfactory when applied to the problem of this paper.

In the L-curve technique for selecting a regularization parameter one plots the misfit RSS against the roughness $||Lm||^2$ on a log-log scale (Aster, Borchers and Thurber 2012). This is done for a range of regularization parameters. The curve usually has an L-shape, and one selects the value of γ corresponding to the "corner" of this curve nearest the origin. We found the position of the corner was not always easily identifiable.

The generalized cross-validation equation (GCV) (Golub, Heath, and Wahba, 1979; Wahba, 1990) is also problematic because it depends on the assumption that noise is uncorrelated. Altman (1990) and Diggle and Hutchinson (1989) found that GCV performed poorly on data with correlated errors.

We find derivations of the AIC and its variants to be opaque (although we have used these variants in the past), and it is not clear to us how to apply AIC fairly to both the spline method and the regularization method. Also, most derivations of AIC appear to assume uncorrelated data errors, sometimes referred to as identically distributed independent (iid) data, which is clearly not the case for our problem. Accordingly, for this paper we derived our own information criteria from the first-principle Bayesian formalism of likelihood and prior (Appendix B). Our BIC_1 is a version of the Schwartz BIC (Schwartz 1978), but without the assumption of iid data (Robert, 2007, p. 352).

Cross-validation splits the data, often into multiple groups, and uses one portion of the data as the validation data and the remaining portions as training data (*e.g.*, Hastie, Tibshirani, and Friedman, 2009). A measure of model error is calculated based on the discrepancy between model estimates from the validation data and the training data. Cross-validation will select the model with the smallest error. This is a nonparametric method, so there are no assumptions about the distribution of data errors. However, it can be computer-intensive (hours on a desktop workstation) depending on the way data are split into groups. If computing power is not an issue, cross-validation appears to provide an adequate method for shoreline model selection, an alternative to the BIC formulas we use.

4.5.2 Practical Issues in Applying Different Methods

The regularization method and basis function methods have some interesting parallels, as well as notable differences in application; Table 4.3 summarizes the differences in the methods. The basis functions that have been previously applied to shoreline studies are Legendre polynomials, trigonometric functions (sinusoids), principal components (eigenbeaches), and cubic B-splines. Continuous uncomplicated sandy shorelines can be nicely represented using any of the basis functions or regularization. Shorelines reflecting uneven variation in rates alongshore, typically due to complex offshore topography, complicate the application of parsimonious methods. Pacific island shorelines, especially, tend to be naturally complex due to the intricate fringing reefs that

surround most of them. Shorelines everywhere are susceptible to construction of jetties, piers, and other features that alter long-term shoreline trends on small spatial scales.

Frazer, Genz, and Fletcher (2009) illustrate how both Legendre polynomials and trigonometric functions cause alongshore ringing in calculated shoreline change rates due to an alongshore discontinuity in actual trends. The alongshore discontinuity in their example was a point of rapid accretion that caused rates to appear like a delta function alongshore. This could also happen on a shoreline at the location of a pier, jetty, or small rocky outcrop. Principal components regression (eigenbeaches) easily accommodates alongshore discontinuities, but as data are used in calculating the principal components, they are contaminated by noise and, traditional parametric methods of estimating uncertainty are inappropriate. A nonparametric method, such as the bootstrap should be used to estimate model parameter uncertainty.

Alongshore discontinuities can be accommodated in a straightforward way with cubic B-splines, but extra care must be taken; because if a discontinuity is allowed, additional knots must be placed at the discontinuity (deBoor 1978): one extra knot for a discontinuity in the second derivative, two extra knots for a discontinuity in the first derivative and three extra knots for a discontinuity in rate. In regularized-ST, a discontinuity in the alongshore derivative of rate is allowed by removing a single row of the second derivative matrix L; to allow a jump in rate, the rows corresponding to the transects that bracket the discontinuity are removed. The BIC_1 formula for use with splines remains the same for models with and without discontinuities. However, if one wishes to compare models with and without discontinuities, extra terms corresponding to the pseudo-determinant of L must be retained in BIC_2 (see Appendix B).

Although B-splines and regularization both provide flexibility in the amount of variation allowed in parameters alongshore, we find that regularization is easier to apply. Selecting the most parsimonious model with B-splines depends on equal knot spacing, so adding extra knots at a particular alongshore position disrupts the knot spacing on either side. Model complexity in regularization relies only on the regularization parameters, so variations in alongshore smoothing have no effect on those parameter.

Table 4.3 The effects of using different basis functions on model estimates.
*Eigenbeaches basis functions are not independent of the data; additional care is required for selecting a parsimonious number of basis functions (*e.g.*, cross-validation)
**Requires modifying second derivative matrix L to circumvent Gibbs effect
***Requires careful knot placement to circumvent Gibbs effect
C_{dd} corr. – covariance matrix must account for spatially correlated errors
Nonparametric – requires nonparametric estimation method (*e.g.*, bootstrap)

	Method	Parsimonious	Defined Everywhere?	Gibbs Effect	Error Est. Issues
	ST	N	N	N	Independent
	Regularized ST	Y	N	N**	C_{dd} corr.
Basis Functions	Spline (B-splines)	Y	Y	N***	C_{dd} corr.
Basis Functions	Polynomial (Legendre, Trigonometric)	Y	Y	Y	C_{dd} corr.
Basis Functions	Eigenbeaches (Principal components)	Y*	N	N	C_{dd} corr.; Nonparametric

Another consideration when analyzing shoreline data is the extent of the region from which shorelines are included in a single regression analysis. Using Legendre functions or trigonometric functions requires sections of the beach that are discontinuous alongshore to be analyzed separately because these basis functions are ineffective in representing alongshore discontinuities. If those sections are located in separate littoral cells, separate analysis is probably desirable anyway because the two beaches may have different natural smoothing in the alongshore direction. Conversely, if the beaches are located in the same littoral cell and separated by a feature such as a river mouth, or if the analysis is focused on identifying a dominant degree of smoothing or aperture of variation over a large region then simultaneous regression of all data is beneficial. In those cases, we believe that B-splines or regularization are the most accurate, although principal component regression may also provide interesting information about the region, depending on the focus of the analysis.

As mentioned above in the introduction, our focus is on methods that provide information about long-term trends in shoreline change for long-term planning purposes. An obvious, but often overlooked, aspect of shoreline change modeling is the practicality of applying the results of scientific studies to planning initiatives. Although the efficacy of scientific results adopted in non-scientific arenas is not the focus of this paper, it is worth mentioning that the simplicity of a model can impact its usability. When shoreline change statistics are used to determine the setback for building structures, coastal decision-makers and coastal property owners naturally take great interest in how that setback is determined, especially given the relatively high market value of coastal properties. The continuing wide application of the single transect method is therefore not surprising, because it is relatively easy to understand and explain, while the concept of basis function expansions can be difficult to explain. Its connection with ST may thus make regularized-ST the most palatable method for planning applications.

4.5.3 Unknown Variance

For some shoreline data sets the data errors are unknown or uncertain. In these situations, a best-estimate scaling factor is typically used to estimate the amplitude of predicted error, based on the data residuals. For example, Anderson and Frazer (in review) modeled the data covariance matrix as $C_d = \alpha \tilde{C}_d$ where α is the best-estimate constant of proportionality that scales $\tilde{C}_d$, the estimated covariance structure matrix, weighted by *a priori* uncertainty estimates (the covariance matrix used in this paper). For unregularized models, such as the spline model, the best estimate of α is

$$\hat{\alpha} = (d - G\hat{m})^T \hat{C}_{dd}^{-1} (d - G\hat{m}) / (N - df),$$

where *df* is the regression degrees of freedom (Eqn. 4.16). It is possible to estimate α when using regularization, but the calculation is not straightforward because the best-fit model parameters depend on α, and one must iterate to find both the value of α and the value of the parameters.

We tested this procedure on our Kailua Beach data, and found that the α was always less than, but close to, one, regardless of how much smoothing was imposed on the model. This indicates that the estimated *a priori* errors slightly exceed the data errors estimated from the data residuals, and so it is conservative to use the *a priori* errors.

4.6 Conclusion

A regularization technique for modeling long-term shoreline change in a parsimonious manner is presented and compared with the ST and B-spline methods. The technique is demonstrated on historic shoreline data from Kailua, Hawaii. The analysis of Kailua Beach data indicates long-term accretion of Kailua Bay focused near the opening of a sand-filled channel toward the center of the beach, consistent with previous studies of the area (Noda, 1989; Norcross, Fletcher, and Merrifield, 2002; Romine *et al.,* 2009). There is general agreement between the three methods tested. Both the spline and regularized-ST methods (parsimony methods) produce shoreline change rates that are smooth alongshore, compared to ST. The parsimony methods both used about six parameters to characterize the variation in rates alongshore. On the other hand, intercept parameters estimated by the parsimony methods showed much higher alongshore variation, compared to rates, and closely resembled those calculated by ST. This phenomenon, also seen in data analysis of Assateague Island and Ocean City, MD, (Anderson and Frazer, in review) suggests that there is little benefit in attempting to reduce the number of intercept parameters. While the variation in rates and intercepts alongshore in the spline model were influenced by the shape of individual basis functions, the regularized rates and intercepts appeared to "trim the hills and fill the valleys" as a result of the smoothing constraints.

Two Bayesian Information Criteria are presented for selecting the most parsimonious model: one for selecting the appropriate regularization parameters in regularized-ST, the other for selecting the suitable number of basis functions for basis function methods. The BIC provides an objective model selection criterion for data with correlated noise.

In applying basis function and regularization methods, spline basis functions (B-splines), principal component regression, and regularization methodologies provide the most flexibility in handling alongshore discontinuities often seen in shoreline behavior. Principal component regression was not favored because its basis functions include noise from the data and it requires nonparametric methods of estimating uncertainty. For shorelines with discontinuities, the model selection process for regularized-ST is easier to code than the B-spline method. Finally, the way that regularization imparts varying degrees of smoothness to alongshore rates may be easier to explain to clients than the action of basis functions, making it a practical choice for use in long-term planning.

4.7 Appendix A. Estimating Data Correlation

The covariance structure matrix C_{corr} is estimated by an iterative process following the procedure presented Chapter Three. We start by setting C_{corr} to the identity matrix. We weight C_{corr} by the data errors (Eqn. 4.14) to form the first covariance matrix. The covariance matrix is then used in the least squares procedure to find the model parameter vector. We subsequently calculate the vector of fitted data (Eqn. 4.8). The fitted data is used to produce residuals; defined as $\rho_{ij} = \hat{d}_{ij} - d_{ij}$, the difference between the fitted data and the observed data. Subscripts *i* and *j* are alongshore location indices and time indices, respectively. We estimate the autocorrelation function of the residuals and use it to construct the correlation matrix C_{corr} using the following equation

$$c_{ii'jj'} = \left(\sum_j \sum_i \rho_{i,j}^2\right)^{-1} \sum_{j=1}^{J} \sum_{k=1}^{I-|i'-i|} \rho_{k,j}\rho_{k+|i'-i|,j} \cdot \delta_{jj'}, \qquad (4.A1)$$

in which *i* and *i'* are location indices, *j* and *j'* are time indices, and $\delta_{jj'}$ is the Kronecker delta used to enforce our assumption that data are not correlated in time. Matrix entries are damped with the taper function

$$T\left(\left|i'-i\right|\right)=\cos^{l}\frac{\pi\left|i'-i\right|}{2(I-1)} \tag{4.A2}$$

to ensure that the matrix is positive definite. The rate of decay for this function is controlled by l. We tried l = 3,6, and 10 for selected combinations of regularization parameters and found that they all produced nearly identical parameter vectors. We used l = 6, which causes the correlation to go nearly to zero by about lag 3/4 I. In all cases, the correlation matrix has ones along the diagonal and entries decline in size with distance from the diagonal.

We repeat the process, beginning with weighting the new correlation matrix by the data errors to produce the next covariance matrix estimate. This process is repeated until correlation matrices from successive iterations are sufficiently close. Our stopping criterion is $\left\|C_{corr}^{(u)}-C_{corr}^{(u-1)}\right\|_2<10^{-3}\left\|C_{corr}^{(u-1)}\right\|_2$ where u is the number of iterations and $\|\cdot\cdot\|_2$ denotes the matrix 2-norm, also called the spectral norm. Depending on the regularization parameter, two to three iterations are required for convergence.

The correlation matrix estimated in the procedure explained above depends on the regularization parameters. To select the particular correlation matrix to use in our study, we estimate correlation matrices for a range of regularization parameters that give results similar to ST at the lower limit and alongshore-linear behavior at the upper limit. We then use the BIC, as explained in the main text and Appendix B, to select the appropriate pair of regularization parameters (one each for rate, intercept). The correlation matrix that is generated with the selected regularization parameters is used in the final analysis.

4.8 Appendix B. Bayesian Information Criteria

We take a Bayesian approach to model selection, and determine the appropriate model by maximizing the posterior probability of a model given the data. Our Bayesian Information Criterion (BIC) is defined as

$$\mathrm{BIC}=-2\ln(p(\psi\,|\,y)) \tag{4.B1}$$

where $p(\psi \mid y)$ is the posterior probability of model ψ given data vector y. Thus, the model with the maximum posterior probability is the one whose BIC score is the minimum of all candidate model scores.

To find the posterior probability, we begin with

$$p(\psi,m,y) = p(\psi,m,y), \tag{4.B2}$$

the joint distribution of ψ, y, and parameter vector m. Applying Bayes' Theorem to both sides gives

$$\begin{aligned} p(\psi,m \mid y)p(y) &= p(y \mid \psi,m)p(\psi,m) \\ &= p(y \mid \psi,m)p(m \mid \psi)p(\psi). \end{aligned} \tag{4.B3}$$

Integration of (4.B3) over the parameter vector m and division by $p(y)$ gives

$$p(\psi \mid y) = p(y)^{-1} p(\psi) \int p(y \mid \psi,m)p(m \mid \psi)dm. \tag{4.B4}$$

We assume $p(y)$ is constant over all models, so (4.B4) becomes

$$p(\psi \mid y) \propto p(\psi) \int p(y \mid \psi,m)p(m \mid \psi)dm. \tag{4.B5}$$

Two versions of the BIC are presented here: BIC_1 for spline models, and BIC_2 for regularized-ST. (More accurately, BIC_1 is applicable to any basis function model that is not regularized, and BIC_2 is applicable to any basis function model that is regularized; recall that ST can be regarded as a basis function model with delta-like basis functions.) As mentioned above, the residual sum of squares RSS is the same in both ICs:

$$\mathrm{RSS} = (y - G\hat{m})^T C_{dd}^{-1} (y - G\hat{m}), \tag{4.B6}$$

in which y is the data vector, G is the system matrix, $\hat{m}$ is the maximum likelihood estimate of the model parameter vector m, and C_{dd} is the data covariance matrix.

4.8.1 BIC$_1$: Basis Function Models

When using basis functions, the model system matrix G has M basis functions, one in each column. We identify a model by its system matrix G, so we substitute G for ψ in (4.B5). The posterior probability of G, given data y is then

$$p(G \mid y) \propto p(G) \int p(y \mid m,G)\, p(m \mid G)\, dm\,. \tag{4.B7}$$

Here, $p(y \mid m,G)$ is the likelihood function by which y is normally distributed with mean Gm and covariance C_{dd}:

$$p(y \mid m,G) = \frac{\exp\left(-\phi(m)\right)}{(2\pi)^{N/2}\left|C_{dd}\right|^{1/2}} \tag{4.B7}$$

where

$$\phi(m) = 2^{-1}(y - Gm)^T C_{dd}^{-1}(y - Gm)\,. \tag{4.B8}$$

Expanding $\phi(m)$ about $\hat{m}$ gives

$$\phi(m) = \phi(\hat{m}) + 2^{-1}(m - \hat{m})^T C_{mm}^{-1}(m - \hat{m}) \tag{4.B9}$$

where $C_{mm} = (G^T C_{dd}^{-1} G)^{-1}$ and $\hat{m} = C_{mm} G^T C_{dd}^{-1} y$. We choose a parameter prior $p(m \mid G)$ that is independent of G and define it formally as the limit $p(m \mid G) = \lim_{\sigma_0 \to \infty} \exp(-(2\sigma_0^2)^{-1} m^T m)$. We choose a model prior $p(G) = (2\pi)^{-K/2}$, where K is the number of columns in G. Both priors are improper, being chosen for

convenience and for consistency with BIC_2 to be derived below. The posterior probability can now be written as

$$p(G \mid y) \propto \frac{\exp\left(-\phi(\hat{m})\right)}{(2\pi)^{K/2}(2\pi)^{N/2}\left|C_{dd}\right|^{1/2}} \int \exp\left(-2^{-1}(m-\hat{m})^T C_{mm}^{-1}(m-\hat{m})\right) dm \,. \quad (4.B10)$$

The integral in (4.B10) can be simplified by noticing that

$$\int \frac{\exp\left(-2^{-1}(m-\hat{m})^T C_{mm}^{-1}(m-\hat{m})\right)}{(2\pi)^{K/2}\left|C_{mm}\right|^{1/2}} dm = 1 \quad (4.B11)$$

because $(2\pi)^{-N/2}\left|C_{mm}\right|^{-1/2} \exp\left(-2^{-1}(m-\hat{m})^T C_{mm}^{-1}(m-\hat{m})\right)$ is the normal distribution of m with mean $\hat{m}$ and covariance C_{mm}, and the integral of a distribution is equal to one. Equation (4.B10) can now be written as

$$p(G \mid y) \propto \frac{\exp\left(-2^{-1}(y-G\hat{m})^T C_{dd}^{-1}(y-G\hat{m})\right)}{(2\pi)^{N/2}\left|C_{dd}\right|^{1/2}\left|C_{mm}\right|^{-1/2}} \quad (4.B12)$$

The BIC_1 is then

$$\begin{aligned} \mathrm{BIC}_1 &= -2\ln p(G \mid y) \\ &= (y-G\hat{m})^T C_{dd}^{-1}(y-G\hat{m}) + \ln\left|C_{mm}^{-1}\right| + \ln\left|C_{dd}\right| + \text{constant} \,. \\ &= \mathrm{RSS} + \ln\left|C_{mm}^{-1}\right| + \ln\left|C_{dd}\right| + \text{constant} \end{aligned} \quad (4.B13)$$

Our procedure assumes that the data covariance matrix is constant, so after discarding constant terms, the BIC_1 becomes

$$\mathrm{BIC}_1 = \mathrm{RSS} + \ln\left|C_{mm}^{-1}\right| . \quad (4.B14)$$

When the data covariance must be estimated from the data, instead of being given *a priori*, we retain the term $\ln|C_{dd}|$.

4.8.2 BIC_2: Regularization Models

We first treat the case of a single regularization parameter γ. The family of models is then most conveniently indexed by γ^2; substituting γ^2 for ψ in (4.B5) gives the posterior probability of γ^2 given data *y*:

$$p(\gamma^2 \mid y) \propto p(\gamma^2) \int p(y \mid m)\, p(m \mid \gamma^2) dm. \tag{4.B15}$$

Here the likelihood $p(y \mid \gamma^2, m)$ may be written $p(y \mid m)$ because γ does not appear in the likelihood equation. As in BIC_1, $p(y \mid m)$ is the likelihood by which *y* is normally distributed with mean *Gm* and covariance C_{dd}:

$$p(y \mid m) = \frac{\exp\left(-2^{-1}(d-Gm)^T C_{dd}^{-1}(d-Gm)\right)}{(2\pi)^{N/2}\left|C_{dd}\right|^{1/2}}.$$

The parameter prior $p(m \mid \gamma^2)$ is the distribution that constrains the model to be smooth. It is a degenerate normal distribution (e.g., Anderson 1958, Chapter 2)

$$p(m \mid \gamma^2) = \frac{\gamma^{K(L)} \exp(-2^{-1}\gamma^2 m^T L^T L m)}{(2\pi)^{K(L)/2} \prod\nolimits' |\lambda_i|_+} \tag{4.B16}$$

in which *L* is a roughening operator, usually the second derivative matrix (equation 4.3); $K(L)$ is the rank of *L,* i.e., the number of nonzero singular values of *L*, which is $M-2$ if *L* is the second derivative operator (recall that *M* is the length of the parameter vector); and $\prod' |\lambda_i|_+$ is the product of those nonzero singular values. Then,

$$p(y \mid m)\, p(m \mid \gamma^2) = \frac{\gamma^{K(L)} \exp\left(-\phi(m,\gamma^2)\right)}{(2\pi)^{(N+K(L))/2} \left|C_{dd}\right|^{1/2} \prod \left|\lambda_i\right|_+} \tag{4.B17}$$

where

$$\phi(m,\gamma^2) = 2^{-1}(y - Gm)^T C_{dd}^{-1}(y - Gm) + 2^{-1}\gamma^2 m^T L^T L m\,. \tag{4.B18}$$

Expanding $\phi(m,\gamma^2)$ about $\hat{m}$ gives

$$\phi(m,\gamma^2) = \phi(\hat{m},\gamma) + 2^{-1}(m - \hat{m})^T C_{mm}^{-1}(m - \hat{m}) \tag{4.B19}$$

where $\hat{m}$ and C_{mm} are defined in equations (4.6) and (4.7) respectively. Then, the integral of (4.B17) over *m* is

$$\int p(y \mid m)\, p(m \mid \gamma^2) dm = \frac{\gamma^{K(L)} \exp\left(-\phi(\hat{m},\gamma)\right)}{(2\pi)^{(N+K(L))/2} \left|C_{dd}\right|^{1/2} \prod \left|\lambda_i\right|_+} \int \exp\left(-2^{-1}(m - \hat{m})^T C_{mm}^{-1}(m - \hat{m})\right) dm$$

$$= \frac{\gamma^{K(L)} \exp\left(-\phi(\hat{m},\gamma)\right) \left|C_{mm}\right|^{1/2}}{(2\pi)^{(N+2)/2} \left|C_{dd}\right|^{1/2} \prod \left|\lambda_i\right|_+}$$

by noticing that the integral of a normal distribution over *m* is equal to one, as in (4.B11).

Including the prior for γ^2, $p(\gamma^2) = \gamma^{-2}$, the non-informative Jeffreys prior, the probability of γ^2 given *y* can now be written as

$$p(\gamma^2 \mid y) \propto \frac{\gamma^{K(L)-2} \exp\left(-2^{-1}(y - Gm)^T C_{dd}^{-1}(y - Gm) - 2^{-2}\gamma^2 m^T L^T L m\right) \left|C_{mm}\right|^{1/2}}{(2\pi)^{(N+2)/2} \left|C_{dd}\right|^{1/2} \prod \left|\lambda_i\right|_+}\,. \tag{4.B20}$$

The BIC_2 is then

$$
\begin{aligned}
\mathrm{BIC}_2 &= -2\ln p(\gamma^2 \mid y) \\
&= (y - G\hat{m})^T C_{dd}^{-1}(y - G\hat{m}) + \gamma^2 \hat{m}^T L^T L\hat{m} + \ln\left|C_{mm}^{-1}\right| - 2\big(K(L)-2\big)\ln(\gamma) \\
&\qquad + \ln\left|C_{dd}\right| + \sum \left|\lambda_i\right|_+ + \text{constant} \\
&= \mathrm{RSS} + \gamma^2 \hat{m}^T L^T L\hat{m} + \ln\left|C_{mm}^{-1}\right| - 2\big(K(L)-2\big)\ln(\gamma) \\
&\qquad + \ln\left|C_{dd}\right| + \sum \left|\lambda_i\right|_+ + \text{constant}.
\end{aligned}
\tag{4.B21}
$$

If we are comparing only models that have the same data covariance matrix C_{dd} and roughening operator L, the terms on the third (and fifth) line of (4.B21) do not change. Thus, after discarding constant terms, we have the BIC_2 in the form

$$
\mathrm{BIC}_2 = \mathrm{RSS} + \gamma^2 \hat{m}^T L^T L\hat{m} + \ln\left|C_{mm}^{-1}\right| - 2\big(K(L)-2\big)\ln(\gamma). \tag{4.B22}
$$

When the data covariance must be estimated from the data, instead of being given *a priori*, we would retain the term $\ln\left|C_{dd}\right|$. More important, if we are comparing models with different roughness operators, we must retain the term $\sum \left|\lambda_i\right|_+$, the logarithm of the pseudo-determinant of L. The roughness matrix will change, for example, if we choose not to penalize roughness over a particular alongshore interval, and therefore discard the rows corresponding to transects in that interval. In general, the transect number of a row is the number of the column in which the value -2 appears. For example, in equation 4.3, the first row gives the roughness (second derivative) at transect 2, and the second row gives the roughness at transect 3.

4.8.2.1 Two Regularization Parameters

In our shoreline problem we smooth the rate and intercept parts of the model separately, so the prior $p(m \mid \gamma^2)$ is replaced by $p(r \mid \gamma_r^2)p(b \mid \gamma_b^2)$ where each factor has the form (4.B16). As rate and intercept parameters occur in pairs, the second derivative matrix is the same for both r and b, with rank $K(L) = M/2 - 2$. However, the derivation

is clearer if we allow the two roughness operators to be distinct, L_r and L_b, say. Proceeding as above gives

$$\begin{aligned}\mathrm{BIC}_2 &= -2\ln p(\gamma_r^2,\gamma_b^2 \mid y) \\ &= \mathrm{RSS} + \ln\left|C_{mm}^{-1}\right| + \gamma_r^2\,\hat{r}^T L_r^T L_r\,\hat{r} - 2\big(K(L_r)-2\big)\ln(\gamma_r) \\ &\quad + \gamma_b^2\,\hat{b}^T L_b^T L_b\,\hat{b} - 2\big(K(L_b)-2\big)\ln(\gamma_b) \\ &\quad + \ln\left|C_{dd}\right| + \sum\left|\lambda_i^{(r)}\right|_+ + \sum\left|\lambda_i^{(b)}\right|_+ + \text{constant}.\end{aligned} \tag{4.B23}$$

In our problem, the roughness operators are the same and do not change, and C_{dd} does not change, so discarding the last line of (4.B23) and collecting terms gives BIC_2 as in equation (4.B22).

Chapter 5
CONCLUDING REMARKS AND FUTURE DIRECTIONS

In this dissertation, shoreline response to a storm was investigated and two new shoreline change methods were introduced. In Chapter Two, analysis of Assateague Island data suggests that storm-induced shoreline change can be modeled as the sum of a transient component that is recovered in a few years and a component that persists until sediment is mobilized by a subsequent storm. This suggests that long-term shoreline change may be coarsely modeled as the cumulative sum of persistent storm components. Since long-term datasets do not have the temporal resolution to model each storm, it is probably best model such data with a trend and transient storm component only. Transient-persistent modeling may be used to generate a rough estimate of long-term rate in short-term, temporally dense shoreline data containing a storm by taking the persistent component from the storm and dividing it by the expected time interval between storms.

In Chapter Three, alongshore correlation in shoreline change prediction is addressed by using a linear combination of B-splines to represent spatial variations of model parameters. In addition to model parsimony, proper treatment of correlated noise was investigated because differences in noise handling techniques affect mean parameter estimates, as well as estimated uncertainties. Correlated noise was best addressed by including a full covariance matrix in the regression model, constructed iteratively from data residuals.

In Chapter Four, a second order Tikhonov regularization technique for modeling long-term shoreline change in a parsimonious manner is presented and compared with the ST and B-spline methods. There is general agreement between the three methods tested, but both the spline and regularized-ST methods (parsimony methods) produce shoreline change rates that are smooth alongshore, compared to ST. On the other hand, intercept parameters estimated by the parsimony methods closely resembled those calculated by ST, suggesting that there is little benefit in attempting to reduce the number of intercept

parameters. The regularized-ST and B-spline methods both provide flexibility in handling alongshore discontinuities often seen in shoreline behavior, but the regularized-ST method may be a more practical choice for use in long-term planning because it is more straightforward to implement and easier to explain to clients.

The work in this dissertation addresses some deficiencies in shoreline change modeling, yet there remains room for improving shoreline analysis and long-term prediction. For example, an inherent limitation in applying long-term historical data trends as a means for indicating future shorelines is that it relies on an underlying assumption that shorelines will continue to behave the same way as they have in the past. This is not necessarily the case. Climate-induced sea level rise is expected to alter historical rates of relative sea level change on a global scale, and future improvements of climate and sea level models may provide regionally specific estimates of sea level rise. A commonly used method for predicting potential shoreline recession due to increased sea level is the Bruun rule (Bruun, 1962, 1988). Considerable controversy exists in the literature as to the efficacy of the Bruun rule (*e.g.*, Thieler *et al.*, 2000; Cooper *et al.*, 2004), so there is a need to understand how better to apply it to different coastal regimes. There is also scope for combining the Bruun rule with historical change rates, perhaps by using the probability calculus of Tarantola and Valette (1982)

Another limitation of the simple cross-shore analysis methods presented here is that they give no indication of the direction that sediment is moving, as noted in the Kailua Beach study; they only identify a change in shoreline position in the cross-shore direction. A natural progression in methodology will be to correlate historic shoreline data with physical drivers such as wave energy. Miller and Dean (2004), Yates *et al.* (2003), and Davidson *et al.* (2013) begin this work by correlating wave and water level data to the distance of shorelines from an equilibrium position. Identifying the equilibrium position is problematic in these methods, but it is a starting point for future research. For example, the concept of relaxation to an equilibrium shoreline could also be extended to include alongshore relaxation in addition to time relaxation. Dean (2002) discusses alongshore relaxation methods used in determining the feasibility of beach

nourishment projects. These methods are mostly variations of the Pelnard-Considère (1956) diffusion equation.

Future advances in shoreline detection and innovative methodologies will undoubtedly contribute to improved analyses.

REFERENCES

Altman, N.S. (1990), Kernel smoothing of data with correlated errors, *Journal of the American Statistical Association*, 85(411), 749-759.

Anderson, T.R., L.N. Frazer, and C.H. Fletcher (2010), Transient and persistent shoreline change from a storm, *Geophysical Research Letters*, 37, L08401.

Anderson, T.W. (1958), *An Introduction to Multivariate Statistical Analysis*, John Wiley and Sons.

Ando, T. (2010), *Bayesian Model Selection and Statistical Modeling,* Chapman and Hall.

"Assateague Island National Seashore North End Restoration Project Timeline," *Assateague Island National Seashore Research in the Park*, National Park Service, 2006, web, August 1, 2009.

Aster, R.C., B. Borchers, and C.H. Thurber (2012), *Parameter Estimation and Inverse Problems, 2nd edition*, Academic Press.

Bauer, B.O. and J.R. Allen (1995), Beach steps: an evolutionary perspective, *Marine Geology*, 123, 143-166.

Bayley, G.V. and J.M. Hammersley (1946), The "Effective" Number of Independent Observations in an Autocorrelated Time Series, *Supplement to the Journal of the Royal Statistical Society*, 8(2), 184-197.

Becker, J.M. Y.L. Firing, J. Aucan, R. Holman, M. Merrifield, and G. Pawlak (2007), Video-based observations of nearshore sand ripples and ripple migration, *Journal of Geophysical Research*, 112, C01007.

Birkemeier, W. A. (1979), The effects of the 19 December 1977 coastal storm on beaches in North Carolina and New Jersey, *Shore Beach*, *47*, 7–15.

Box, G.E.P. (1954), The Exploration and Exploitation of Response Surfaces: Some General Considerations and Examples, *Biometrics*, 10(1), 16-60.

Box, G.E.P. and G.C. Tiao (1973), *Bayesian Inference in Statistical Analysis,* Redding, Massachusetts: Addison-Wesley.

Box, G.E.P., G.M. Jenkins, and G.C. Reinsel (1994), *Time Series Analysis: Forecasting and Control. 3rd Ed.,* Upper Saddle River, New Jersey: Prentice-Hall.

Bracewell, R.N. (2000), *The Fourier Transform and Its Applications, 3rd ed.,* New York: McGraw-Hill.

Buckland, S.T., K.P. Burnham, and N.H. Augustin (1997), Model selection: an integral part of inference, *Biometrics*, 53, 603-618.

Burnham, K.P. and D.R. Anderson (2002), *Model Selection and Multimodel Inference,* 2nd edition, New York: Springer-Verlag.

Buttolph, A.M., W.G. Grosskopf, G.P. Bass, and N.C. Kraus (2006), Natural Sand Bypassing and Response of Ebb Shoal to Jetty Rehabilitaion, Ocean City Inlet, MD, USA, *Proceedings 30th Coastal Engineering Conference,* World Scientific Press, 3.344-3.356.

Cacchione, D.A., B.R. Richmond, P. Howd, and M. D'Iorio (2002), Sand transport within a reef channel off Kailua, Oahu, Hawaii, *AGU Ocean Sciences Meeting,* Honolulu, Hawaii.

Claeskens, G. and N.L. Hjort (2008), *Model Selection and Model Averaging,* Cambridge University Press.

Cooper, J., G. Andrew, and O.H.Pilkey (2004), Sea-level rise and shoreline retreat: time to abandon the Bruun Rule, *Global and planetary change*, 43(3), 157-171.

Crowell, M., B.C. Douglas, S.P. Leatherman (1997), On Forecasting Future U.S. Shoreline Positions: A Test of Algorithms, *J. Coastal Res., 13***,** 1245–1255.

Crowell, M., M. Honeycutt, and D. Hatheway (1999), Coastal Erosion Hazards Study: Phase One Mapping. *Journal of Coastal Research,* Special Issue 28, 10-20.

Crowell, M., S.P. Leatherman, and M.K. Buckley (1991), Historical shoreline change: error analysis and mapping accuracy, *J. Coastal Res., 7***,** 839–852.

Crowell, M., S.P. Leatherman, and M.K. Buckley (1993), Shoreline Change Rate Analysis: Long Term Versus Short Term Data, *Shore and Beach,* 61(2), 13-20.

Dail, H.J., M.A. Merrifield, and M. Bevis (2000), Steep beach morphology changes due to energetic wave forcing, *Marine Geology*, 162(2-4), 443-458.

Davidson, M.A., R.P. Lewis, and I.L. Turner (2010), Forecasting seasonal to multi-year shoreline change, *Coastal Engineering*, 57(6), 620-629.

Davidson, M.A., K.D. Splinter, and I.L. Turner (2013), A simple equilibrium model for predicting shoreline change, *Coastal Engineering,* 73, 191-202.

de Boor, C. (1978), *A Practical Guide to Splines*, New York: Spinger-Verlag.

Dean, R.G. (1991), Equilibrium Beach Profiles: Characteristics and Applications, *Journal of Coastal Research*, 7(1), 53-84.

Dean, R.G. (2002), *Beach nourishment: Theory and Practice*, World Scientific, Singapore.

Dean, R.G. and M. Perlin (1977), Coastal engineering study of Ocean City Inlet, Maryland, *Proceedings Coastal Sediments '77*, ASCE, Reston, Virginia, 520-540.

Dean, R.G. and S.B. Malakar (1999), Projected Flood Hazard Zones in Florida, *Journal of Coastal Research,* Special Issue 28, 85-94.

Diggle, P.J. and M.F. Hutchinson (1989), On spline smoothing with autocorrelated errors, *Australian Journal of Statistics*, 31(1), 166-182.

Dolan, R., M.S. Fenster, and S.J. Holme (1991), Temporal Analysis of Shoreline Recession and Accretion, *Journal of Coastal Research*, 7(3), 723-744.

Dosso, S.E., P.L. Neilsen, and M.J. Wilmut (2006), Data error covariance in matched-field geoacoustic inversion, *Acoustical Society of America*, 119(1), 208-219.

Douglas, B. C., M. Crowell, and S. P. Leatherman (1998), Considerations for shoreline position prediction, *J. Coastal Res.*, *14*, 1025–1033.

Douglas, B. C., and M. Crowell (2000), Long-term shoreline position prediction and error propagation, *J. Coastal Res.*, *16*, 145–152.

Fenster, M.S., R. Dolan and J.F. Elder (1993), A new method for predicting shoreline positions from historical data, *Journal of Coastal Research*, 9(1), 147-171.

Fenster, M.S., R. Dolan, and R.A. Morton (2001), Coastal Storms and Shoreline Change: Signal or Noise? *Journal of Coastal Research*, 17(3), 714-720.

Field, M. E. (1979), Sediments, shallow subbottom structure, and sand resources of the inner continental shelf, Central Delmarva Peninsula, CERC-TP-79-2, U.S Army Engineer Waterways Experiment Station, Vicksburg, MS.

Fletcher, C. H., J. J. B. Rooney, M. Barbee, S.-C. Lim, B. M. Richmond (2003), Mapping Shoreline Change Using Digital Orthophotogrammetry on Maui, Hawaii, *J. Coastal Res., Special Issue 38*, 106–124.

Ford, M. (2013), Shoreline changes interpreted from multi-temporal aerial photographs and high resolution satellite images: Wotje Atoll, Marshall Islands, *Remote Sensing of Environment*, 135, 130-140.

Frazer, L.N., A. S. Genz, and C.H. Fletcher (2009a), Toward parsimony in shoreline change prediction I: methods, *J. Coastal Res., 25*, 366–379.

Frazer, L.N., T. R. Anderson, and C.H. Fletcher (2009b), Modeling storms improves estimates of shoreline change, *Geophys. Res. Lett., 36*, L20404, doi:10.1029/2009GL40061.

Galgano, F. A. and B. C. Douglas (2000), Shoreline Position Prediction: Methods and Errors, *Environmental Geosciences, 7*, 23-31.

Galgano, F.A., B.C. Douglas, and S.P. Leatherman (1998), Trends and Variability of Shoreline Position, *Journal of Coastal Research*, Special Issue 26: 282-291.

Genz, A. S., C. H. Fletcher, R. A. Dunn, L. N. Frazer, and J. J. Rooney (2007), The Predictive Accuracy of Shoreline Change Rate Methods and Alongshore Beach Variation on Maui, Hawaii, *J. Coastal Res. 23*, 87–105.

Genz, A.S., L.N. Frazer, and C.H. Fletcher (2009), Toward parsimony in shoreline change prediction (II): Applying basis function methods to real and synthetic data, *J. Coastal Res., 25*, 380-392.

Hansen, P.C. and D.P. O'Leary (1993), The use of the L-curve in the regularization of discrete ill-posed problems, *SIAM Journal on Scientific Computing*, 14(6), 1487-1503.

Hapke, C.J., E.A. Himmelstoss, M. Kratzman, J.H. List, and E.R. Thieler (2010), National assessment of shoreline change; historical shoreline change along the New England and Mid-Atlantic coasts: *U.S. Geological Survey Open-File Report 2010-1118*, 57 p., available at http://pubs.usgs.gov/of/2010/1118/.

Harney, J.N. and C.H. Fletcher (2003), A Budget of Carbonate Framework and Sediment Production, Kailua Bay, Oahu, Hawaii, *Journal of Sedimentary Research*, 73(6), 856-868.

Hastie, T., R. Tibshirani, and J. Friedman (2009), *The Elements of Statistical Learning, 2nd Edition*. New York: Springer-Verlag.

Himmelstoss, E.A., M. Kratzmann, C. Hapke, E.R. Thieler, and J. List (2010), The National Assessment of Shoreline Change: A GIS Compilation of Vector Shorelines and Associated Shoreline Change Data for the New England and Mid-Atlantic Coasts: *U.S. Geological Survey Open-File Report 2010-1119*, available at http://pubs.usgs.gov/of/2010/1119/.

Honeycutt, M. G., M. Crowell, and B.C. Douglas (2001), Shoreline-Position Forecasting: Impact of Storms, Rate-Calculation Methodologies, and Temporal Scales, *Journal of Coastal Research,* 17(3)**,** 721-730.

Hurvich, C.M. and C.-L. Tsai (1989), Regression and time series model selection in small samples, *Biometrika*, 76, 297-307.

Hwang, D.J. (2005), *Hawaii Coastal Hazard Mitigation Guidebook*. Honolulu, Hawaii: University of Hawaii Sea Grant College Program.

Kane, H. H., C.H. Fletcher, B.M. Romine, T.R. Anderson, L.N. Frazer, and M.M. Barbee (2012), Vulnerability Assessment of Hawai'i's Cultural Assets Attributable to Erosion Using Shoreline Trend Analysis Techniques, *Journal of Coastal Research*, *28*(3), 533-539.

Kochel, R.C., and Dolan, R. (1986), The role of overwash on a mid-atlantic coast barrier island, *Journal of Geology,* 94, 902-906.

Komar, P.D. (1998), *Beach Processes and Sedimentation, Second Edition*, Upper Saddle River, New Jersey: Prentice Hall.

Kraus, N.C. (2000), Reservoir model of ebb-tidal shoal evolution and sand bypassing, *J. Waterw. Port Coastal Ocean Eng.,* 126, 305–313.

Kriebel, D. L. (1987), Beach recovery following Hurricane Elena, *Coastal Sediments*, *87*, 990–1005.

Leatherman, S.P. (1979), Interaction between overwash and Aeolian processes on migrating barrier islands, *AAPG Bull,* 63, 486-487.

Leatherman, S.P. (1984), Shoreline evolution of North Assateague Island, Maryland, *Shore and Beach*, 52(3), 3-10.

Leatherman, S.P. and M. Crowell (1997), Beach Erosion Trends and Shoreline Forecasting, *Journal of Coastal Research,* 13(4), iii-iv.

Lesser, G.R., J.A. Roelvink, J.A.T.M. van Kester, and G.S. Stelling (2004), Development and validation of a three dimensional morphological model, *Journal of Coastal Engineering*, 51, 883-915.

Long, J.W. and N.G. Plant (2012), Extended Kalman Filter framework for forecasting shoreline evolution, *Geophysical Research Letters*, 39, L13603.

McQuarrie, A.D.R. and C.-L. Tsai (1998), *Regression and Time Series Model Selection*, Singapore: World Sci.

Menke, W. (2012), *Geophysical Data Analysis: Discrete Inverse Theory, 3rd Edition*, San Diego, California: Academic Press.

Miller, J.K. and R.G. Dean (2004), A simple new shoreline change model, *Coastal Engineering*, 17(3), 531-556.

Miller, J.K. and R.G. Dean (2007), Shoreline variability via empirical orthogonal function analysis: Part I temporal and spatial characteristics, *Coastal Engineering*, 54, 111-131.

Morton, R. A. (1988), Nearshore responses to great storms, in *Sedimentologic consequences of convulsive geologic events*, edited by H. E. Clifton, pp. 7–22, Geol. Soc. Am., Boulder, CO.

Morton, R. A., J. G. Paine, and J. G. Gibeaut (1994), Stages and durations of post-storm beach recovery, southeastern Texas coast, USA, *J. Coast. Res.*, *10*, 884–908.

Morton, R. A., M.P. Leach, J.G. Paine, and M.A. Cardoza (1993), Monitoring beach changes using GPS surveying techniques, *Journal of Coastal Research*, 702-720.

National Research Council, (1990), *Managing Coastal Erosion,* Washington, D.C.: National Academy Press, 182 p.

Niedoroda, A. W., D. J. P. Swift, T.S. Hopkins, and C.-M. Ma (1984), Shoreface Morphodynamics on wave-dominated coasts, *Marine Geology*, 60:331-354.

Noda, E.K. and Associates, Inc. (1989), Hawaii shoreline erosion management study, overview and case studies – Makaha, Oahu; Kailua-Lanikai, Oahu; Kukuiula-Poipu, Kauai, *Report for the Hawaii Coastal Zone Management Program.*

Norcross, Z.M., C.H. Fletcher, and M. Merrified (2002), Annual and interannual changes on a reef-fringed pocket beach: Kailua Bay, Hawaii, *Marine Geology*, 190, 553-580.

Pelnard-Considère (1956), Essai de theorie de l'evolution des formes de rivage enplages de sables et de galets, *4th Journees de l'Hydraulique, Les Energies de la Mer*, Question III, Rapport No. 1.

Plant, N.G., S.G.J. Aarninkhof, I.L. Turner, and K.S. Kingston (2007), The Performance of Shoreline Detection Models Applied to Video Imagery, *Journal of Coastal Research*, 23(3), 658-670.

Ramsey, K. W., D.J. Leathers, D.V. Wells, and J.H. Talley (1998), Summary report: The coastal storms of January 27–29 and February 4-6, 1998, Delaware and Maryland, Open File Report No. 40, Delaware Geological Survey, Newark, DE.

Robert, C.P. (2007), *The Bayesian Choice*, 2nd Edition, Springer-Verlag.

Roelvink, J.A. and G.K.D.M. Van Banning (1994), Design and development of Delft3D and application to coastal morphodynamics, In: Verwey, Minns, Babovic, Maksimovic (Eds.), *Hydroinformatics* '94, Rotterdam, The Netherlands: Balkema, pp. 451-455.

Romine, B.M. and C.H. Fletcher (2012), Armoring on eroding coasts leads to beach narrowing and loss on Oahu, Hawaii, *in* Pitfalls of Shoreline Stabilization: Selected Case Studes, J.A.G. Cooper and O.H. Pilkey (eds.), Coastal Research Library 3, DOI 10.1007/978-94-007-4123-2_10, Springer Science and Business Media, Dordrecht, Netherlands.

Romine, B.M., C.H. Fletcher, L.N. Frazer, A.S. Genz, A.S., M.M. Barbee, and S.-C. Lim (2009), Historical shoreline change, southeast Oahu, Hawaii: applying polynomial

models to calculate shoreline change rates, *Journal of Coastal Research*, 25(6), 1236-1253.

Rosati, J. D., and B. A. Ebersole (1996), Littoral impact of Ocean City Inlet, Maryland, USA, *Proceedings of the 25th International Conference,* American Society of Civil Engineers, 2779-2792.

Ruggiero, P. and J.H. List (2009), Improving Accuracy and Statistical Reliability of Shoreline Position and Change Rate Estimates, *Journal of Coastal Research*, 25(5), 1069 – 1081.

Sallenger Jr, A. H., W. B. Krabill, R. N. Swift, J. Brock, J. List, M. Hansen, R. A. Holman *et al*. (2003), Evaluation of airborne topographic lidar for quantifying beach changes, *Journal of Coastal Research,* 19(1), 125-133.

Schupp, C. A., G. P. Bass, and W. G. Grosskopf (2007), Sand bypassing restores natural processes to Assateague Island, Maryland, *Coastal Sediments '07:Proceedings of the sixth international symposium on coastal engineering and science of coastal sediment processes,* American Society of Civil Engineers,1340-1353.

Schwartz, G. (1978), Estimating the dimension of a model, *The Annals of Statistics*, 6(2), 461-464.

Sea Engineering (1988), Oahu Shoreline Study, City and County of Honolulu Department of Land Utilization.

Short, A.D. (1979), Three dimensional beach stage model, *J. Geol*, 87, 553-571.

Stockdon, H.F., A.H. Sallenger Jr., J.H. List, and R.A. Holman (2002), Estimation of Shoreline Position and Change using Airborne Topographic Lidar Data, *Journal of Coastal Research*, 18(3), 502-513.

Sugiura, N. (1978), Further analysis of the data by Akaike's information criterion and the finite corrections, *Communications in Statistics, Theory and Methods*, A7, 13-26.

Tarantola, A. and B. Valette (1982), Inverse problems – quest for information, *Journal of Geophysics*, 50, 159-170.

Thieler, E.R., E.A. Himmelstoss, J.L. Zichichi, and A. Ergul (2009), Digital Shoreline Analysis System (DSAS) version 4.0 – An ArcGIS extension for calculating shoreline change: *U.S. Geological Survey Open-File Report 2008-1278*.

Thieler, E.R., O.H. Pilkey Jr., R.S. Young, D.M. Bush, and F. Chai (2000), The use of mathematical models to predict beach behavior for US coastal engineering: a critical review, *Journal of Coastal Research*, 16(1), 48-70.

U.S. Department of Energy (2011), *Buildings Energy Data Book*, [pdf] Washington, D.C.: U.S. Department of Energy, Office of Energy Efficiency and Renewable Energy, Building Technologies Program, p. 3-10, Available at: <http://buildingsdatabook.eere.energy.gov/> [Accessed 16 April 2013].

Yates, M.L., R.T. Guza, and W.C. O'Reilly (2009), Equilibrium shoreline response: Observations and modeling, *Journal of Geophysical Research: Oceans*, 114, C09014.

Zellner, A. and G.C. Tiao (1964), Bayesian Analysis of the Regression Model with Autocorrelated Errors, *J. Amer. Statist. Assoc.*, 59, 763.

Zhang, K., B. Douglas, and S. Leatherman (2001), Beach erosion potential for severe nor'easters, *J. Coastal Res., 17*, 309–321.

Zhang, K., B. Douglas, and S. Leatherman (2002a), Do Storms Cause Long-Term Beach Erosion along the U.S. East Barrier Coast? *J. Geology, 110*, 493–502.

Zhang, K. W. Huang, B. Douglas and S. Leatherman (2002b), Shoreline position variability and long-term trend analysis, *Shore and Beach*, 70(2), 31–35.